JOURNAL OF NATURAL PRODUCTS

pubs.acs.org/jnp

Article

The Chemistry of Kratom [*Mitragyna speciosa*]: Updated Characterization Data and Methods to Elucidate Indole and Oxindole Alkaloids

Laura Flores-Bocanegra, Huzefa A. Raja, Tyler N. Graf, Mario Augustinović, E. Diane Wallace, Shabnam Hematian, Joshua J. Kellogg, Daniel A. Todd, Nadja B. Cech, and Nicholas H. Oberlies*

Cite This: *J. Nat. Prod.* 2020, 83, 2165−2177

Read Online

ACCESS | Metrics & More | Article Recommendations | Supporting Information

ABSTRACT: Two separate commercial products of kratom [*Mitragyna speciosa* (Korth.) Havil. Rubiaceae] were used to generate reference standards of its indole and oxindole alkaloids. While kratom has been studied for over a century, the characterization data in the literature for many of the alkaloids are either incomplete or inconsistent with modern standards. As such, full ^{1}H and ^{13}C NMR spectra, along with HRESIMS and ECD data, are reported for alkaloids **1**−**19**. Of these, four new alkaloids (**7**, **11**, **17**, and **18**) were characterized using 2D NMR data, and the absolute configurations of **7**, **17**, and **18** were established by comparison of experimental and calculated ECD spectra. The absolute configuration for the *N*(4)-oxide (**11**) was established by comparison of NMR and ECD spectra of its reduced product with those for compound **7**. In total, 19 alkaloids were characterized, including the indole alkaloid mitragynine (**1**) and its diastereoisomers speciociliatine (**2**), speciogynine (**3**), and mitraciliatine (**4**); the indole alkaloid paynantheine (**5**) and its diastereoisomers isopaynantheine (**6**) and epiallo-isopaynantheine (**7**); the *N*(4)-oxides mitragynine-*N*(4)-oxide (**8**), speciociliatine-*N*(4)-oxide (**9**), isopaynantheine-*N*(4)-oxide (**10**), and epiallo-isopaynantheine-*N*(4)-oxide (**11**); the 9-hydroxylated oxindole alkaloids speciofoline (**12**), isorotundifoleine (**13**), and isospeciofoleine (**14**); and the 9-unsubstituted oxindoles corynoxine A (**15**), corynoxine B (**16**), 3-epirhynchophylline (**17**), 3-epicorynoxine B (**18**), and corynoxeine (**19**). With the ability to analyze the spectroscopic data of all of these compounds concomitantly, a decision tree was developed to differentiate these kratom alkaloids based on a few key chemical shifts in the ^{1}H and/or ^{13}C NMR spectra.

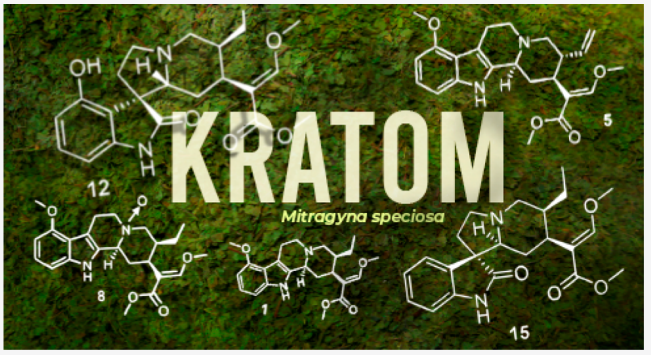

The scientific literature on the chemical composition of kratom [*Mitragyna speciosa* (Korth.) Havil. Rubiaceae] dates back nearly 100 years, when the most studied alkaloid from this plant, mitragynine (**1**), was reported in 1921.[1] The introduction to that paper concludes with the following prescient statements: "*According to Redley . . . Mitragyne [sic] speciosa is used in Perak against the opium habit, whilst, according to Dr. P.P. Laidlaw, mitragynine is a local anaesthetic, which finding is of interest, since the alkaloid contains an ester grouping.*" At that time, there was uncertainty on the use of kratom. Interestingly, a century later, this uncertainty continues, including in the scientific literature, the popular press, and even government regulatory bodies. Many questions persist such as, does kratom ameliorate pain, can it be used as an opioid substitute, does it relieve opioid withdrawal symptoms, does its use precipitate trips to the emergency room, and is kratom harmful, harmless, or somewhere in between? Addressing these questions requires a thorough understanding of the chemical composition of kratom.

In the past decade there has been an explosion in the biomedical literature regarding at least some of the above questions, particularly case reports (Figure S1). There are reports that speak to its ability to address pain, broadly defined.[2−5] However, there are a similar number that suggest that it has opioid-like properties and, thus, may be an addiction liability.[6−15] Toward that end, the U.S. Food and Drug Administration has threatened to classify kratom as a schedule I controlled substance more than once, although at the writing of this paper, it has not done so.[16−19]

As part of a project to study the potential for interactions between herbal medicines and drugs,[20−24] our team was

Received: March 7, 2020
Published: June 29, 2020

https://dx.doi.org/10.1021/acs.jnatprod.0c00257
J. Nat. Prod. 2020, 83, 2165−2177

charged with generating reference standards of the kratom alkaloids. In doing so, we found many challenges and opportunities, largely due to gaps in the literature. Extensive chemical studies have been performed over the last century, resulting in the isolation of at least 54 alkaloids from the plant (see Figure S2), starting with the isolation of the main alkaloid, mitragynine (**1**), in 1921 by Ellen Field.[1] More than four decades later, and over a series of three manuscripts, Becket et al. and Zacharias et al. worked on the isolation, structure elucidation, and absolute configuration of **1**.[25−27] Contemporaneously, the mitragynine diastereoisomers speciociliatine (**2**) and speciogynine (**3**) were reported.[28] A dozen years later, the fourth diastereoisomer, mitraciliatine (**4**), was described from the leaves of *M. speciosa*.[29] Like many alkaloids, a majority of isolation studies on new compounds from kratom were carried out between the 1960s and 1980s.[30−32] However, due to the growing popularity of this plant near the end of the last century, there was a renewed interest, resulting in the isolation of additional alkaloids (particularly minor constituents, which could be isolated due to advances in HPLC).[33,34] Despite this, most of the pharmacological studies on constituents from kratom have focused on mitragynine (**1**) and 7-hydroxymitragynine (see Figure S1). In general, the tetracyclic indole and pentacyclic oxindole alkaloids isolated from *M. speciosa* embody a few variations, which, collectively, show the interrelatedness of these compounds (see Figure S2). Some key motifs of the 54 known compounds from *M. speciosa* include a hydroxy or methoxy group at C-9, unsaturation at C-3, C-5, or C-18, hydroxylation at C-7, and various configurations at C-3, C-7, and/or C-20 (see Figure S2).[30−32]

It was necessary to isolate standards for the alkaloids present in the plant, because even though there are over 50 kratom alkaloids reported, only 13 are commercially available (Figure S2). Moreover, in some cases we found that the quality of the commercial standards was not optimal, being mixtures, or were not even the correct compound.[35,36] From a pharmacological testing point of view, this is a serious problem, especially for scientists that do not have the training or collaborations to verify structural identity, as it could perpetuate erroneous findings in the literature. For these reasons, we strove to develop a series of reference standards, being able to isolate and characterize 19 kratom alkaloids (**1**−**19**), including four new analogues (**7**, **11**, **17**, and **18**). In doing so, we quickly realized that the reported spectroscopy data for some of the known compounds were limited, as is the case for many natural products.[37−41] Thus, we took the opportunity to contribute by analyzing the NMR, HRESIMS, and ECD data for **1**−**19**, comparing the key differences between analogues.

RESULTS AND DISCUSSION

While there are some challenges associated with acquiring kratom plant material,[42] two different sources could be obtained on the kilogram scale, which were termed "Green Maeng Da" and "White Jongkong" by the suppliers. These samples were slightly different in appearance, with the former being ground leaf fragments (internally coded as K49) and the latter being a fine powder (internally coded as K52) (see Figure S6). The taxonomy of these was examined using a combination of molecular methods, specifically DNA barcoding and maximum likelihood phylogenetic analysis. For the purpose of molecular identification, the most widely recommended loci were analyzed, including the plastid intergenic spacer *trnH-psbA*, *matK*, and the nuclear ribosomal internal transcribed spacer (ITS), since these three regions have been designated as the official DNA barcodes for the plant kingdom.[43,44] Of these, *trnH-psbA* is a widely used plastid marker, which displays a high rate of insertion and deletion and, as such, is widely used for plant barcoding studies.[45−47] All three regions indicated that samples K49 and K52 could be unequivocally identified as *Mitragyna speciosa*. Maximum likelihood analysis of the partial *matK* region placed both commercial samples in a strongly supported clade (100% bootstrap support) with the published sequences for *M. speciosa* (Figure S3). Importantly, this analysis included a partial *matK* sequence from a recently sequenced genome of *M. speciosa* (BioProject: PRJNA325670). In addition, a BLAST search of *matK* using the BOLDSYSTEMS database (version 4) showed that samples K49 and K52 had ≥99% sequence similarity to *M. speciosa* (Figures S4 and S5). As a confirmatory measure, maximum likelihood analysis using the ITS region also indicated that both samples formed a strongly supported clade (≥99% bootstrap support) with published sequence data of *M. speciosa* (Figure S6). Based on uncorrected p-distances calculated for *trnH-psbA*, there was ≥99% sequence similarity to sequences of *M. speciosa*. This means that samples K49 and K52 were more similar to sequences of *M. speciosa* and more dissimilar to sequences of *M. diversifolia*, *M. hirsuta*, and *M. rotundifolia* (Tables S1 and S2). In short, three different methods all indicated that these materials were derived from *M. speciosa*. The sequence data were deposited in GenBank: *matK*: MT114409 and MT114408, *trnH-psbA*: MT114410 and MT114411, and ITS: MT111840, MT111841, MT111842, and MT111843.

Even though the sources of kratom (i.e., K49 and K52) were demonstrated to be *M. speciosa* based on DNA barcoding, chromatographic profiles generated via UPLC-HRESIMS (Figure S7) showed clear differences in the profile of secondary metabolites. For instance, mitragynine (**1**) was the most abundant alkaloid in the K49 materials, while the K52 materials contained higher levels of speciofoline (**12**) and related alkaloids. While those differences may be somewhat surprising, varied chemical composition for different sources of *M. speciosa* has been documented, where plant age, environmental factors, and processing conditions impact on the suite of kratom alkaloids.[48,49] For example, in one published study the content of **1** derived from a Thai specimen was approximately five times higher than that derived from a Malaysian specimen.[50] Additionally, alkaloid differences between *M. speciosa* grown in Asia/Africa vs the United States have been noted.[49,51] Thus, for the purpose of generating structurally diverse kratom alkaloid reference standards, we selected sample K49 for the isolation of indole-type alkaloids and sample K52 for the isolation of oxindole-type alkaloids using an alkaloid partitioning scheme. The indole alkaloids mitragynine (**1**), speciociliatine (**2**), speciogynine (**3**), mitraciliatine (**4**), paynantheine (**5**),[52] isopaynantheine (**6**),[29] epiallo-isopaynantheine (**7**), mitragynine-*N*(4)-oxide (**8**),[53] speciociliatine-*N*(4)-oxide (**9**),[53] isopaynantheine-*N*(4)-oxide (**10**),[54] and epiallo-isopaynantheine-*N*(4)-oxide **11** were isolated from the Green Maeng Da product (K49; see Figure S8), while the oxindole alkaloids speciofoline (**12**),[55] isorotundifoleine (**13**),[56] isospeciofoleine (**14**),[57] corynoxine A (**15**),[58,59] corynoxine B (**16**),[59] 3-epirhynchophylline (**17**), 3-epicorynoxine B (**18**), and corynoxeine (**19**) were isolated from the White Jongkong product (K52; see Figure S9). Details of the structure elucidation for these compounds,

https://dx.doi.org/10.1021/acs.jnatprod.0c00257
J. Nat. Prod. 2020, 83, 2165−2177

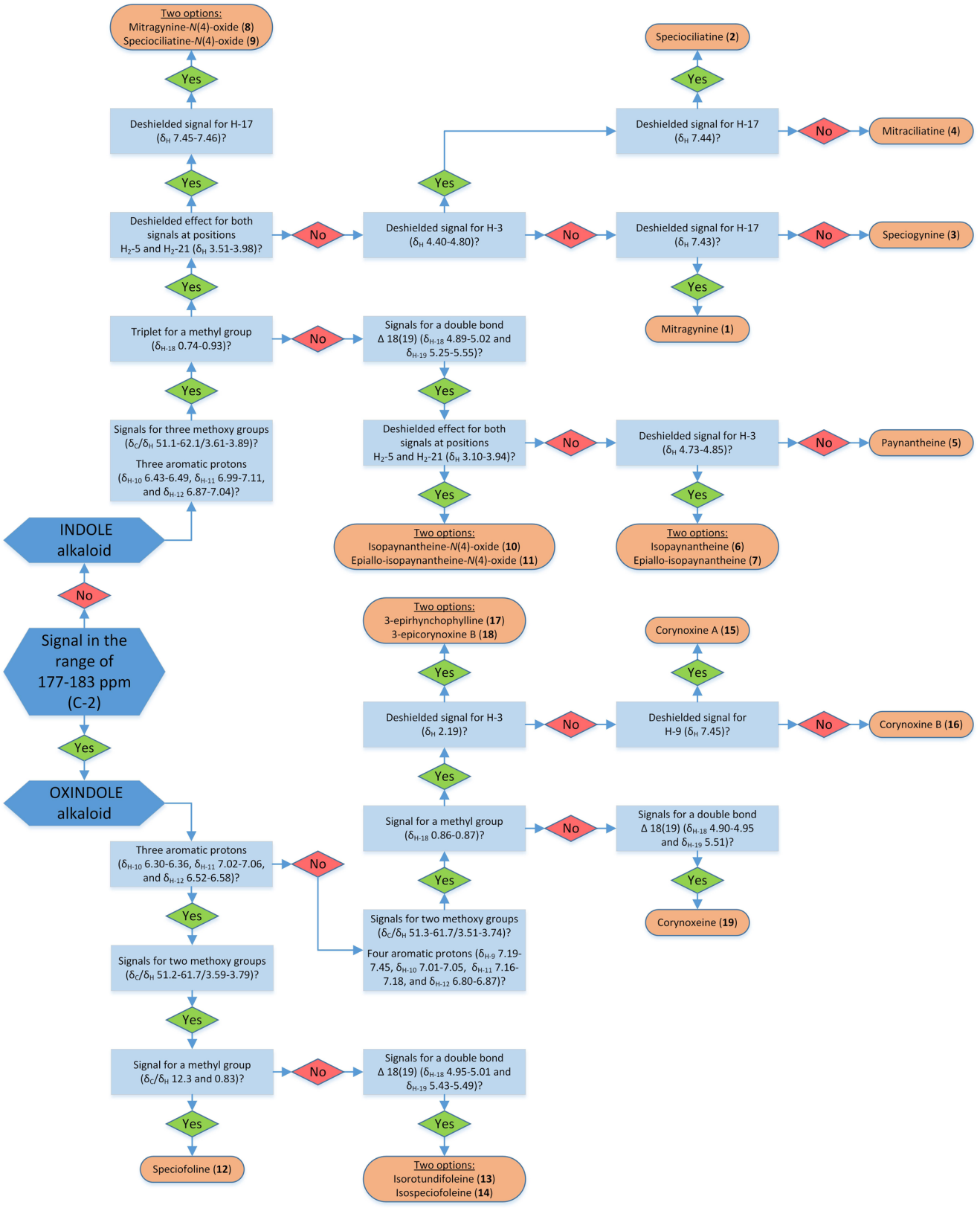

Figure 1. Decision tree for differentiating among **1**−**19** based on key NMR signals. As a single starting point, the ^{13}C NMR signal for the lactam moiety is used to distinguish between oxindole (present) and indole (absent) kratom alkaloids. Once the broad structural class is determined, ^{1}H NMR data can be used via a flowchart as a guide to elucidate the structure of these alkaloids.

including the identification of four new kratom alkaloids (i.e., **7**, **11**, **17**, and **18**), are presented below, using a suite of spectroscopic and spectrometric techniques (HRESIMS), including ECD. In doing so, a decision tree was developed that can be used to differentiate between these kratom alkaloids based on a few key signals in the ^{1}H and/or ^{13}C

https://dx.doi.org/10.1021/acs.jnatprod.0c00257
J. Nat. Prod. 2020, 83, 2165−2177

NMR spectra (Figure 1). This flow diagram was designed to be helpful for those with only a limited understanding of structure elucidation, focusing on key signals that serve to differentiate between the various kratom alkaloid chemotypes.

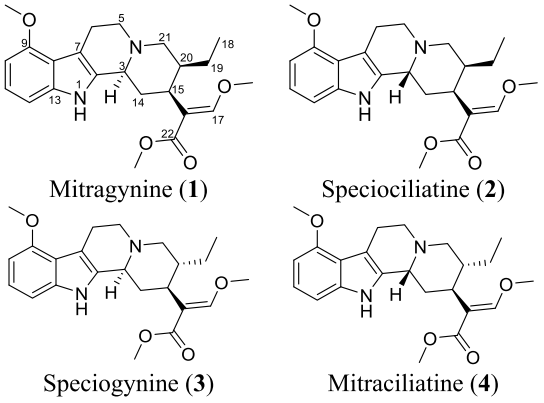

Indole Alkaloids: Mitragynine (1) and Its Diastereoisomers (2−4). Four diastereoisomers with a molecular formula of $C_{23}H_{30}N_2O_4$ were isolated, specifically mitragynine (**1**), speciociliatine (**2**), speciogynine (**3**), and mitraciliatine (**4**), all of which were verified via HRESIMS data, where the protonated molecule displayed *m/z* 399.2274, 399.2273, 399.2274, and 399.2275 ions, respectively (Figures S10−S13). While the absolute amounts likely vary in different kratom plant materials, the quantity of compound **1** isolated was at least 20 times greater than that for each of the other diastereoisomers (i.e., >450 mg of **1** vs ∼20 mg of **2**, **3**, or **4**). The ^{1}H and ^{13}C NMR data matched with those reported previously,[60] and key characteristics included (1) eight sp^2 signals in the ^{13}C NMR spectrum assignable to the indole moiety (C-2 and C-7 to C-13); (2) two doublets ($\delta_{H\text{-}10}$ 6.44−6.49 and $\delta_{H\text{-}12}$ 6.87−7.01) and one triplet ($\delta_{H\text{-}11}$ 6.99−7.07), all corresponding to the indole moiety; (3) signals for the vinylic proton at C-17 (δ_C/δ_H 160.2−160.7/7.32−7.44); (4) three methoxy groups attached to C-9, C-17, and C-22 (δ_C/δ_H 51.1−61.9/3.66−3.89); and (5) the methyl group at C-19 (δ_C/δ_H 11.1−13.0/0.74−0.89). Importantly, a thorough analysis of the differences between the characteristic signals permitted the unequivocal identification of compounds **1**−**4**. For example, as Lee and colleagues described,[61] when a deshielded proton singlet assignable to H-17 appeared at δ_H 7.43 or 7.44 (i.e., compounds **1** and **2**, respectively), it was indicative of the α orientation of H-20. Alternatively, a more shielded chemical shift for H-17 (i.e., δ_H 7.32 and 7.35 for compounds **4** and **3**, respectively) indicated the β orientation for H-20.[61] Additionally, the orientation of H-20 could be confirmed orthogonally via the chemical shift of C-18, at δ_C of 12.5 or 13.0 (i.e., compounds **2** and **1**, respectively) for the α orientation and δ_C of 11.1 (i.e., for both **3** and **4**) for the β orientation. On the other hand, the presence of a broad singlet at δ_H 4.40 or 4.80 (i.e., compounds **2** and **4**) agreed with the β orientation for H-3, but a signal at δ_H 3.20 or 3.21 (i.e., compounds **1** and **3**) indicated the opposite orientation for the same proton (i.e., H-3α). Indeed, the $\Delta\delta_{H\text{-}3}$ values of the α and β orientations depend on the dihedral angle and the distance between H-3 and the nitrogen lone pair. An anticoplanar arrangement, as seen in the axial H-3 of the *trans*-fused system in compound **1** or **3** (i.e., α orientation), leads to shielding relative to the *syn*-coplanar arrangement of the equatorial proton (i.e., β orientation) in compound **2** or **4**, which have a dihedral angle of ∼60° with the nitrogen lone pair. The donation of electron density into the antibonding orbital (i.e., $n \rightarrow \sigma^*$) of the axial C−H bond (i.e., α orientation) effectively results in the weakening of that bond and strong shielding of the proton (Figure S18).[62,63] Key NMR signals for **1**−**4** are outlined (Table 1), and in addition, full 1D NMR spectra and tables are reported in the Supporting Information (Figures S14−S17 and Table S4). Moreover, ECD spectra presented an additional approach for confirming the absolute configuration for these corynanthe-type alkaloids. It has been established that the Cotton effect between 250 and 300 nm could be used to establish the orientation of H-3, where a negative Cotton effect correlates with the β orientation (i.e., compounds **2** and **4**) and a positive Cotton effect for the α orientation for H-3 (i.e., compounds **1** and **3**; see Figure S19).[61]

Indole Alkaloids: Paynantheine and Its Diastereoisomers (Compounds 5−7). The structures of paynantheine (**5**) and isopaynantheine (**6**) were established by comparisons with literature data.[57] Their molecular formulas were confirmed by HRESIMS as $C_{23}H_{28}N_2O_4$, where the protonated molecule showed an *m/z* of 397.2119 and 397.2117, respectively (Figures S20 and S21). The NMR data of **5** and **6** resembled those for compounds **1**−**4**, sharing the previously enumerated characteristic signals for the indole ring. The main difference was the absence of signals for the C-20 ethyl moiety and its replacement for a vinylic moiety, as evidenced by two doublets of doublets (δ_H 4.89−5.01) and a doublet of doublet of doublets or a doublet of triplets (δ_H 5.25−5.57), consistent with a Δ18(19) double bond ($\delta_{C\text{-}18}$

Table 1. Characteristic ^{1}H and ^{13}C NMR Data for Compounds 1−4 ($CDCl_3$, 400 and 100 MHz, Respectively)[a]

	mitragynine (**1**)			speciociliatine (**2**)			speciogynine (**3**)			mitraciliatine (**4**)		
position	δ_C	type	δ_H (*J* in Hz)	δ_C	type	δ_H (*J* in Hz)	δ_C	type	δ_H (*J* in Hz)	δ_C	type	δ_H (*J* in Hz)
3	61.3	CH	3.20, d (8.4)	54.7	CH	4.40, bs	61.9	CH	3.21, m	53.9	CH	4.80, s
10	99.9	CH	6.45, d (7.7)	99.8	CH	6.47, d (7.7)	99.8	CH	6.44, d (7.8)	99.7	CH	6.49, d (7.6)
11	122.0	CH	7.00, t (7.9)	122.4	CH	7.02, t (8.0)	122.4	CH	6.99, t (7.9)	122.6	CH	7.07, t (7.9)
12	104.3	CH	6.90, d (8.1)	104.5	CH	6.91, d (8.1)	104.5	CH	6.87, d (8.0)	104.9	CH	7.01, d (8.0)
17	160.7	CH	7.43, s	160.6	CH	7.44, s	160.4	CH	7.35, bs	160.2	CH	7.32, s
18	13.0	CH_3	0.87, t (7.3)	12.5	CH_3	0.89, t (7.9)	11.1	CH_3	0.85, t (7.2)	11.1	CH_3	0.74, t (7.0)
9-OCH_3	55.5	CH_3	3.87, s	55.3	CH_3	3.88, s	55.4	CH_3	3.85, s	55.3	CH_3	3.89, s
17-OCH_3	61.7	CH_3	3.73, s	61.7	CH_3	3.78, s	61.9	CH_3	3.72, s	61.8	CH_3	3.77, s
22-OCH_3	51.5	CH_3	3.71, s	51.6	CH_3	3.66, s	51.1	CH_3	3.72, s	51.5	CH_3	3.68, s
NH			7.74, bs			8.00, bs			7.94, bs			8.98, bs

[a]See Table S4 for a full comparison of the ^{1}H and ^{13}C NMR data for **1**−**4** (Supporting Information).

https://dx.doi.org/10.1021/acs.jnatprod.0c00257
J. Nat. Prod. 2020, 83, 2165−2177

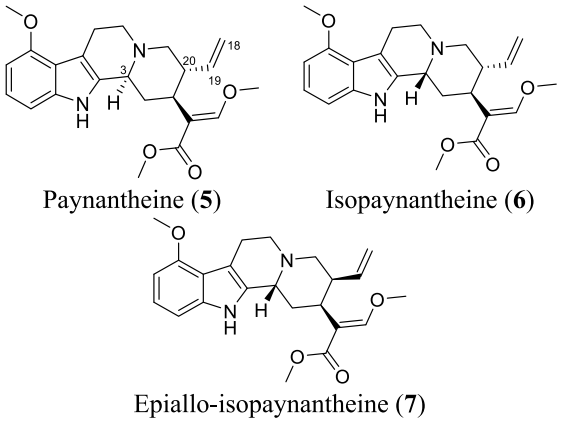

115.7−116.7 and $\delta_{C\text{-}19}$ 137.9−139.4). As with **1**−**4**, the orientation of H-3 was deduced from chemical shift data, where the H-3α orientation was noted for **5** (δ_H 3.20), while the more deshielded shift in **6** (δ_H 4.73) indicated the H-3β orientation. These assignments were supported by the ECD spectra, where **5** and **6** had opposite Cotton effects at 250−300 nm. Specifically, a negative Cotton effect confirmed the β orientation (i.e., **6**) and a positive Cotton effect confirmed the α orientation (i.e., **5**) for H-3 (see Figure S33). Comparisons of the key NMR signals for compounds **5** and **6** are shown in Table 2, and the full 1D NMR spectroscopic data are reported in the Supporting Information (Figures S23−S24 and Table S5).

Compound **7** was isolated as an optically active yellow powder (α_D^{20} +41, *c* 0.1 $CHCl_3$), with a molecular formula of $C_{23}H_{28}N_2O_4$, deduced by HRESIMS, where the protonated molecule showed an *m*/*z* of 397.2115 (Figure S22). The ^1H and ^{13}C NMR data of **7** resembled those of compounds **5** and **6**, sharing all the characteristic signals for an indole alkaloid with Δ18(19) unsaturation (see Tables 2 and S5 and Figures S23−S25). These observations, along with differences in chromatographic retention times (**5**: 7.5 min, **6**: 7.0 min, and **7**: 9.0 min; see Figure S34), suggested that **7** was a new diastereoisomer of **5** and **6**. The HSQC data, along with COSY and HMBC correlations, were used to elucidate the structure of **7** (Figures S26−S28). For example, three isolated spin systems (specifically, H-10/H-11/H-12, H_2-5/H_2-6, and H-3/H_2-14/H-15/H-20/H_2-21/H-19/H_2-18) and key HMBC correlations (i.e., H-3 to C-2/C-7, H-17 to C-15/C-22, H_2-18 to C-20, CH_3O-9 to C-9, CH_3O-17 to C-17, and CH_3O-22 to C-22) were used to confirm the skeleton for the proposed structure (Figure 2).

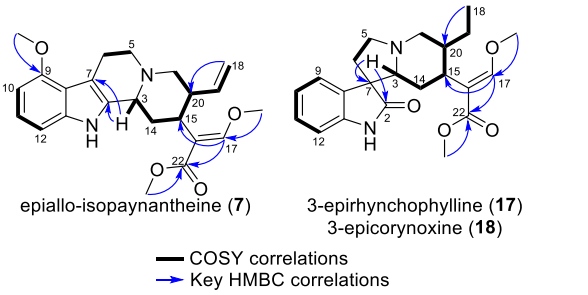

Figure 2. Key correlations observed in the COSY and HMBC spectra for compounds **7**, **17**, and **18**. The latter two have the same 2D structure and thus the same correlations.

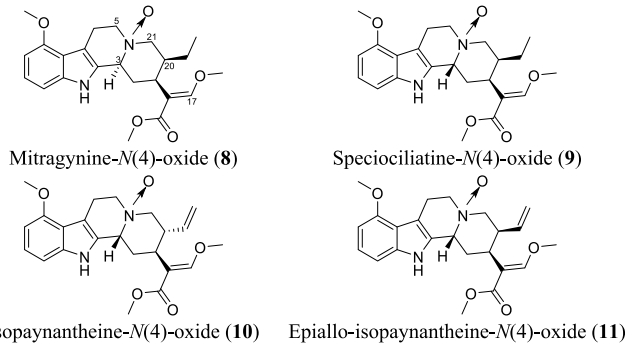

To establish the absolute configuration of **7**, several complementary lines of reasoning were used. For instance, the deshielded signal at 4.85 ppm suggested H-3β, since that was similar to the chemical shift for the same position in compounds **2** ($\delta_{H\text{-}3}$ 4.40), **4** ($\delta_{H\text{-}3}$ 4.80), and **6** ($\delta_{H\text{-}3}$ 4.73), all of which have been established to be H-3β. Moreover, biogenetic assumptions were used for the C-15 configuration, since all the indole alkaloids from *M. speciosa* (42 compounds, to date) have the H-15α orientation.[32] Those considerations narrowed the possibilities for compound **7** to either the pseudo (i.e., 3β, 15α, and 20β) or epiallo (i.e., 3β, 15α, and 20α) orientation.[61] The known compound isopaynantheine (**6**) has

Table 2. Characteristic ^1H and ^{13}C NMR Data for Compounds 5−7 ($CDCl_3$, 400 and 100 MHz, Respectively)[a]

	paynantheine (5)			isopaynantheine (6)			epiallo-isopaynantheine (7)		
position	δ_C	type	δ_H (*J* in Hz)	δ_C	type	δ_H (*J* in Hz)	δ_C	type	δ_H (*J* in Hz)
3	60.1	CH	3.20, m	53.8	CH	4.73, bs	53.9	CH	4.85, bs
10	99.9	CH	6.45, d (7.8)	99.7	CH	6.49, d (7.6)	99.7	CH	6.49, d (7.8)
11	122.1	CH	7.00, t (7.9)	122.6	CH	7.07, t (7.9)	122.9	CH	7.08, t (7.9)
12	104.3	CH	6.88, d (8.0)	105.0	CH	7.02, d (8.1)	105.0	CH	7.01, d (8.1)
17	160.0	CH	7.33, s	160.2	CH	7.28, s	160.3	CH	7.28, s
18	115.7	CH_2	5.01, dd (17.3, 2.0)	116.7	CH_2	4.96, dd (17.2, 1.8)	117.2	CH_2	4.98, dd (17.3, 1.7)
			4.96, dd (10.4, 2.1)			4.89, dd (10.2, 1.8)			4.91, dd (10.3, 1.8)
19	139.4	CH	5.55, dt (17.9, 9.3)	137.9	CH	5.29, ddd (18.0, 10.3, 8.3)	137.1	CH	5.27, ddd (18.0, 10.3, 8.3)
9-OCH_3	55.4	CH_3	3.88, s	55.3	CH_3	3.89, s	55.3	CH_3	3.88, s
17-OCH_3	61.7	CH_3	3.78, s	61.7	CH_3	3.76, s	61.7	CH_3	3.76, s
22-OCH_3	51.5	CH_3	3.69, s	51.4	CH_3	3.67, s	51.5	CH_3	3.67, s
NH			7.85, s			8.91, s			9.12, s

[a]See Table S5 for a full comparison of the ^1H and ^{13}C NMR data for **5**−**7** (Supporting Information).

https://dx.doi.org/10.1021/acs.jnatprod.0c00257
J. Nat. Prod. 2020, 83, 2165−2177

the pseudo configuration, and thus, compound **7** is the 20-epimer of **6** (i.e., H-20α), yielding an overall configuration of epiallo; those considerations were used to suggest the trivial name epiallo-isopaynantheine (**7**). In addition, ECD spectroscopy was used as an orthogonal probe of the proposed configuration. The spectrum for the epiallo configuration (i.e., 3β, 15α, and 20α) was calculated using a time-dependent DFT (TDDFT) method at the B3LYP/6-31G+(d) level of theory, demonstrating concordance, including the aforementioned negative Cotton effect at ca. 275 nm that confirmed the H-3β orientation (Figure 3). The NOESY spectra of compounds

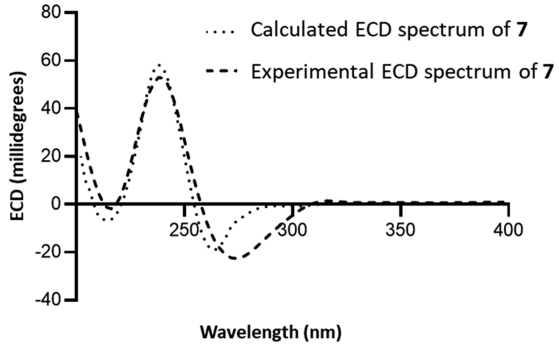

Figure 3. Experimental ECD spectrum of **7** in CH_3OH at 0.2 mg/mL (dashed line) and calculated ECD spectrum of (3*R*,15*S*,20*S*)-**7** (dotted line).

6 and **7** were compared as well (Figures S29−S31). However, these data were inconclusive, since clear differences could not be discerned. This could be explained based on atomic distances, which were measured for the most stable conformers; in all cases these distances were <5 Å (Figure S31). Collectively, the amalgamation of NMR and ECD data and biogenetic considerations were used to establish the (3*R*,15*S*,20*S*) absolute configuration of the new indole alkaloid, epiallo-isopaynantheine (**7**).

***N*(4)-Oxides of Indole Alkaloids (8−11).** Compounds **8** and **9** had identical molecular formulas ($C_{23}H_{30}N_2O_5$), as determined by HRESIMS, where the protonated molecules displayed an *m*/*z* of 415.2234 (**8**) and 415.2237 (**9**) (see Figures S35 and S36). This indicated that **8** and **9** had one extra oxygen atom compared to the diastereoisomers **1**−**4**. ^{1}H and ^{13}C NMR spectra of both had strong similarities to the spectroscopic data reported for mitragynine-*N*(4)-oxide, sharing the characteristic NMR signals for the *N*(4)-oxide indole alkaloids ($\delta_{H\text{-}10}$ 6.43, $\delta_{H\text{-}11}$ 6.99−7.03, $\delta_{H\text{-}12}$ 6.92−6.95, $\delta_{C\text{-}17}/\delta_{H\text{-}17}$ 161.3−161.5/7.45−7.46, $\delta_{C\text{-}18}/\delta_{H\text{-}18}$ 11.8−12.7/0.85−0.93, $\delta_{C\text{-}21}/\delta_{H\text{-}21}$ 68.5−68.6/3.53−3.72, $\delta_{C\text{-}5}/\delta_{H\text{-}5}$ 65.8−65.9/3.51−3.98, and three methoxy groups δ_C/δ_H 51.6−62.1/3.61−3.86).[30] The main difference between the spectra for compounds **8** and **9**, relative to those discussed above for **1**−**4**, was deshielding of the signals attributed to H-3, H_2-5, and H_2-21, which was caused by a coordinate covalent bond in the *N*(4)-oxide group. There is an important distinction with the *N*-oxides, relative to the other kratom alkaloids, in that the $\Delta\delta_{H\text{-}3}$ value is small (~0.12 ppm) and does not correlate with the orientation of H-3. As noted in the discussion of **1**−**4**, the $\Delta\delta_{H\text{-}3}$ values of diastereoisomers mainly depend on the extent of interaction between the nitrogen free electron pair and the C−H antibonding orbitals. However, for the *N*-oxides, such an effect is not possible, since the electron pair is shared with the oxygen (i.e., N^+-O^- group). For the *N*-oxides, the positive charge on the nitrogen has a strong electron-withdrawing inductive effect, resulting in decreased electron density regardless of whether the α-protons are axial or equatorial. In both compounds, the deshielded signal for the vinylic proton at $\delta_{H\text{-}17}$ 7.45−7.46 indicated the α orientation for H-20, analogous to compounds **1** and **2**. In addition, H-15 was presumed to have the α orientation, based on the biogenetic considerations discussed for compound **7**. Therefore, **8** and **9** could have the allo (i.e., 3α, 15α, and 20α) or the epiallo (i.e., 3β, 15α, and 20α) configurations. This illustrates another advantage of analyzing the ECD spectra of kratom alkaloids, particularly the Cotton effect at ca. 275 nm. Compounds **8** and **9** had opposite effects at ca. 275 nm, where a positive Cotton effect correlated with the H-3α orientation (i.e., **8**) and a negative Cotton effect indicated the H-3β orientation (i.e., **9**). In turn, these data allowed us to assign these compounds as mitragynine-*N*(4)-oxide (**8**)[30] and speciociliatine-*N*(4)-oxide (**9**). This is the first report of NMR characterization data for **9**, and key NMR signals for **8** and **9** are collated in Table 3, with full 1D NMR data reported in the Supporting Information (see Figures S39 and S40 and Table S6).

A similar set of observations were used to assign the structures of compounds **10** and **11**, which were isolated as orange powders with a molecular formula of $C_{23}H_{28}N_2O_5$ as calculated by HRESIMS via a protonated molecule with an

Table 3. Characteristic ^{1}H and ^{13}C NMR Data for Compounds 8−11 ($CDCl_3$, 400 and 100 MHz, Respectively)[a]

	mitragynine-*N*(4)-oxide (**8**)			speciociliatine-*N*(4)-oxide (**9**)			isopaynantheine-*N*(4)-oxide (**10**)			epiallo-isopaynantheine-*N*(4)-oxide (**11**)		
position	δ_C	type	δ_H (*J* in Hz)	δ_C	type	δ_H (*J* in Hz)	δ_C	type	δ_H (*J* in Hz)	δ_C	type	δ_H (*J* in Hz)
3	66.9	CH	5.16, s	66.0	CH	5.04, d (12.5)	69.2	CH	5.04, bs	69.6	CH	4.91, bs
10	99.7	CH	6.43, d (7.7)	99.8	CH	6.43, d (7.7)	99.9	CH	6.49, d (7.8)	99.8	CH	6.48 d (7.7
11	123.3	CH	7.03, t (7.9)	122.7	CH	6.99, t (7.9)	123.8	CH	7.11, t (7.9)	123.6	CH	7.10, t (7.9)
12	105.2	CH	6.95, d (8.1)	106.3	CH	6.92, bs	105.1	CH	7.03, d (8.2)	105.2	CH	7.04, d (8.1)
17	161.5	CH	7.45, s	161.3	CH	7.46, s	160.5	CH	7.31, s	160.5	CH	7.30, s
18	12.7	CH_3	0.93, t (7.2)	11.8	CH_3	0.85, t (7.4)	118.0	CH_2	5.02, dd (17.5, 1.0)	117.8	CH_2	5.02, d (17.2)
									4.95, dd (10.2, 1.7)			4.94, dd (10.3, 1.6)
9-OCH_3	55.2	CH_3	3.85, s	55.3	CH_3	3.86, s	55.3	CH_3	3.88, s	55.3	CH_3	3.87, s
17-OCH_3	62.1	CH_3	3.80, s	61.9	CH_3	3.85, s	62.0	CH_3	3.80, s	62.0	CH_3	3.79, s
22-OCH_3	51.6	CH_3	3.61, s	51.8	CH_3	3.68, s	51.6	CH_3	3.68, s	51.6	CH_3	3.68, s
NH			9.46, s						8.84, s			

[a]See Table S6 for a full comparison for the ^{1}H and ^{13}C NMR data for **8**−**11** (Supporting Information).

https://dx.doi.org/10.1021/acs.jnatprod.0c00257
J. Nat. Prod. 2020, 83, 2165−2177

m/z of 413.2079 (**10**) and 413.2077 (**11**) (Figures S37 and S38). For instance, the NMR data for **10** and **11** were similar to those reported for isopaynantheine-*N*(4)-oxide (Table 3). These NMR data also resembled those of **8** and **9**, where the main difference was the lack of the C-20 ethyl group (**10** and **11**), which was replaced with a vinylic group (see Table 3). In both cases, the signals for the vinylic proton appeared at $\delta_{H\text{-}17}$ 7.30−7.31, which was similar to the shifts in compounds **6** and **7**. Again, ECD data were helpful, where the negative Cotton effects at ca. 275 nm correlated with the H-3β orientation for both **10** and **11** (Figure S47). Additionally, a comparison of the ECD spectra of compounds **10** and **6** showed striking similarities; the same was true when comparing compounds **11** and **7** (see Figure S46). Therefore, compound **10** had the pseudo configuration (3β, 15α, and 20β; i.e., as seen in **6**) and **11** had the epiallo configuration (3β, 15α, and 20α; i.e., as seen in **7**). To confirm the absolute configuration of the new compound **11**, the method described by Shellard and colleagues[53] was used. Briefly, **11** was reduced by addition of H_2SO_4, and the reaction product should correspond to the indole alkaloid without the oxide. Indeed, the ^{1}H NMR spectrum for the reduced product of **11** matched the spectrum of **7** (Figure S46). Collectively, these data permitted the characterization of these compounds as isopaynantheine-*N*(4)-oxide (**10**) and the new kratom alkaloid epiallo-isopaynantheine-*N*(4)-oxide (**11**). The spectroscopic data for both are reported in the Supporting Information (Figures S41−S45 and Table S6).

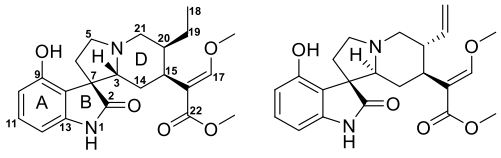

Speciofoline (**12**)

Isorotundifoleine (**13**)

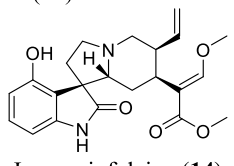

Isospeciofoleine (**14**)

Oxindole Alkaloids: 9-Hydroxylated Oxindoles like Speciofoline (12−14). Compound **12** had a molecular formula of $C_{22}H_{28}N_2O_5$, based on the protonated HRESIMS molecule with an m/z of 401.2067 (Figure S48). Comparison of the NMR data with key NMR signals in the ^{1}H and ^{13}C spectra reported previously permitted the identification of this compound as speciofoline (**12**) (Table 4).[55,56] This compound, which is one of the main alkaloids present in kratom (e.g., >55 mg isolated in this study), was first reported in 1963.[55] We have included the full spectroscopic data for **12** to serve as a reference point when analyzing the spectroscopic data for some of the more minor oxindole alkaloids. For instance, the C-ring (i.e., the pyrollidine ring) of **12** is connected to the γ-lactam (i.e., B-ring) through a C-7 spiro carbon, and this results in characteristic signals in the ^{13}C NMR spectrum at δ_C 180.2 and 57.3 for the carbonyl in the oxindole ring and the spiro C-7 carbon, respectively (Table 4); the lactam signal, in particular, serves to quickly differentiate between indole and oxindole alkaloids (see Figure 1). Other important NMR signals, which are similar to those discussed above for the indole alkaloids, include (1) signals for the indole system ($\delta_{H\text{-}10}$ 6.35, $\delta_{H\text{-}11}$ 7.05 and $\delta_{H\text{-}12}$ 6.53); (2) a vinylic H-17 (δ_C/δ_H 159.8/7.38); (3) two methoxy groups at C-17 and C-22 (δ_C/δ_H 61.3/3.79 and δ_C/δ_H 51.7/3.65, respectively), and (4) a methyl group ($\delta_{C\text{-}18}/\delta_{H\text{-}18}$ 12.3/0.83). Key NMR signals for **12** are tabulated (Table 4), and the full 1D NMR spectroscopic data are reported in the Supporting Information (Figure S51 and Table S7).

Additionally, two other 9-hydroxylated oxindole alkaloids were isolated and characterized as isorotundifoleine (**13**) and isospeciofoleine (**14**). The molecular formula for both isomers was $C_{22}H_{26}N_2O_5$ as measured by HRESIMS based on protonated molecules with m/z values of 399.1909 and 399.1906, respectively (Figures S49 and S50). The structures were elucidated by comparing the NMR data with those reported previously (Table 4),[56,57] and the full assignment of the ^{1}H and ^{13}C NMR spectroscopic data for both are reported in the Supporting Information (Figures S52 and S53 and Table S7); this is the first report of comprehensive NMR data for **13**. The NMR data for both **13** and **14** resembled those described above for speciofoline (**12**), with a major difference being the absence of the methyl group (i.e., C-18 in **12** at δ_C/δ_H 12.3/0.83), which was replaced by the Δ18(19) double bond (δ_C/

Table 4. Characteristic ^{1}H and ^{13}C NMR Data for Compounds 12−14 ($CDCl_3$, 500 and 125 MHz, Respectively)[a]

	speciofoline (**12**)			isorotundifoleine (**13**)			isospeciofoleine (**14**)		
position	δ_C	type	δ_H (J in Hz)	δ_C	type	δ_H (J in Hz)	δ_C	type	δ_H (J in Hz)
2	180.2	C		177.7	C		179.1	C	
3	63.8	CH	3.06, dd (11.7, 3.6)	66.6	CH	3.39, dd (12.5, 3.6)	68.7	CH	2.68, dd (11.6, 3.2)
7	57.3	C		55.9	C		57.5	C	
9	154.6	C		155.1	C		154.6	C	
10	111.9	CH	6.35, d (7.6)	112.1	CH	6.30, dd (7.6, 0.8)	111.4	CH	6.36, dd (7.6, 0.7)
11	129.6	CH	7.05, t (8.0)	129.2	CH	7.02, dd (8.3, 7.7)	129.6	CH	7.06, dd (8.3, 7.7)
12	101.1	CH	6.53, d (8.3)	100.3	CH	6.52, dd (8.5, 0.8)	101.0	CH	6.58, d (8.3)
17	159.8	CH	7.38, s	159.8	CH	7.27, s	159.9	CH	7.19, s
18	12.3	CH_3	0.83, d (7.4)	116.4	CH_2	5.01, m 4.96, m	116.4	CH_2	4.97, m 4.95, m
19	24.2	CH_2	1.21, dqd (14.0, 6.8, 2.8)	138.8	CH	5.43, dt (18.7, 9.1)	138.6	CH	5.49, dt (17.3, 9.5)
17-OCH_3	61.3	CH_3	3.79, s	61.7	CH_3	3.79, s	61.5	CH_3	3.71, s
22-OCH_3	51.7	CH_3	3.65, s	51.3	CH_3	3.68, s	51.2	CH_3	3.59, s
NH			8.44, s			7.45,s			7.60, s

[a]See Table S7 for a full comparison of the ^{1}H and ^{13}C NMR data for **12−14** (Supporting Information).

https://dx.doi.org/10.1021/acs.jnatprod.0c00257
J. Nat. Prod. 2020, 83, 2165−2177

δ_H 116.4/4.95−5.01 and δ_C/δ_H 138.6−138.8/5.43−5.49, respectively, for **13** and **14**). As with the indole alkaloids, ECD spectra were instrumental in assigning the configuration of these compounds, especially for analyzing the C-7 spiro center. According to the literature, the negative Cotton effect at 290 nm confirmed the (7*R*) configuration in compounds **12** and **13**, and the positive Cotton effect agreed with the (7*S*) configuration in compound **14**. Additionally, the negative Cotton effect around 250 nm confirmed the H-3β orientation in compounds **12** and **14**, whereas the opposite Cotton effect demonstrated the H-3α orientation in **13**. These results agreed with the rules for ECD spectra for the 9-hydroxylated oxindole alkaloids, and a calculated ECD spectrum was generated for **12** as a confirmatory measure (see Figure S54).[56,64]

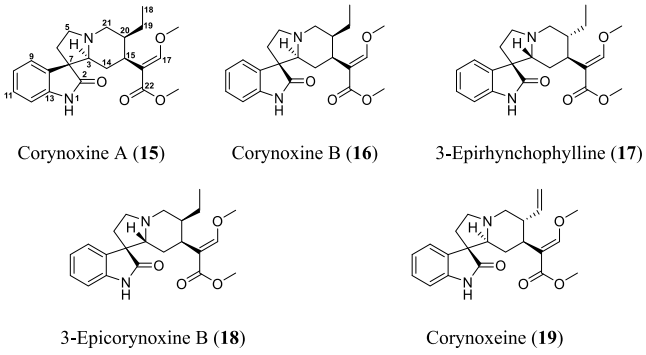

Corynoxine A (**15**) Corynoxine B (**16**) 3-Epirhynchophylline (**17**)

3-Epicorynoxine B (**18**) Corynoxeine (**19**)

Oxindole Alkaloids: 9-Unsubstituted Oxindoles Such as Corynoxine A (15−19). Two closely related isomers, **15** and **16**, were isolated with a molecular formula of $C_{22}H_{28}N_2O_4$, based on HRESIMS protonated molecules with *m*/*z* values of 385.2119 (i.e., **15**) and 385.2127 (i.e., **16**) (Figures S55 and S56). The compounds were characterized using ^{1}H and ^{13}C NMR data as corynoxine A (**15**) and corynoxine B (**16**), based on concordance with published data for synthetic standards of these compounds (Tables 5 and S8 and Figures S60 and S61).[65] In addition, the NMR data for **15** and **16** resembled those described for **12**, with the main difference being replacement of the C-9 phenolic group with an aromatic proton, which resulted in a pattern of two doublets and two triplets of doublets for the protons in the oxindole ring (H-9 to H-12, see Table 5). Both **15** and **16** had the allo configuration (i.e., 3α, 15α, and 20α), with opposite configurations at the spiro C-7, being (7*S*) for **15** and (7*R*) for **16**. As Trager and colleagues reported,[64] the configuration at C-7 can be deduced based on the chemical shift for the H-9 signal. For instance, when presuming the allo configuration, the presence of a deshielded signal for H-9 (δ_H 7.45) confirmed the (7*S*) configuration for **15** and the (7*R*) configuration in **16** due to the more shielded signal for H-9 (δ_H7.19). While **15** was stable, an interesting challenge with compound **16** was its interconversion to **15** over a period of about 8 days in $CDCl_3$ (see Figure S62). As reported previously,[66] the epimerization process increases under acidic conditions via an intermolecular Mannich reaction, resulting in a ratio of ∼70:30 of **15** and **16**, respectively (see Figure S62). As such, only the ECD spectrum of **15** is reported, supporting the (7*S*) and the allo configurations based on negative Cotton effects around 290 and 250 nm (Figure S76).

Compounds **17** and **18** were isolated as optically active powders ($[\alpha]_D^{23}$ −30 (*c* 0.1, $CHCl_3$) and $[\alpha]_D^{24}$ −46 (*c* 0.1, $CHCl_3$), respectively). Their molecular formulas were established as $C_{22}H_{28}N_2O_4$ based on the HRESIMS proto-

Table 5. Characteristic ^{1}H and ^{13}C NMR Data for Compounds 15−19 ($CDCl_3$, 500 and 125 MHz, Respectively)[a]

	corynoxine A (**15**)			corynoxine B (**16**)			3-epirhynchophylline (**17**)			3-epicorynoxine B (**18**)			corynoxeine (**19**)		
position	δ_C	type	δ_H (*J* in Hz)	δ_C	type	δ_H (*J* in Hz)	δ_C	type	δ_H (*J* in Hz)	δ_C	type	δ_H (*J* in Hz)	δ_C	type	δ_H (*J* in Hz)
2	182.4	C		182.3	C		181.2	C		182.2	C		181.0	C	
3	73.2	CH	2.41, dd (11.3, 2.7)	76.5	CH	2.24, bd (11.2)	77.4	CH	2.19, dd (11.4, 2.4)	77.0	CH	2.19, d (10.9)	75.2	CH	2.30, dd (11.3, 2.5)
9	125.0	CH	7.45, d (7.4)	123.2	CH	7.19, d (7.4)	123.3	CH	7.20, d (7.5)	123.4	CH	7.20, d (7.8)	123.5	CH	7.22, d (7.8)
10	122.5	CH	7.05, td (7.6, 1.0)	122.5	CH	7.01, td (7.5, 1.0)	122.5	CH	7.02, td (7.6, 1.0)	122.9	CH	7.02, td (7.5)	122.7	CH	7.05, td (7.6, 1.0)
11	127.4	CH	7.17, td (7.7, 1.3)	127.9	CH	7.16, td (7.7, 1.0)	127.8	CH	7.16, td (7.7, 1.2)	128.1	CH	7.17, t (7.7)	128.0	CH	7.18, td (7.7, 1.2)
12	109.5	CH	6.86, d (7.7)	109.5	CH	6.87, d (7.7)	109.1	CH	6.81, d (7.7)	109.6	CH	6.80, d (7.7)	109.2	CH	6.82, d (7.7)
18	13.0	CH_3	0.87, t (7.4)	13.4	CH_3	0.86, t (7.4)	13.5	CH_3	0.86, t (7.4)	13.3	CH_3	0.86, t (7.3)	115.6	CH_2	4.95, ddd (17.2, 2.01, 0.8) 4.90, dd (10.2, 2.1)
19	19.4	CH_2	1.10, dqd (15.7, 7.8, 2.9) 1.65, dq (14.3, 7.2)	19.3	CH_2	1.77, ddq (14.2, 11.1, 7.1) 1.18, m	19.3	CH_2	1.78, ddq (13.6, 11.2, 7.2) 1.18, dq (14.7, 7.7)	19.8	CH_2	1.80, m 1.17, dq (14.5, 7.3)	139.6	CH	5.51, dt (18.0, 9.1)
17-OCH_3	61.2	CH_3	3.51, s	61.6	CH_3	3.57, s	61.7	CH_3	3.67, s	61.7	CH_3	3.69, s	61.7	CH_3	3.74, s
22-OCH_3	51.3	CH_3	3.59, s	51.4	CH_3	3.61, s	51.4	CH_3	3.63, s	51.4	CH_3	3.63, s	51.4	CH_3	3.62, s
NH			8.40, s			8.91, s			7.62, s			7.33, s			7.53, s

[a]See Table S8 for a full comparison of the ^{1}H and ^{13}C NMR data for **15−19** (Supporting Information).

https://dx.doi.org/10.1021/acs.jnatprod.0c00257
J. Nat. Prod. 2020, 83, 2165−2177

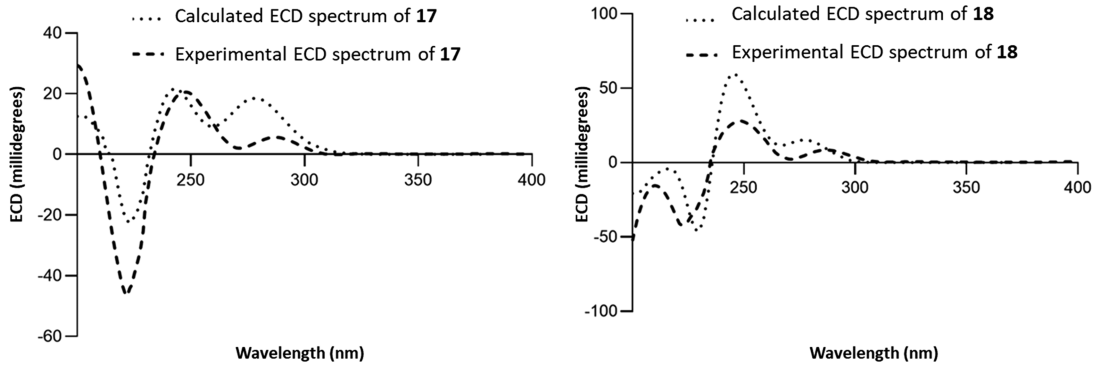

Figure 4. (A) Experimental ECD spectra of **17** in CH_3OH at 0.2 mg/mL (dashed lines) and calculated ECD spectrum of (3*R*,7*R*,15*S*,20*R*)-**17** (dotted lines). (B) Experimental ECD spectra of **18** in CH_3OH at 0.2 mg/mL (dashed lines) and calculated ECD spectrum of (3*R*,7*R*,15*S*,20*S*)-**18** (dotted lines).

nated molecule with *m*/*z* values of 385.2119 (i.e., **17**) and 385.2120 (i.e., **18**) (Figures S57 and S58). The ^1H and ^{13}C NMR spectra of these compounds were similar to those of **15** and **16** (Table 5). These data, along with their different retention times (**17**: 2.76 min and **18**: 2.87 min) (see Figures S57 and S58), suggested that **17** and **18** were new isomers of **15** and **16**. The HSQC data, along with COSY and HMBC correlations, were used to confirm the proposed structures. In both cases, three isolated spin systems (specifically H-9/H-10/H-11/H-12, H_2-5/H_2-6, and H-3/H_2-14/H-15/H-20/H_2-21/H_2-19/H_3-18) and key HMBC correlations (i.e., H-3 to C-2/C-7, H-17 to C-15/C-22, H_3-18 to C-20, CH_3O-17 to C-17, and CH_3O-22 to C-22) were used to confirm the 2D structures of **17** and **18** (see Figures 2 and S63−S66 and S69−S72). Similar to the discussion for **6** and **7**, the correlations observed in the NOESY spectra for **17** and **18** were not useful to determine the relative configuration for these compounds (Figures S67 and S73). The absolute configuration of these molecules was proposed based on ECD experiments, following the rules described for the 9-unsubstituted oxindole alkaloids. In particular, the related isomer rhyncophylline served as a reference, since the crystal structure for this compound has been published and the ECD data were well described.[64,67] For instance, both **17** and **18** had the (7*R*) configuration, based on positive Cotton effects around 290 nm, and the H-3β orientation, as noted by positive Cotton effects around 250 nm (Figure S76). Using biogenetic reasoning for the H-15α orientation, along with the evidence observed in the ECD data, we deduced that compounds **17** and **18** should have the pseudo (i.e., 3β, 15α, and 20β) or epiallo (i.e., 3β, 15α, and 20α) configurations. To evaluate that presumption, the ECD spectra for the diastereoisomers at C-20 were calculated using a TDDFT method at the B3LYP/6-31G+(d) level of theory. The results showed that the calculated ECD spectrum for H-20β matched with the ECD spectrum for **17**, and similarly, the calculated ECD spectrum for an analogue with the H-20α orientation matched with the ECD spectrum for compound **18** (Figure 4). NMR data, biogenetic considerations, and the examination of ECD spectra were used to establish the absolute configuration of the new oxindole alkaloids (3*R*,7*R*,15*S*,20*R*)-3-epirhynchophylline (**17**) and (3*R*,7*R*,15*S*,20*S*)-3-epicorynoxine B (**18**).

Compound **19** was isolated as a white powder, and its molecular formula was established as $C_{22}H_{26}N_2O_4$, based on the HRESIMS protonated molecule with an *m*/*z* of 383.1964 (Figure S59). The NMR data for this compound showed strong similarities to the data of **15**−**18**, where the main differences were the absence of the signals for the C-20 ethyl group, which was replaced by a vinylic group (Tables 5 and S8). The NMR data (Figure S75 and Table S8) matched with those reported for corynoxeine.[68] ECD data corroborated the H-3α orientation based on the negative Cotton effect around 250 nm, and the (7*R*) configuration based on the positive Cotton effect around 290 (Figure S76).

To add complementary data to the structural characterization of the kratom alkaloids, an attempt was made to analyze compounds **1**, **6**, **7**, **15**, **17**, and **18** by VCD, so as to examine a range of both indole and oxindole alkaloids. However, in all cases the similarities between calculated and experimental data were low, ranging between 57.7% and 70.0% (Table S9). In contrast, prominent recent VCD results published in this *Journal* report similarities ranging from 74.1% to 98.5%.[69−73] In particular, we were surprised at the lack of concordance with the data for mitragynine (**1**), since it has been so well characterized, including by X-ray crystallography.[27] Thus, the purity of **1**, **6**, **7**, **15**, **17**, and **18**, was examined after the completion of the VCD studies, and indeed, it was obvious that the compounds decomposed during the experiments (see Figure S77). On the basis of the ^1H NMR spectra (data not shown), we hypothesize that epimers were formed, likely as a result of the VCD data being recorded at elevated temperatures in $CHCl_3$ for up to 18 h; the epimerization potential of these compounds has been reported.[66] While disappointing, we determined that analysis of VCD spectra is not helpful for this class of compounds, at least with current technologies, due to their lack of stability under the analytical conditions.

In summary, 19 reference standards were isolated from kratom plant materials, including the two new indole alkaloids **7** and **11** and the two new oxindole alkaloids **17** and **18**. To characterize their structures, including absolute configuration, a combination of mass spectrometry and NMR and ECD spectroscopy was utilized. An added benefit of analyzing the NMR spectroscopy data for a suite of closely related compounds was that it facilitated the development of a decision tree (Figure 1). Using only a few key NMR signals, even a relative novice should be able to narrow the possible structures for at least these kratom alkaloids, and an expert is encouraged to examine a full suite of NMR data in relation to those reported in the Supporting Information. It is our hope that improvements in the structural characterization of the kratom alkaloids will result in more clarity in the biomedical literature on this interesting class of compounds.

https://dx.doi.org/10.1021/acs.jnatprod.0c00257
J. Nat. Prod. 2020, 83, 2165−2177

EXPERIMENTAL SECTION

General Experimental Procedures. Optical rotations were obtained in $CHCl_3$ using a Rudolph Research Autopol III polarimeter. UV and ECD spectra were acquired on a Varian Cary 100 Bio UV−vis spectrophotometer and an Olis DSM 17 CD spectrophotometer, respectively. A Chiral*IR-2X* dual-source, dual-polarization-modulated FT-VCD spectrometer was used to carry out IR and VCD measurements. NMR experiments were conducted using either a JEOL ECA-500 NMR spectrometer operating at 500 MHz for ^{1}H and 125 MHz for ^{13}C or a JEOL ECS-400 NMR spectrometer equipped with a high-sensitivity JEOL Royal probe operating at 400 MHz for ^{1}H and 100 MHz for ^{13}C; the residual solvent signals were utilized for referencing. HRESIMS was performed on a Thermo LTQ Orbitrap XL mass spectrometer equipped with an electrospray ionization source. UPLC was carried out on a Waters Acquity system with data collected and analyzed using Thermo Xcalibur software. HPLC was carried out using a Varian ProStar HPLC system equipped with ProStar 210 pumps and a ProStar 335 photodiode array detector (PDA), with data collected and analyzed using Galaxie Chromatography Workstation software (version 1.9.3.2). For preparative HPLC, a series of Phenomenex columns were used, including a Kinetex C_{18} (5 μm; 250 × 21.2 mm), a Luna CN (5 μm; 250 × 21.2 mm), and a Luna PFP (5 μm; 250 × 21.2 mm) all at a 20 mL/min flow rate. For UPLC, a Waters BEH C_{18} column (1.7 μm; 50 × 2.1 mm) was used with a 0.6 mL/min flow rate. Flash chromatography was performed on a Teledyne ISCO Combi*Flash* Rf 200 using various sizes of Silica Gold columns and monitored by UV and evaporative light-scattering detectors.

Plant Material, DNA Extraction, PCR, and Sequencing for Molecular Identification. The commercial kratom products used to prepare extracts [i.e., Green Maeng Da (K49, batch: M-1005, 4 kg) and White Jongkong (K52, batch: BN-1006, 1 kg)] were identified by DNA barcoding. The manufacturers reported these as both from Southeast Asia, with K49 being chipped leaf materials and K52 being a fine powder. Samples were handled using methods described previously for the DNA barcoding of commercial mushroom products.[74] Briefly, one scintillation vial was made from each product (see Figure S6), where the vial was filled with plant material from the top and middle layers of the commercial product, and these were labeled with product name, lot number, and batch number and stored at ambient temperature in a bench drawer. For DNA extractions, approximately 5 mg of plant powder was taken from the scintillation vial and transferred to a bashing bead tube with DNA lysis buffer provided by Zymo Research Quick-DNA plant/seed miniprep DNA extraction kit. DNA was extracted using procedures outlined in the Zymo Research plant DNA extraction kit. The plastid gene *matK* was PCR amplified with primer combination matK-xf and matK-MALP;[75,76] for *psbA-trnH* primer combination *psbA-trnH*[77] and for nuclear ITS, primer combinations ITS-u1 and ITS-u4[78] were used for PCR and sequencing. All PCRs were amplified on an Applied Biosystems Veriti thermal cycler using PuReTaq Ready-To-Go PCR beads (GE Healthcare) with the above primers. The PCR reaction was carried out in 25 μL containing 5 μL of template DNA, 2.5 μL of BSA, 2.5 μL of 50% DMSO, and 1 μL of each forward and reverse primer at a concentration of 10 μM. The rest of the volume was made up to 25 μL by adding molecular biology grade water from Fisher Scientific. PCR thermocycler parameters for all fragments are outlined (Table S3). The PCR products were then run on an ethidium bromide-stained 1% agarose gel (Fisher Scientific) along with a 1 kb DNA ladder (Promega) to estimate the size of the amplified band. PCR products were purified using a Wizard SV gel and PCR clean-up system. Sanger sequencing of the purified PCR products was performed at Eurofins Genomics (http://www.operon.com/default.aspx) using BigDye Terminator v3.1 cycle sequencing. The sequencing was accomplished bidirectionally using both strands with the same primers used for the PCR amplification. Sequences were generated on an Applied Biosystems 3730XL high-throughput capillary sequencer. For both sequencing reactions, approximately 15 μL of PCR template was used along with 2 μM sequencing primers. Sequences were assembled with Sequencher 5.3 (Gene Codes), optimized, and then corrected manually when necessary; the latter step was to ensure that the computer algorithm was assigning proper base calls. Each sequence fragment was subjected to an individual NCBI GenBank, Basic Local Alignment Search Tool (BLAST) search as well as the BOLDSYSTEMS database to verify identity.

BLAST Search and DNA Barcoding. For identification of kratom plant material via DNA barcoding, one plastid region (*matK*) was utilized for plant identification by BLAST searching against the BOLDSYSTEMS database version 4. In addition, the sequences of *matK* were compared against an authentic partial sequence of *matK* from the *Mitragyna speciosa* genome assembly (Center for Food Safety and Applied Nutrition (CFSAN), part of the USDA). Uncorrected p-distances were calculated in Geneious, a bioinformatics desktop software package (http://www.biomatters.com), for sequences obtained from the *psbA-trnH* plastid region, which is considered as one of the most variable regions of angiosperm plants, as well as for the nuclear ITS region for the published sequence data from GenBank for *Mitragyna* spp.[79−81] including *M. speciosa* and the newly obtained sequences in this study. The p-distances were obtained by dividing the number of nucleotide differences by the total number of nucleotides being compared. An arbitrary cut-off proxy of ≥98−100% was applied as a criterion to designate similar species; therefore, to be considered the same species based on *psbA-trnH* and ITS sequence comparison, the taxa being compared would have ≥98% sequence similarity.

Molecular Phylogenetic Analysis. Maximum likelihood analysis was performed separately for both the nuclear ITS and the plastid *matK* region to place the kratom samples into a phylogenetic framework with published sequences of *M. speciosa*. Methods for maximum likelihood analysis have been outlined previously.[82] *Nauclea officinalis* (Rubiaceae) was used as an outgroup taxon in both nuclear ITS and *matK* analyses.

Extraction and Isolation of Kratom Alkaloids from Green Maeng Da. The kratom plant material (Green Maeng Da, 4 kg; Figure S8) was extracted with 10 L of $CHCl_3$−CH_3OH (1:1) and 500 mL of 10% aqueous KOH by maceration over 24 h at room temperature. The mixture was filtered, and the solvent was evaporated under reduced pressure. The dried extract was reconstituted in a solution of 1 M HCl and hexanes (1:1), transferred into a separatory funnel, and shaken vigorously. The hexanes phase was drawn off, the pH of the aqueous phase was adjusted to 9.0 with dropwise addition of concentrated NH_4OH, and the alkaloids were extracted as the free base with $CHCl_3$; after washing with neutral water, the organic phase was dried to yield 12 g of the alkaloid extract. This material was fractionated by normal-phase flash chromatography using a silica column (120 g) and a gradient solvent system of hexanes−$CHCl_3$−CH_3OH at a flow rate of 85 mL/min over 67 min to yield 11 pooled fractions.

Fraction 4 (500 mg) was subjected to reverse-phase HPLC using a CN column and a gradient system of 40:60 to 100:0 of CH_3OH−H_2O (10 mM NH_4OAc in both phases) over 20 min with a flow rate of 20 mL/min. This process yielded eight subfractions, and fraction 8 was identified as compound **1** (450.5 mg).

Fraction 9 (1.1 g) was fractionated by normal-phase flash chromatography using a silica column (12 g) and a gradient system of hexanes−EtOAc−CH_3OH using a flow rate of 30 mL/min to generate four subfractions. Subfraction 2 (40 mg) was purified by preparative HPLC over a CN column using a gradient of 70:30 to 100:0 of CH_3OH−H_2O (10 mM NH_4OAc in both phases) over 20 min with a flow rate of 20 mL/min. This process yielded compounds **4** (13.1 mg) and **6** (15.2 mg). Subfraction 4 (800 mg) was subjected to flash chromatography using a silica column (12 g) via a gradient of $CHCl_3$−CH_3OH (10 mM NH_4OAc in both phases) over 60 min with a flow rate of 30 mL/min to generate five fractions (F9-4_1 through F9-4_5). Fraction F9-4_3 was subjected to preparative HPLC over a Kinetex column using a gradient of 60:40 to 70:30 of CH_3OH−H_2O (10 mM NH_4OAc in both phases) over 30 min with a flow rate of 20 mL/min; three fractions were collected, and the first fraction was characterized as compound **2** (20.5 mg). Fraction F9-4_4 (300 mg) was subjected to flash chromatography using a silica column (4 g) and

https://dx.doi.org/10.1021/acs.jnatprod.0c00257
J. Nat. Prod. 2020, 83, 2165−2177

a gradient of hexanes−acetone−CH_3OH over 20 min at a flow rate of 18 mL/min to generate eight fractions. The second fraction was resolved by preparative HPLC over a CN column using a gradient of 50:50 to 100:0 of CH_3OH−H_2O (10 mM NH_4OAc in both phases) over 20 min with a flow rate of 20 mL/min; this process yielded 16.5 mg of compound **7**. The seventh fraction (16 mg) from F9-4_4 was subjected to preparative HPLC using a CN column and a gradient of 40:60 to 90:10 of CH_3OH−H_2O (10 mM NH_4OAc in both phases) over 20 min with a flow rate of 20 mL/min; two fractions were collected, and the first fraction was characterized as compound **11** (2.3 mg). Fraction F9-4_5 (40 mg) was subjected to preparative HPLC over a Kinetex column with a gradient of 50:50 to 100:0 of CH_3OH−H_2O (10 mM NH_4OAc in both phases) over 35 min with a flow rate of 20 mL/min; the third fraction was identified as **8** (10.5 mg).

Fraction 6 (680 mg) was subjected to a second fractionation using flash chromatography over a silica column (12 g) and a gradient of $CHCl_3$−CH_3OH (10 mM NH_4OAc in both phases) over 60 min with a flow rate of 30 mL/min to generate five subfractions. Subfraction 1 (47 mg) was subjected to preparative HPLC over a CN column and a gradient system of 55:45 to 100:0 CH_3OH−H_2O (10 mM NH_4OAc in both phases) over 25 min; the first and second fractions were identified as **5** (9.8 mg) and **3** (18.3 mg), respectively.

Fraction 8 (1.3 g) was fractionated by flash chromatography using a silica column (12 g) with a gradient of $CHCl_3$−CH_3OH (10 mM NH_4OAc in both phases) over 25 min with a flow rate of 30 mL/min to generate four subfractions. Subfractions 3 (12.8 mg) and 4 (7.0 mg) were purified by preparative HPLC over a CN column and a gradient system of 50:50 to 100:0 CH_3OH−H_2O (10 mM NH_4OAc in both phases) over 15 min at a flow rate of 20 mL/min to yield compounds **9** (5.7 mg) and **10** (4.5 mg), respectively.

Extraction and Isolation of Kratom Alkaloids from White Jongkong. The plant material (White Jongkong, 1 kg; Figure S9) was extracted exhaustively using the same procedure described above, to obtain 1.0 g of the dried extract. Normal-phase flash chromatography was used to separate the extract using a silica column (24 g) and a gradient system of hexanes−$CHCl_3$−CH_3OH over 52 min at a flow rate of 35 mL/min to generate 13 fractions. Fractions 3 (100 mg) and 4 (80 mg) were purified, separately, by preparative HPLC using a PFP column and a gradient of 70:30 to 100:0 CH_3OH−H_2O (10 mM NH_4OAc in both phases) over 20 min at a flow rate of 20 mL/min to yield 38.2 mg of **15** (from fraction 3) and, separately, 52.5 mg of **16** and 3.5 mg of **13** (from fraction 4).

Fraction 5 (81 mg) was subjected to preparative HPLC over a PFP column using a gradient of 70:30 to 100:0 CH_3OH−H_2O (10 mM NH_4OAc in both phases) over 20 min at a flow rate of 20 mL/min to generate nine subfractions, and subfraction 4 was identified as compound **12** (55.0 mg).

Fractions 6 (156 mg) and 7 (84 mg) were combined based upon their similar HPLC chromatographic profiles. The resulting fraction (240 mg) was resolved by flash chromatography over a silica column (12 g) using a gradient of hexanes−$CHCl_3$−CH_3OH over 25 min at a flow rate of 18 mL/min to generate 11 subfractions. Subfraction 2 (10.0 mg) was subjected to semipreparative HPLC over a PFP column using a gradient of 50:50 to 100:0 CH_3OH−H_2O (10 mM NH_4OAc in both phases) over 20 min at a flow rate of 4.0 mL/min, yielding **17** (2.0 mg). Subfraction 4 (15 mg) was subjected to preparative HPLC over a PFP column using a gradient of 60:40 to 100:0 CH_3OH−H_2O (10 mM NH_4OAc in both phases) over 20 min at a flow rate of 20.0 mL/min, yielding **14** (3.6 mg). Subfraction 5 (13 mg) was subjected to preparative HPLC over a PFP column using a gradient of 50:50 to 100:0 CH_3OH−H_2O (10 mM NH_4OAc in both phases) over 20 min at a flow rate of 20.0 mL/min to generate four subfractions, where subfractions 2 and 3 were identified as **19** (1.7 mg) and **18** (1.1 mg), respectively.

*Epiallo-isopaynantheine (**7**):* yellowish solid powder; $[\alpha]_D^{20}$ +41 (*c* 0.1, $CHCl_3$); UV (CH_3OH) λ_{max} (log ε) 233 (3.7), 339 (2.9) nm; ^1H and ^{13}C NMR see Table 2 and Table S5; HRESIMS *m*/*z* 397.2115 $[M + H]^+$ (calcd for $C_{23}H_{29}N_2O_4$, 397.2127).

*Epiallo-isopaynantheine-N(4)-oxide (**11**):* orange powder; $[\alpha]_D^{23}$ +33 (*c* 0.1, $CHCl_3$); UV (CH_3OH) λ_{max} (log ε) 219 (3.2), 244 (3.9) nm; ^1H and ^{13}C NMR see Table 3 and Table S6; HRESIMS *m*/*z* 413.2077 $[M + H]^+$ (calcd for $C_{23}H_{29}N_2O_5$, 413.2076).

*3-Epirhyncophylline (**17**):* white powder; $[\alpha]_D^{23}$ −30 (*c* 0.1, $CHCl_3$); UV (CH_3OH) λ_{max} (log ε) 219 (3.3), 244 (3.6) nm; ^1H and ^{13}C NMR see Table 5 and Table S8; HRESIMS *m*/*z* 385.2119 $[M + H]^+$ (calcd for $C_{22}H_{29}N_2O_4$, 385.2127).

*3-Epicorynoxine B (**18**):* white powder; $[\alpha]_D^{24}$ −46 (*c* 0.1, $CHCl_3$); UV (CH_3OH) λ_{max} (log ε) 217 (3.4), 246 (3.7) nm; ^1H and ^{13}C NMR see Table 5 and Table S8; HRESIMS *m*/*z* 385.2120 $[M + H]^+$ (calcd for $C_{22}H_{29}N_2O_4$, 385.2127).

Computational Methods. The minimum energy structures were built with Spartan'10 software (Wavefunction Inc., Irvine, CA, USA). The conformational analysis was performed using the Monte Carlo search protocol under the MMFF94 molecular mechanics force field.

For the ECD prediction, the resulting conformers were minimized using the DFT method at the B3LYP/6-311G+(2d,p) level of theory. Then, the TDDFT method at the B3LYP/6-31G+(d) level of theory was employed for ECD calculations. The calculated excitation energy (nm) and rotatory strength in dipole velocity and dipole length forms were simulated into an ECD curve. All calculations were performed employing the Gaussian'09 program package (Gaussian Inc., Wallingford, CT, USA).

■ ASSOCIATED CONTENT

Supporting Information

The Supporting Information is available free of charge at https://pubs.acs.org/doi/10.1021/acs.jnatprod.0c00257.

^1H NMR, ^{13}C NMR, and HRESIMS data for compounds **1**−**19**; 2D NMR data (COSY, HSQC, and HMBC) for new compounds **7**, **11**, **17**, and **18**; ECD data for compounds **1**−**14** and **16**−**19** (PDF)

■ AUTHOR INFORMATION

Corresponding Author

Nicholas H. Oberlies − *Department of Chemistry and Biochemistry, University of North Carolina at Greensboro, Greensboro, North Carolina 27402, United States;* orcid.org/0000-0002-0354-8464; Email: Nicholas_Oberlies@uncg.edu

Authors

Laura Flores-Bocanegra − *Department of Chemistry and Biochemistry, University of North Carolina at Greensboro, Greensboro, North Carolina 27402, United States;* orcid.org/0000-0002-1393-7834

Huzefa A. Raja − *Department of Chemistry and Biochemistry, University of North Carolina at Greensboro, Greensboro, North Carolina 27402, United States;* orcid.org/0000-0002-0824-9463

Tyler N. Graf − *Department of Chemistry and Biochemistry, University of North Carolina at Greensboro, Greensboro, North Carolina 27402, United States;* orcid.org/0000-0003-4145-2815

Mario Augustinović − *Department of Chemistry and Biochemistry, University of North Carolina at Greensboro, Greensboro, North Carolina 27402, United States*

E. Diane Wallace − *Department of Chemistry and Biochemistry, University of North Carolina at Greensboro, Greensboro, North Carolina 27402, United States*

Shabnam Hematian − *Department of Chemistry and Biochemistry, University of North Carolina at Greensboro, Greensboro, North Carolina 27402, United States;* orcid.org/0000-0002-0788-7615

https://dx.doi.org/10.1021/acs.jnatprod.0c00257
J. Nat. Prod. 2020, 83, 2165−2177

Joshua J. Kellogg − *Department of Chemistry and Biochemistry, University of North Carolina at Greensboro, Greensboro, North Carolina 27402, United States;* orcid.org/0000-0001-8685-0353

Daniel A. Todd − *Department of Chemistry and Biochemistry, University of North Carolina at Greensboro, Greensboro, North Carolina 27402, United States*

Nadja B. Cech − *Department of Chemistry and Biochemistry, University of North Carolina at Greensboro, Greensboro, North Carolina 27402, United States;* orcid.org/0000-0001-6773-746X

Complete contact information is available at: https://pubs.acs.org/10.1021/acs.jnatprod.0c00257

Notes

The authors declare no competing financial interest.

■ ACKNOWLEDGMENTS

This project was supported by the National Institutes of Health/National Center for Complementary and Integrative Health via the Center of Excellence for Natural Product Drug Interaction Research (NaPDI Center, U54 AT008909), including an Administrative Supplement for Validation Studies of Analytical Methods for Dietary Supplements and Natural Products. We thank our colleagues from UNC Greensboro (S. Knowles, Z. Al Subeh, and K. Cank) for evaluating the NMR decision tree.

■ REFERENCES

(1) Field, E. *J. Chem. Soc., Trans.* **1921**, *119*, 887−891.
(2) Vermaire, D. J.; Skaer, D.; Tippets, W. *A. A. Pract.* **2019**, *12*, 103−105.
(3) Schmuhl, K. K.; Gardner, S. M.; Cottrill, C. B.; Bonny, A. E. *Subst. Abus.* **2019**, 1−4.
(4) Coe, M. A.; Pillitteri, J. L.; Sembower, M. A.; Gerlach, K. K.; Henningfield, J. E. *Drug Alcohol Depend.* **2019**, *202*, 24−32.
(5) Buresh, M. *J. Addict. Med.* **2018**, *12*, 481−483.
(6) Corkery, J. M.; Streete, P.; Claridge, H.; Goodair, C.; Papanti, D.; Orsolini, L.; Schifano, F.; Sikka, K.; Korber, S.; Hendricks, A. *J. Psychopharmacol.* **2019**, *33*, 1102−1123.
(7) Murthy, P.; Clark, D. *Paediatr. Child. Health.* **2019**, *24*, 12−14.
(8) Mackay, L.; Abrahams, R. *Can. Fam. Physician* **2018**, *64*, 121−122.
(9) Cumpston, K. L.; Carter, M.; Wills, B. K. *Am. J. Emerg. Med.* **2018**, *36*, 166−168.
(10) Castillo, A.; Payne, J. D.; Nugent, K. *Proc. (Bayl. Univ. Med. Cent.)* **2017**, *30*, 355−357.
(11) Galbis-Reig, D. *Wmj.* **2016**, *115*, 49−52.
(12) Karinen, R.; Fosen, J. T.; Rogde, S.; Vindenes, V. *Forensic Sci. Int.* **2014**, *245*, No. e29-e32.
(13) Forrester, M. B. *J. Addict. Dis.* **2013**, *32*, 396−400.
(14) Holler, J. M.; Vorce, S. P.; McDonough-Bender, P. C.; Magluilo, J., Jr.; Solomon, C. J.; Levine, B. *J. Anal. Toxicol.* **2011**, *35*, 54−9.
(15) McWhirter, L.; Morris, S. *Eur. Addict. Res.* **2010**, *16*, 229−31.
(16) The New York Times. April 17, 2019. https://www.nytimes.com/2019/04/17/us/kratom-overdose-deaths.html (accessed October 25, 2019).
(17) U.S. Food & Drug Administration. February 21, 2018 https://www.fda.gov/news-events/press-announcements/fda-oversees-destruction-and-recall-kratom-products-and-reiterates-its-concerns-risks-associated (accessed October 25, 2019).
(18) United States Drug Enforcement Administration. August 30, 2016. https://www.dea.gov/press-releases/2016/08/30/dea-announces-intent-schedule-kratom (accessed October 25, 2019).
(19) Forbes. October 13, 2016. https://www.forbes.com/sites/davidkroll/2016/08/30/dea-to-place-kratom-mitragynine-on-schedule-i-premature-move-may-compromise-research-benefits/#679fe47d2b8f (accessed October 25, 2019).
(20) Johnson, E. J.; González-Peréz, V.; Tian, D.-D.; Lin, Y. S.; Unadkat, J. D.; Rettie, A. E.; Shen, D. D.; McCune, J. S.; Paine, M. F. *Drug Metab. Dispos.* **2018**, *46*, 1046−1052.
(21) Tian, D.-D.; Kellogg, J. J.; Okut, N.; Oberlies, N. H.; Cech, N. B.; Shen, D. D.; McCune, J. S.; Paine, M. F. *Drug Metab. Dispos.* **2018**, *46*, 552.
(22) Gufford, B. T.; Chen, G.; Lazarus, P.; Graf, T. N.; Oberlies, N. H.; Paine, M. F. *Drug Metab. Dispos.* **2014**, *42*, 1675−1683.
(23) Kellogg, J. J.; Paine, M. F.; McCune, J. S.; Oberlies, N. H.; Cech, N. B. *Nat. Prod. Rep.* **2019**, *36*, 1196−1221.
(24) Brantley, S. J.; Gufford, B. T.; Dua, R.; Fediuk, D. J.; Graf, T. N.; Scarlett, Y. V.; Frederick, K. S.; Fisher, M. B.; Oberlies, N. H.; Paine, M. F. *CPT: Pharmacometrics Syst. Pharmacol.* **2014**, *3*, 107.
(25) Beckett, A. H.; Shellard, E. J.; Tackie, A. N. *Planta Med.* **1965**, *13*, 241−246.
(26) Beckett, A.; Shellard, E.; Phillipson, J.; Lee, C. M. *Planta Med.* **1966**, *14*, 277−288.
(27) Zacharias, D.; Rosenstein, R.; Jeffrey, G. *Acta Crystallogr.* **1965**, *18*, 1039−1043.
(28) Beckett, A. H.; Shellard, E. J.; Phillipson, J. D.; Lee, C. M. *Planta Med.* **1966**, *14*, 277−288.
(29) Shellard, E.; Houghton, P.; Resha, M. *Planta Med.* **1978**, *34*, 253−263.
(30) Takayama, H.; Ishikawa, H.; Kurihara, M.; Kitajima, M.; Aimi, N.; Ponglux, D.; Koyama, F.; Matsumoto, K.; Moriyama, T.; Yamamoto, L. T.; Watanabe, K.; Murayama, T.; Horie, S. *J. Med. Chem.* **2002**, *45*, 1949−1956.
(31) Takayama, H. *Chem. Pharm. Bull.* **2004**, *52*, 916−928.
(32) Takayama, H.; Kitajima, M.; Kogure, N. *Curr. Org. Chem.* **2005**, *9*, 1445−1464.
(33) Marston, A.; Hostettmann, K. *Nat. Prod. Rep.* **1991**, *8*, 391−413.
(34) Stead, P. Isolation by Preparative HPLC. In *Natural Products Isolation*; Cannell, R. J. P., Ed.; Humana Press: Totowa, NJ, 1998; pp 165−208.
(35) Betz, J. M.; Brown, P. N.; Roman, M. C. *Fitoterapia* **2011**, *82*, 44−52.
(36) Li, S.; Yuan, W.; Deng, G.; Wang, P.; Yang, P.; Aggarwal, B. *Pharm. Crops* **2011**, *2*, 28−54.
(37) Napolitano, J. G.; Lankin, D. C.; Chen, S. N.; Pauli, G. F. *Magn. Reson. Chem.* **2012**, *50*, 569−575.
(38) Niemitz, M.; Laatikainen, R.; Chen, S. N.; Kleps, R.; Kozikowski, A. P.; Pauli, G. F. *Magn. Reson. Chem.* **2007**, *45*, 878−882.
(39) Seebacher, W.; Simic, N.; Weis, R.; Saf, R.; Kunert, O. *Magn. Reson. Chem.* **2003**, *41*, 636−638.
(40) Sy-Cordero, A. A.; Pearce, C. J.; Oberlies, N. H. *J. Antibiot.* **2012**, *65*, 541−9.
(41) Kao, D.; Flores-Bocanegra, L.; Raja, H. A.; Darveaux, B. A.; Pearce, C. J.; Oberlies, N. H. *Phytochemistry* **2020**, *172*, 112238.
(42) https://www.fda.gov/news-events/public-health-focus/fda-and-kratom (accessed January 20, 2020).
(43) Hollingsworth, M. L.; Andra Clark, A.; Forrest, L. L.; Richardson, J.; Pennington, R. T.; Long, D. G.; Cowan, R.; Chase, M. W.; Gaudeul, M.; Hollingsworth, P. M. *Mol. Ecol. Resour.* **2009**, *9*, 439−457.
(44) Kress, W. J.; Wurdack, K. J.; Zimmer, E. A.; Weigt, L. A.; Janzen, D. H. *Proc. Natl. Acad. Sci. U. S. A.* **2005**, *102*, 8369−8374.
(45) Kress, W. J.; Erickson, D. L. *PLoS One* **2007**, *2*, No. e508.
(46) Li, X.; Yang, Y.; Henry, R. J.; Rossetto, M.; Wang, Y.; Chen, S. *Biol. Rev.* **2015**, *90*, 157−166.
(47) Ebihara, A.; Nitta, J. H.; Ito, M. *PLoS One* **2010**, *5*, No. e15136.
(48) Brown, P. N.; Lund, J. A.; Murch, S. J. *J. Ethnopharmacol.* **2017**, *202*, 302−325.

(49) Raffa, R. B. *Kratom and Other Mitragynines: The Chemistry and Pharmacology of Opioids from a Non-opium Source*; CRC Press, 2014.
(50) Takayama, H.; Kurihara, M.; Kitajima, M.; Said, I. M.; Aimi, N. *Tetrahedron* **1998**, *54*, 8433−8440.
(51) León, F.; Habib, E.; Adkins, J. E.; Furr, E. B.; McCurdy, C. R.; Cutler, S. J. *Nat. Prod. Commun.* **2009**, *4*, 907−910.
(52) Beckett, A.; Shellard, E.; Phillipson, J.; Lee, C. M. *J. Pharm. Pharmacol.* **1965**, *17*, 753−755.
(53) Shellard, E. J.; Hougton, P. J.; Resha, M. *Planta Med.* **1978**, *33*, 223−227.
(54) Cao, X.-F.; Wang, J.-S.; Wang, X.-B.; Luo, J.; Wang, H.-Y.; Kong, L.-Y. *Phytochemistry* **2013**, *96*, 389−396.
(55) Beckett, A. H.; Lee, C. M.; Tackie, A. N. *Tetrahedron Lett.* **1963**, *4*, 1709−1714.
(56) Hemingway, S. R.; Houghton, P. J.; Phillipson, J. D.; Shellard, E. J. *Phytochemistry* **1975**, *14*, 557−563.
(57) Ali, Z.; Demiray, H.; Khan, I. A. *Tetrahedron Lett.* **2014**, *55*, 369−372.
(58) Cu, N. *Bull. Soc. Chim. Fr.* **1957**, 1292−1294.
(59) Shellard, E. *Planta Med.* **1978**, *34*, 26−36.
(60) Kitajima, M.; Misawa, K.; Kogure, N.; Said, I. M.; Horie, S.; Hatori, Y.; Murayama, T.; Takayama, H. *J. Nat. Med.* **2006**, *60*, 28−35.
(61) Lee, C. M.; Trager, W. F.; Beckett, A. H. *Tetrahedron* **1967**, *23*, 375−385.
(62) 1H NMR Properties of Piperidine Derivatives. In *Studies in Organic Chemistry*; Rubiralta, M.; Giralt, E.; Diez, A., Eds.; Elsevier, 1991; Vol. *43*, pp 34−87.
(63) Alkorta, I.; Elguero, J. *Magn. Reson. Chem.* **2004**, *42*, 955−961.
(64) Trager, W.; Lee, C. M.; Phillipson, J.; Haddock, R.; Dwuma-Badu, D.; Beckett, A. *Tetrahedron* **1968**, *24*, 523−543.
(65) Xu, J.; Shao, L.-D.; Li, D.; Deng, X.; Liu, Y.-C.; Zhao, Q.-S.; Xia, C. *J. Am. Chem. Soc.* **2014**, *136*, 17962−17965.
(66) Berner, M.; Tolvanen, A.; Jokela, R. Acid-catalysed Epimerization of Bioactive Indole Alkaloids and Their Derivatives. In *Studies in Natural Products Chemistry*; Atta ur Raman, Ed.; Elsevier, 2001; Vol. *25*, pp 3−42.
(67) Laus, G.; Wurst, K. *Helv. Chim. Acta* **2003**, *86*, 181−187.
(68) Wanner, M. J.; Ingemann, S.; van Maarseveen, J. H.; Hiemstra, H. *Eur. J. Org. Chem.* **2013**, *2013*, 1100−1106.
(69) Reinhardt, J. K.; Klemd, A. M.; Danton, O.; De Mieri, M.; Smieško, M.; Huber, R.; Bürgi, T.; Gründemann, C.; Hamburger, M. *J. Nat. Prod.* **2019**, *82*, 1424−1433.
(70) Bustos-Brito, C.; Joseph-Nathan, P.; Burgueño-Tapia, E.; Martínez-Otero, D.; Nieto-Camacho, A.; Calzada, F.; Yépez-Mulia, L.; Esquivel, B.; Quijano, L. *J. Nat. Prod.* **2019**, *82*, 1207−1216.
(71) El-Kashef, D. H.; Daletos, G.; Plenker, M.; Hartmann, R.; Mándi, A.; Kurtán, T.; Weber, H.; Lin, W.; Ancheeva, E.; Proksch, P. *J. Nat. Prod.* **2019**, *82*, 2460−2469.
(72) Cao, F.; Meng, Z.-H.; Mu, X.; Yue, Y.-F.; Zhu, H.-J. *J. Nat. Prod.* **2019**, *82*, 386−392.
(73) Arreaga-González, H. M.; Rodríguez-García, G.; del Río, R. E.; Ferreira-Sereno, J. A.; García-Gutiérrez, H. A.; Cerda-García-Rojas, C. M.; Joseph-Nathan, P.; Gómez-Hurtado, M. A. *J. Nat. Prod.* **2019**, *82*, 3394−3400.
(74) Raja, H. A.; Baker, T. R.; Little, J. G.; Oberlies, N. H. *Food Chem.* **2017**, *214*, 383−392.
(75) Dunning, L. T.; Savolainen, V. *Bot. J. Linn. Soc.* **2010**, *164*, 1−9.
(76) Ford, C. S.; Ayres, K. L.; Toomey, N.; Haider, N.; Van Alphen Stahl, J.; Kelly, L. J.; Wikström, N.; Hollingsworth, P. M.; Duff, R. J.; Hoot, S. B. *Bot. J. Linn. Soc.* **2009**, *159*, 1−11.
(77) Pawar, R. S.; Handy, S. M.; Cheng, R.; Shyong, N.; Grundel, E. *Planta Med.* **2017**, *83*, 921−936.
(78) Cheng, T.; Xu, C.; Lei, L.; Li, C.; Zhang, Y.; Zhou, S. *Mol. Ecol. Resour.* **2016**, *16*, 138−149.
(79) Löfstrand, S. D.; Krüger, Å.; Razafimandimbison, S. G.; Bremer, B. *Syst. Bot.* **2014**, *39*, 304−315.
(80) Razafimandimbison, S. G.; Bremer, B. *Am. J. Bot.* **2002**, *89*, 1027−1041.
(81) Tnah, L.; Lee, S.; Tan, A.; Lee, C.; Ng, K.; Ng, C.; Farhanah, Z. N. *Food Control* **2019**, *95*, 318−326.
(82) Raja, H. A.; Miller, A. N.; Pearce, C. J.; Oberlies, N. H. *J. Nat. Prod.* **2017**, *80*, 756−770.

https://dx.doi.org/10.1021/acs.jnatprod.0c00257
J. Nat. Prod. 2020, 83, 2165−2177

Supporting Information

The Chemistry of Kratom [*Mitragyna speciosa*]: Updated Characterization Data and Methods to Elucidate Indole and Oxindole Alkaloids

Laura Flores-Bocanegra, Huzefa A. Raja, Tyler N. Graf, Mario Augustinović, E. Diane Wallace, Shabnam Hematian, Joshua J. Kellogg, Daniel A. Todd, Nadja B. Cech, and Nicholas H. Oberlies*

Index of Figures

Index of Tables

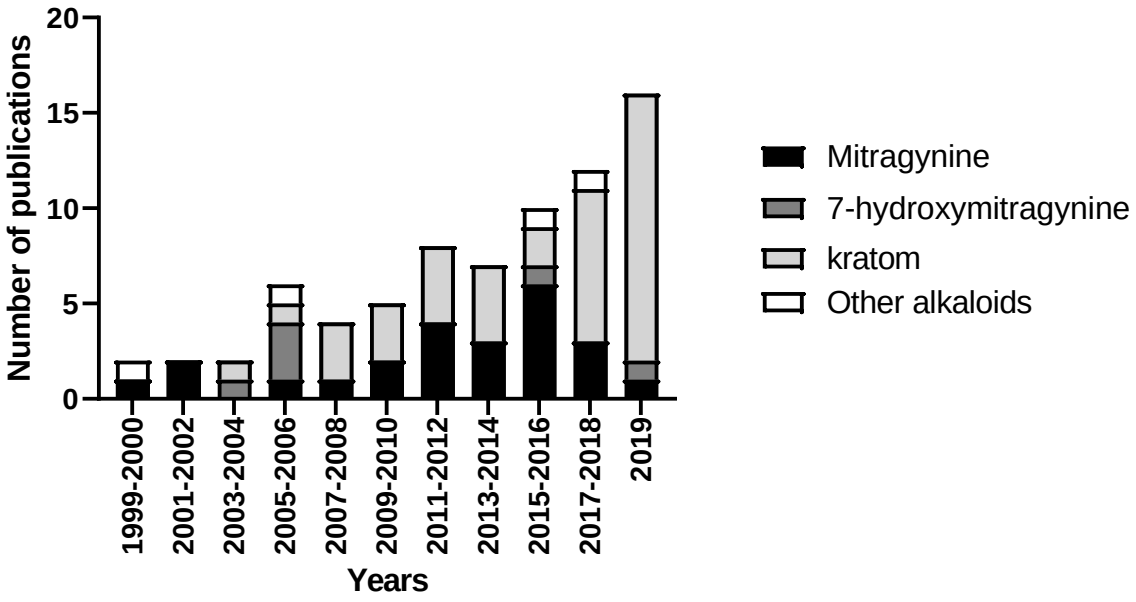

Figure S1. Histogram showing the number of papers about the pharmacological properties for kratom (presumably an extract of *M. speciosa*) and/or the kratom alkaloids mitragynine, 7-hydroxymitragynine and others, published in the past 20 years. This search was performed using "SciFinder" and "PubMed" with the research topic "Kratom" and "*Mitragyna speciosa*". The search was refined by looking only at those papers published that applied *in vitro* and/or *in vivo* pharmacological studies as well as those for case reports.

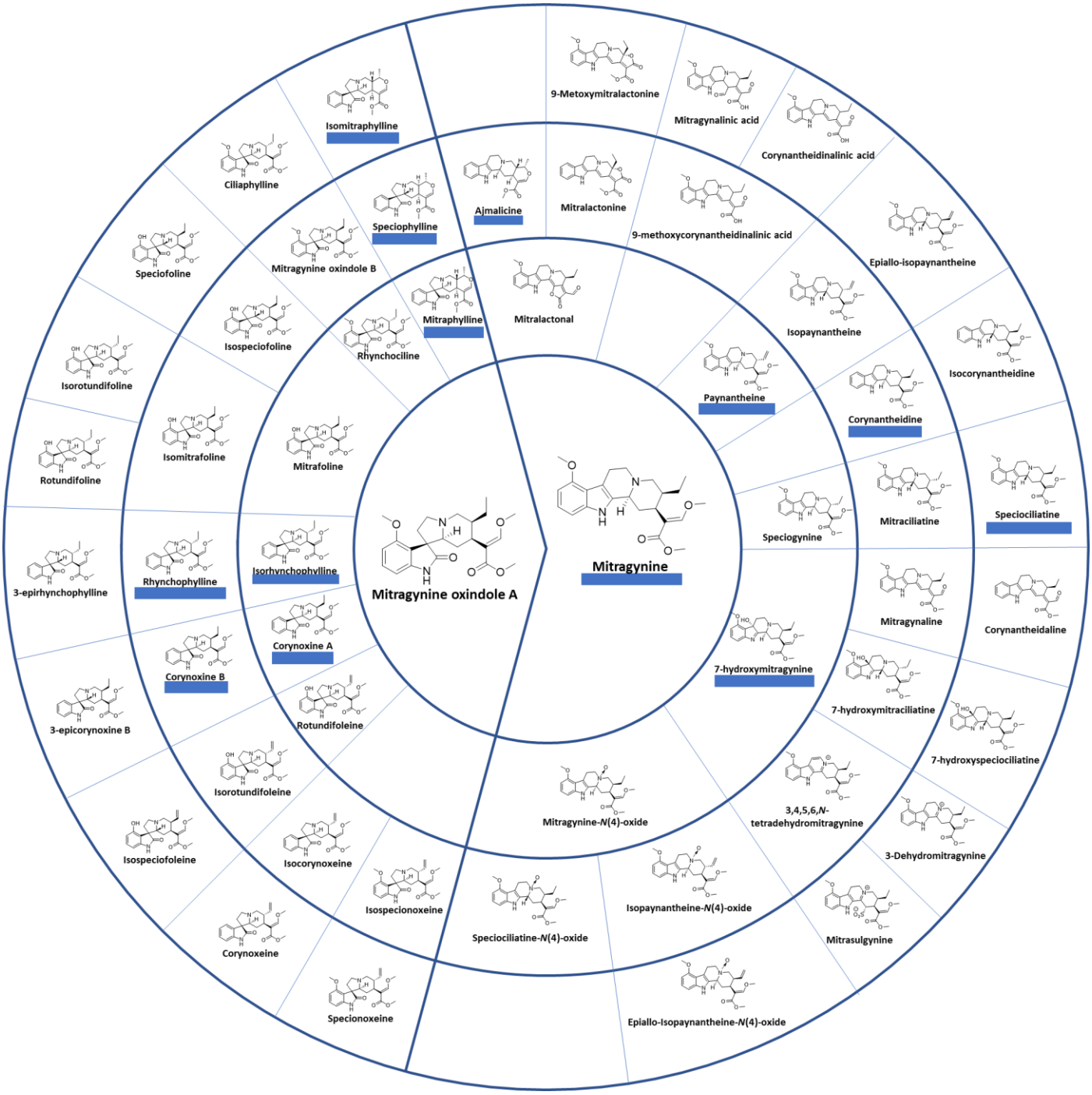

Figure S2. Schematic representation of the 54 compounds that have been reported from *Mitragyna speciosa*, showing the interrelatedness of the structures. Compounds to the right are indole alkaloids, while those to the left are oxindole alkaloids. Compounds underlined in blue are commercially available (as of 2019); however, we strongly recommend verifying both the purity and identity of any purchased standards.

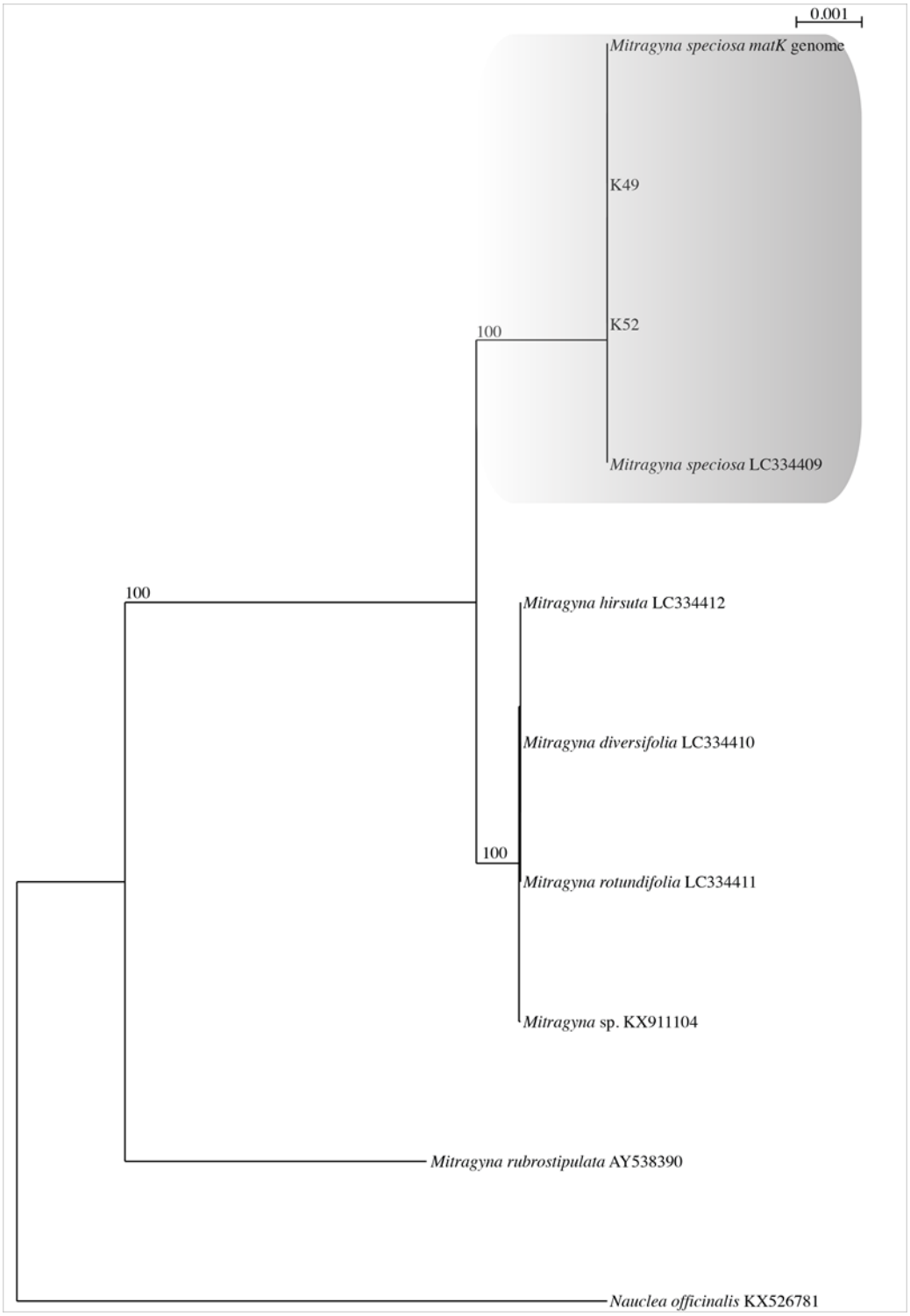

Figure S3. Phylogenetic tree (RAxML; -lnL = 2220.13) inferred from the DNA sequence data from the plastid region (*matK*; 1525 bp). K49 and K52 form a strongly supported clade with published sequence data of *Mitragyna speciosa*, including a partial sequence of *matK* from the *Mitragyna speciosa* genome assembly; BioProject: PRJNA325670 (Center for Food Safety and Applied Nutrition (CFSAN), part of the FDA). Numbers refer to RAxML bootstrap support values ≥ 70% based on 1000 replicates. Clades with samples from the present study are highlighted in gray. Bar indicates nucleotide substitutions per site. The tree was rooted to *Nauclea officinalis*

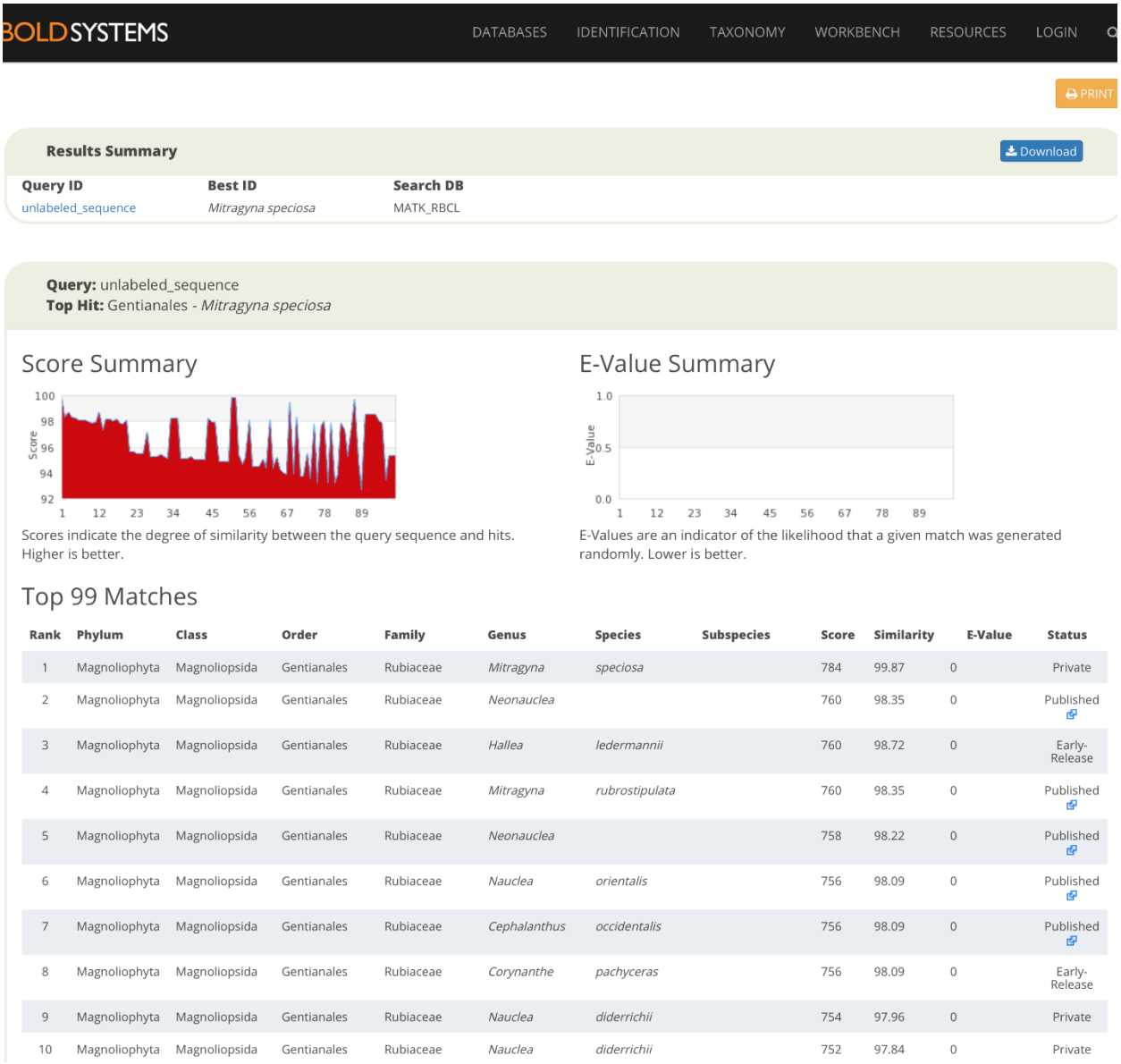

Figure S4. Graphical overview of the BLAST results (January 2020) in BOLD database using *matK* (core locus of The Consortium for the Barcode of Life; CBOL). Sample K49 shows ≥ 99% similarity with *Mitragyna speciosa*. Only the top 10 results are shown.

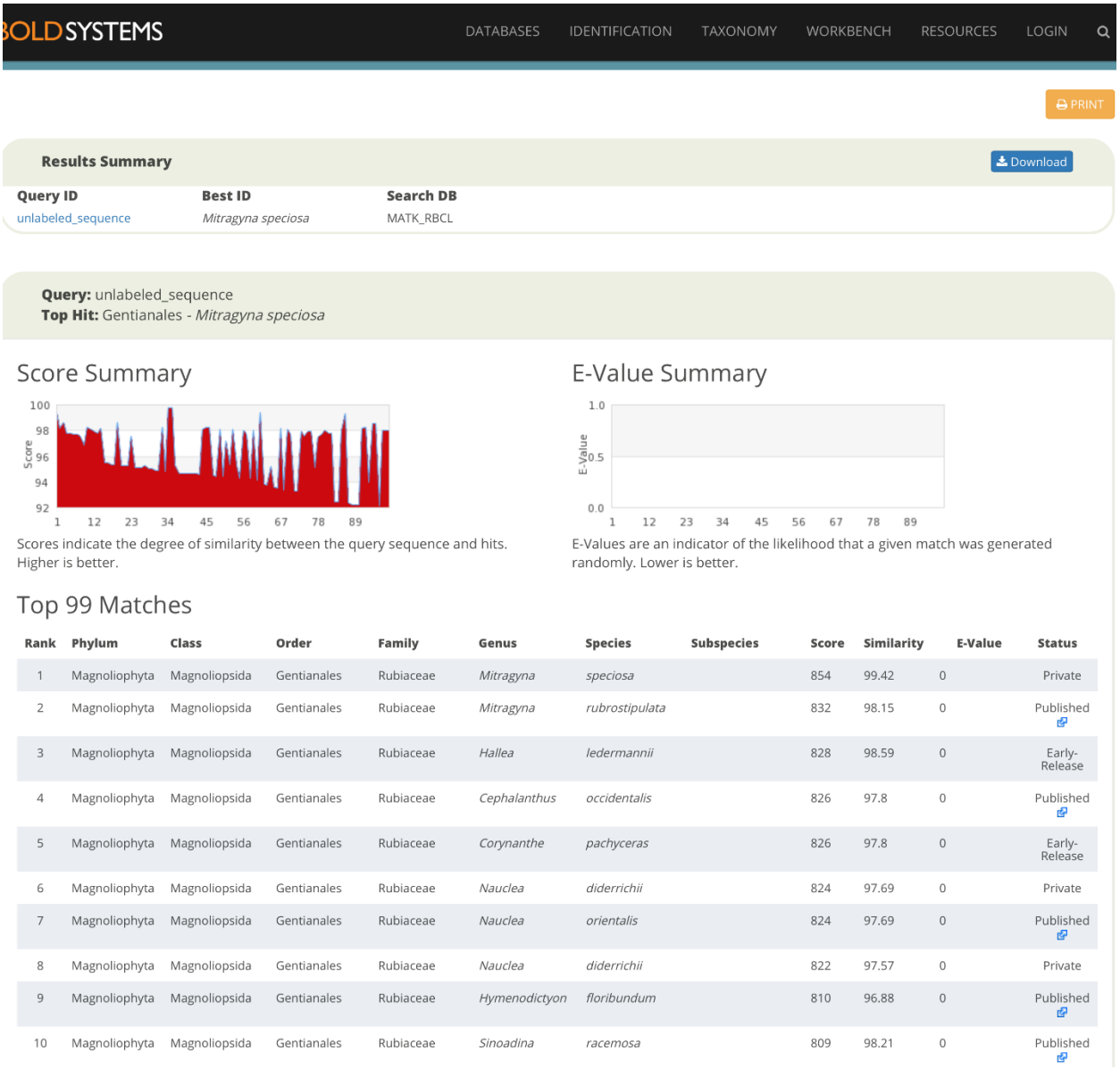

Figure S5. Graphical overview of the BLAST results (January 2020) in BOLD database using *matK* (core locus of The Consortium for the Barcode of Life; CBOL). Sample K52 shows ≥ 99% similarity with *Mitragyna speciosa.* Only the top 10 results are shown.

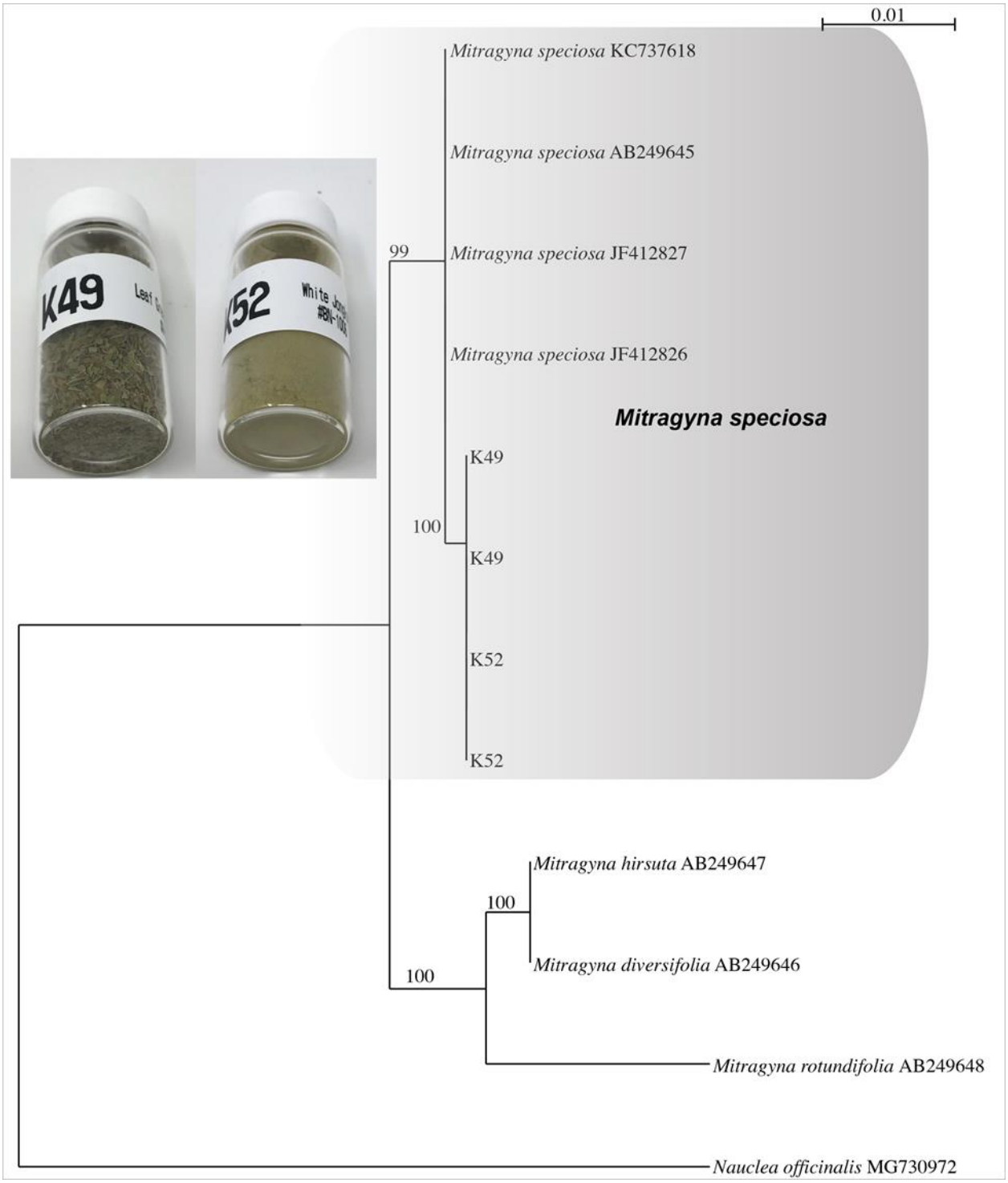

Figure S6. Phylogenetic tree (RAxML; -lnL = 1252.61) inferred from the DNA sequence data from the Internal Transcribed Spacer region (ITS; 662 bp). K49 and K52 form a strongly supported clade with published sequence data of *Mitragyna speciosa* with ≥ 99% bootstrap support. Numbers refer to RAxML bootstrap support values ≥ 70% based on 1000 replicates. Clades with samples from the present study are highlighted in gray. Bar indicates nucleotide substitutions per site. The tree was rooted to *Nauclea officinalis*. Sample vials of K49 and K52 materials are shown on the left.

Table S1. Uncorrected p-Distances from the *trnH-psbA* Region Indicating that Kratom Samples Barcoded in Our Study Have Higher Sequence Similarity with *Mitragyna speciosa*. Regions with N at the beginning and end of the nucleotide alignment were not taken into consideration for uncorrected p-distances. Comparisons were made using the listed species. *Mitragyna speciosa* MH069946; *Mitragyna speciosa* LC334417; *Mitragyna diversifolia* LC334418; *Mitragyna rotundifolia* LC334419; and *Mitragyna hirsuta* LC334420.

	K49	K52	Mitragyna_...	Mitragyna_...	Mitragyna_...	Mitragyna_...	Mitragyna_...
K49		100%	100%	100%	95%	95%	95%
K52	100%		100%	100%	95%	95%	95%
Mitragyna_speciosaM...	100%	100%		100%	95%	95%	95%
Mitragyna_speciosa_L...	100%	100%	100%		95%	95%	95%
Mitragyna_diversifolia_...	95%	95%	95%	95%		100%	100%
Mitragyna_rotundifolia...	95%	95%	95%	95%	100%		100%
Mitragyna_hirsuta_LC3...	95%	95%	95%	95%	100%	100%	

Table S2. Uncorrected p-Distances from the ITS Region Indicating that Kratom Samples Barcoded in Our Study Have Higher Sequence Similarity with *Mitragyna speciosa*. Regions with N at the beginning and end of the nucleotide alignment were not taken into consideration for uncorrected p-distances. Comparisons were made using the listed species. *Mitragyna speciosa* JF412826; *Mitragyna speciosa* JF412827; *Mitragyna speciosa* KC737618; *Mitragyna speciosa* AB249645; *Mitragyna diversifolia* AB249646; *Mitragyna hirsuta* AB249647; *Mitragyna rotundifolia* AB249648; and *Nauclea officinalis* MG730972.

	K49_1_ITS	K49_2_ITS	K52_1_ITS	K52_2_ITS	JF412826...	JF412827...	KC73761...	AB24964...	AB24964...	AB24964...	AB24964...	MG73097...
K49_1_ITS		100%	100%	100%	100%	100%	100%	100%	98%	98%	97%	92%
K49_2_ITS	100%		100%	100%	100%	100%	100%	100%	98%	98%	96%	92%
K52_1_ITS	100%	100%		100%	100%	100%	100%	100%	98%	98%	97%	92%
K52_2_ITS	100%	100%	100%		100%	100%	100%	100%	98%	98%	97%	92%
JF412826_Mitragyna_...	100%	100%	100%	100%		100%	100%	100%	98%	98%	97%	92%
JF412827_Mitragyna_...	100%	100%	100%	100%	100%		100%	100%	98%	98%	97%	92%
KC737618_Mitragyna...	100%	100%	100%	100%	100%	100%		100%	98%	98%	97%	91%
AB249645_Mitragyna...	100%	100%	100%	100%	100%	100%	100%		98%	98%	97%	91%
AB249646_Mitragyna...	98%	98%	98%	98%	98%	98%	98%	98%		100%	98%	89%
AB249647_Mitragyna...	98%	98%	98%	98%	98%	98%	98%	98%	100%		98%	89%
AB249648_Mitragyna...	97%	96%	97%	97%	97%	97%	97%	97%	98%	98%		89%
MG730972_Nauclea_...	92%	92%	92%	92%	92%	92%	91%	91%	89%	89%	89%	

Table S3. Primers and PCR Protocols for Plant Identification.

Locus	Primer	Primer Sequence 5'-3'	Direction	PCR protocol*
The chloroplast maturase K gene (*matK*)	matK-xf matK-MALP	TAATTTACGATCAATTCATTC ACAAGAAAGTCGAAGTAT	Forward Reverse	1. 98˚C – 45 sec 2. 98˚C – 10 sec 3. 54˚C – 30 sec 4. 72˚C – 40 sec 5. Repeat 2–4 for 35 cycles 6. 72˚C – 10 min 7. 4˚C on hold
The chloroplast intergenic region (*trnH-psbA*)	psbA trnH	GTTATGCATGAACGTAATGCTC CGCGCATGGTGGATTCACAATCC	Forward Reverse	1. 94˚C – 5 min 2. 94˚C – 1 min 3. 50˚C – 1 min 4. 72˚C – 2 min 5. Repeat 2–4 for 35 cycles 6. 72˚C – 7 min 7. 4˚C on hold
The internal transcribed spacer (ITS) of nuclear ribosomal DNA	ITS-u1 ITS-u4	GGAAGKARAAGTCGTAACAAGG RGTTTCTTTTCCTCCGCTTA	Forward Reverse	1. 94˚C – 4 min 2. 94˚C – 30 sec 3. 55˚C or 58˚C – 40 sec 4. 72˚C – 1 min 5. Repeat 2–4 for 34 cycles 6. 72˚C – 10 min 7. 4˚C on hold

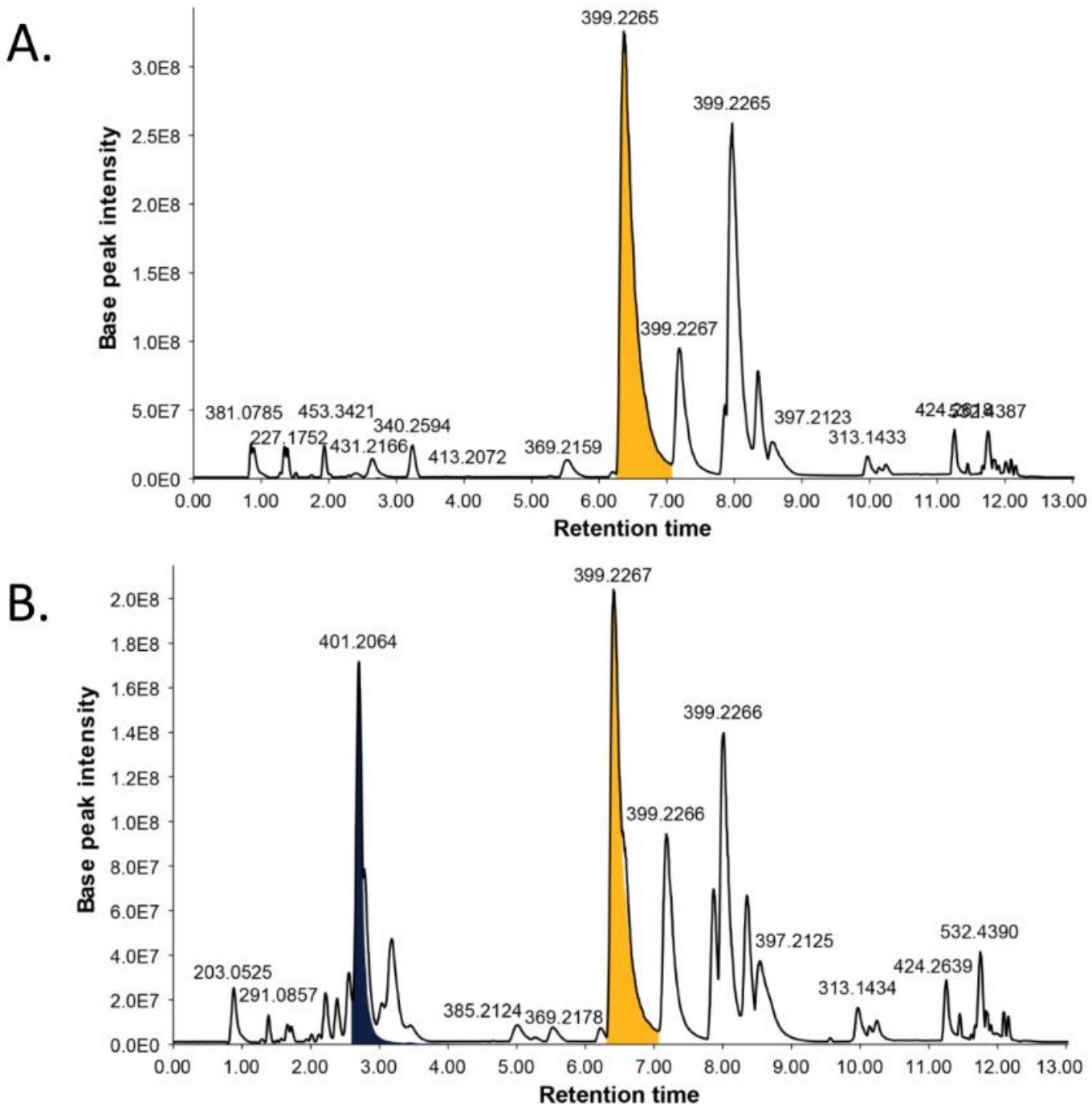

Figure S7. Chromatographic profiles of the two sources of kratom, specifically A) Green Maeng Da (K49) and B) White Jongkong (K52). The major compound present in K49 is mitragynine (**1**, yellow peak). However, in K52 speciofoline (**12**, black peak) has a much higher abundance. The chromatograms were acquired in the reverse phase using a UPLC system coupled with HRESIMS.

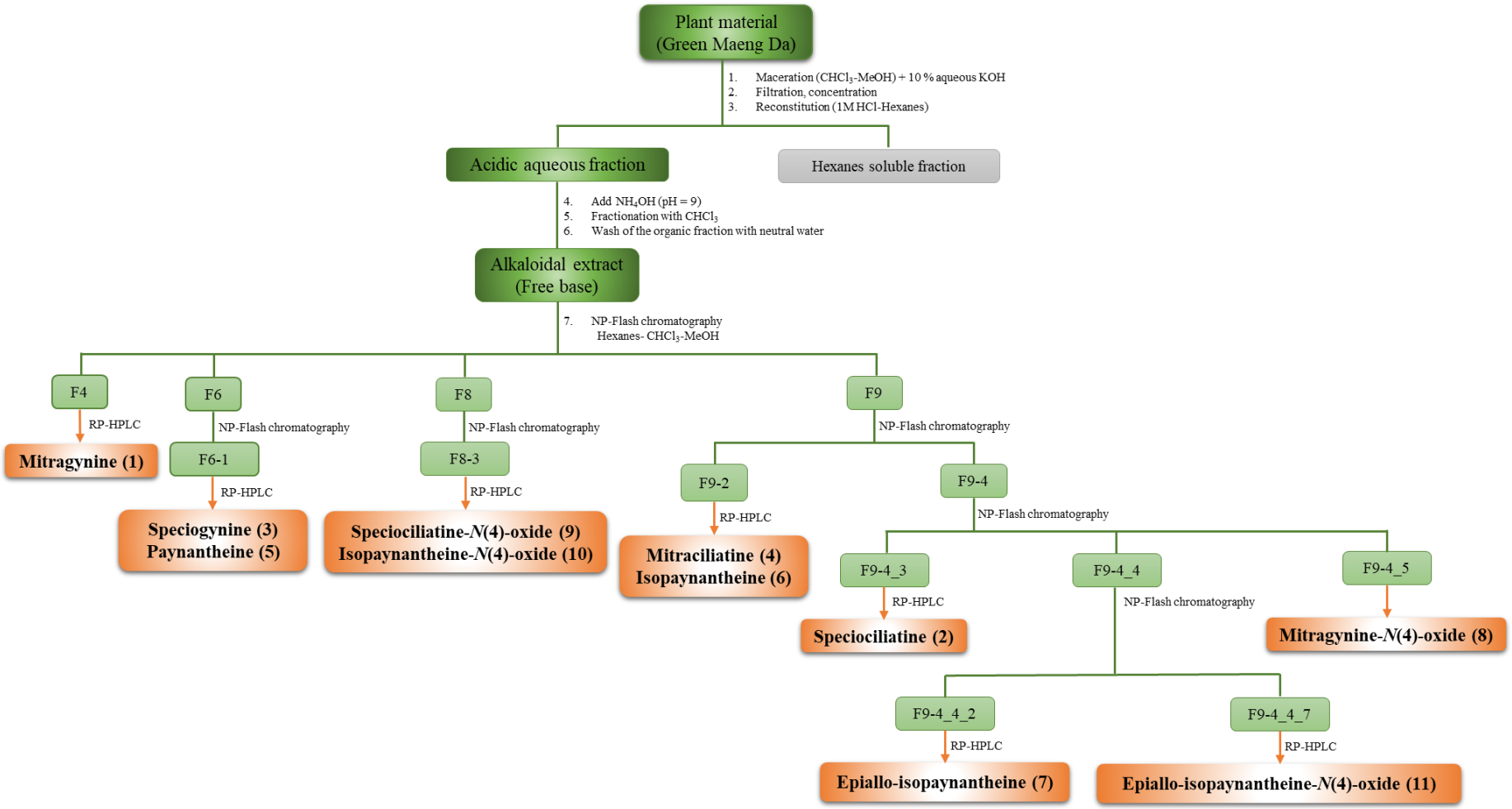

Figure S8. Workflow for the isolation of the alkaloids from the kratom product termed Green Maeng Da (i.e., sample K49).

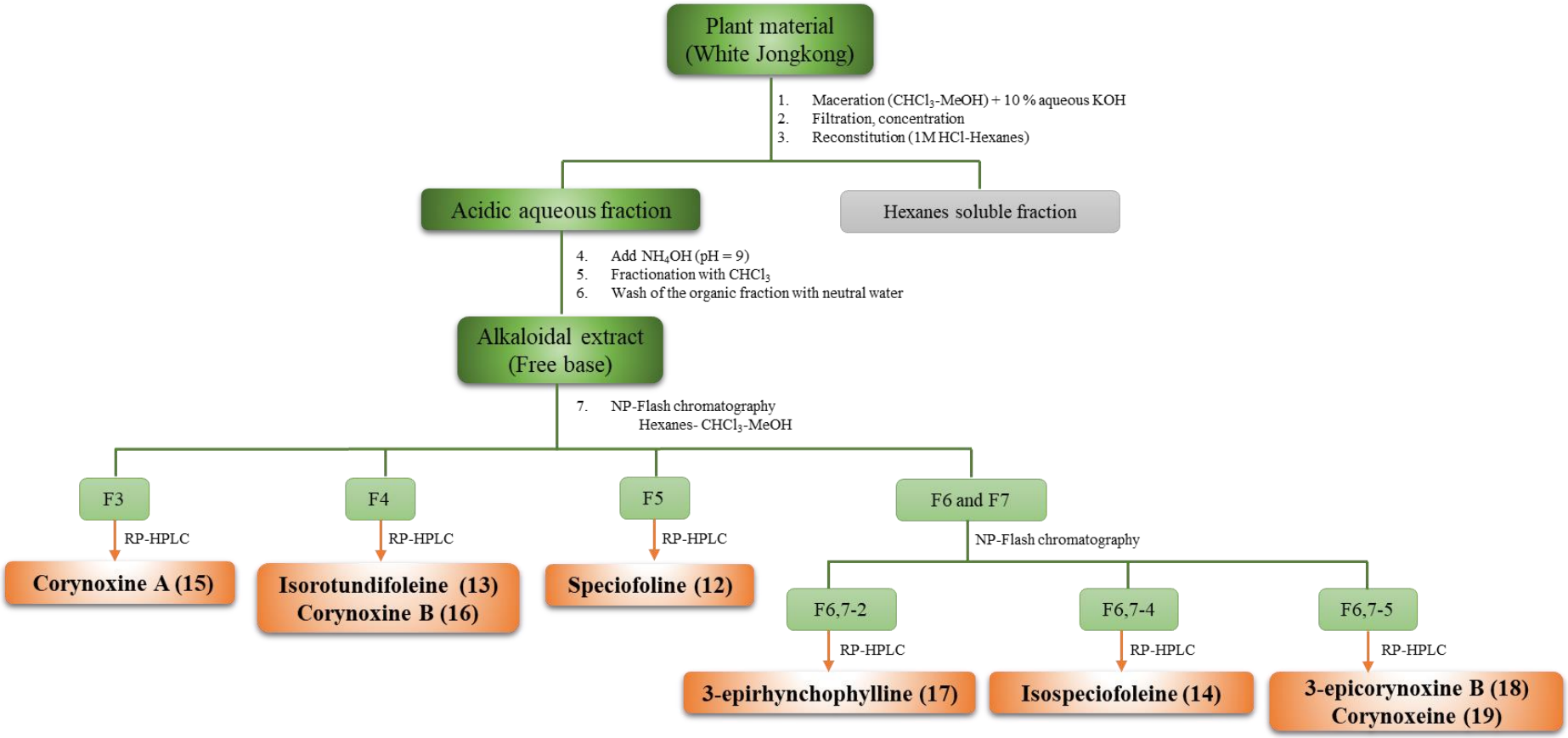

Figure S9. Workflow for the isolation of the alkaloids from the kratom product termed White Jongkong (i.e., sample K52).

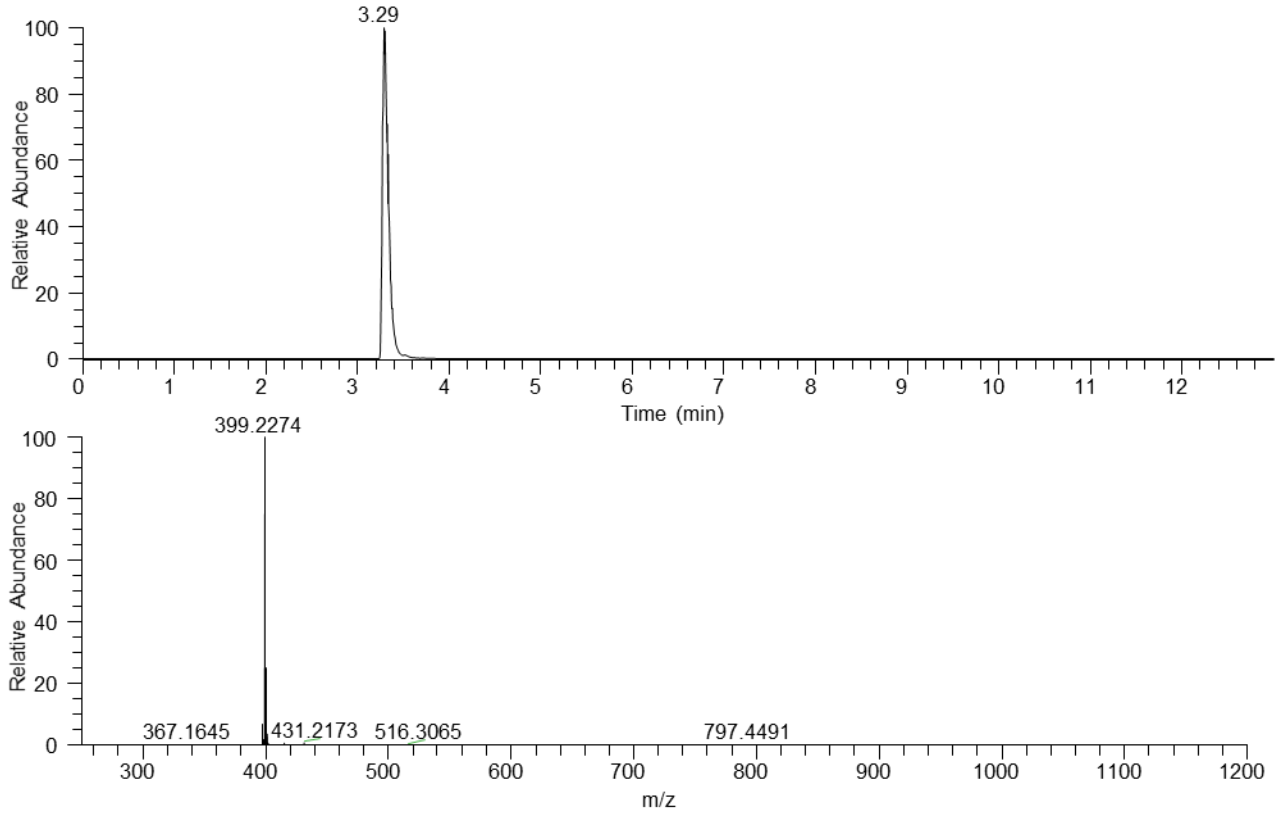

Figure S10. UPLC-HRESIMS data for mitragynine (**1**).

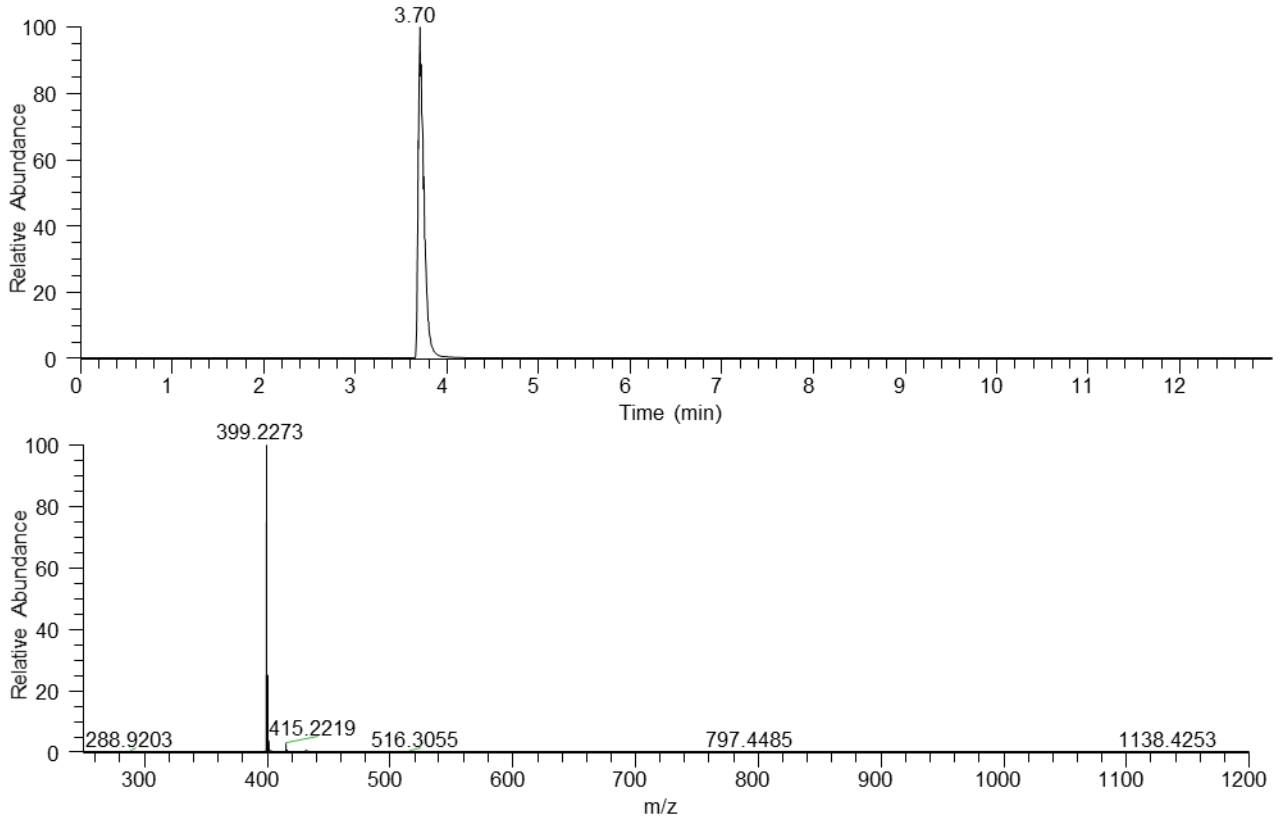

Figure S11. UPLC-HRESIMS data for speciociliatine (**2**).

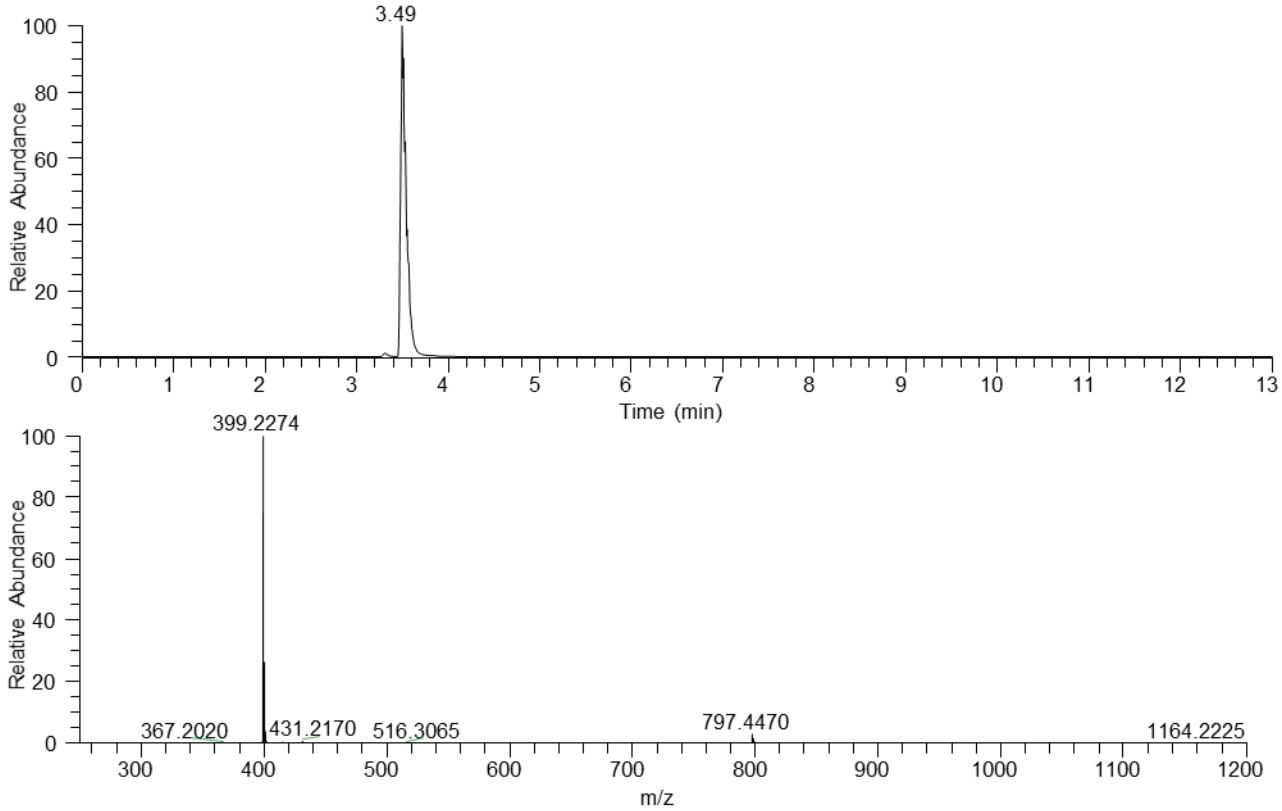

Figure S12. UPLC-HRESIMS data for speciogynine (**3**).

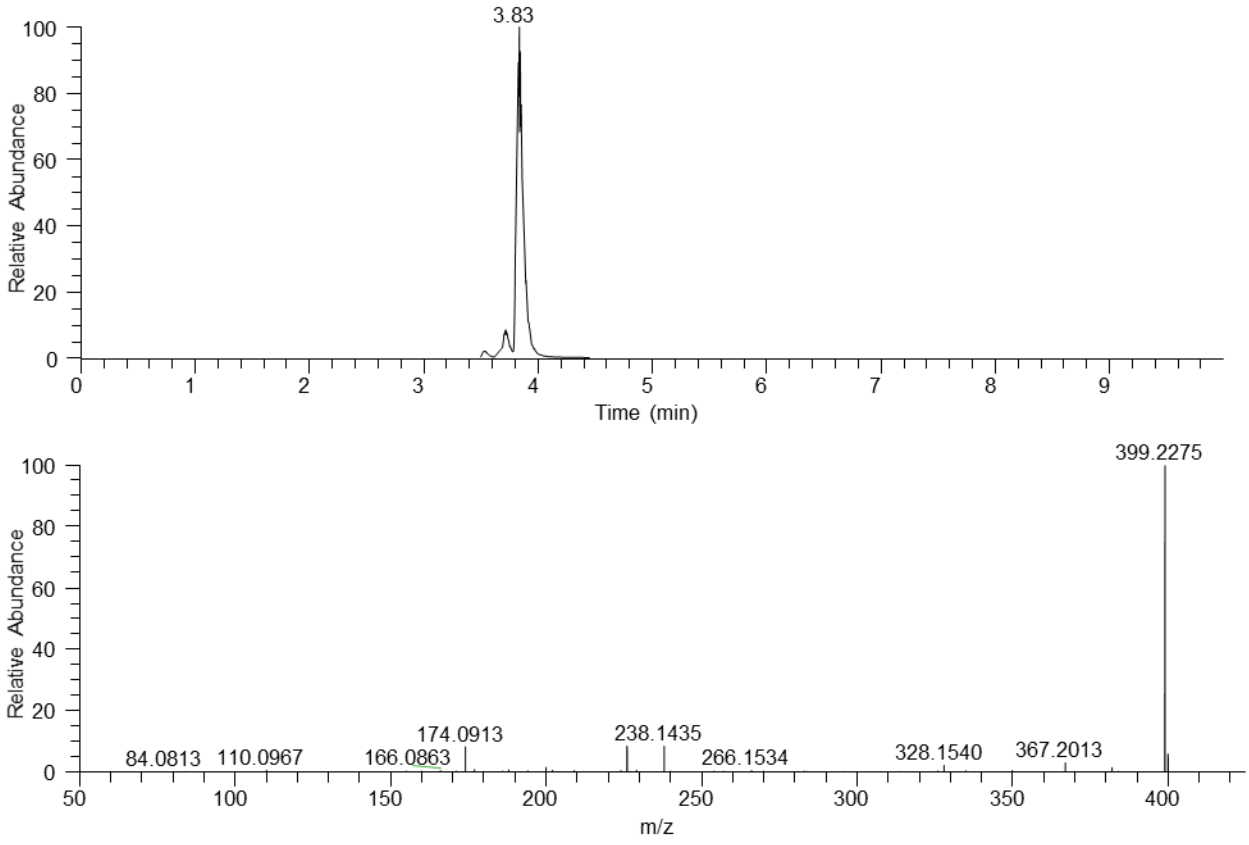

Figure S13. UPLC-HRESIMS data for mitraciliatine (**4**).

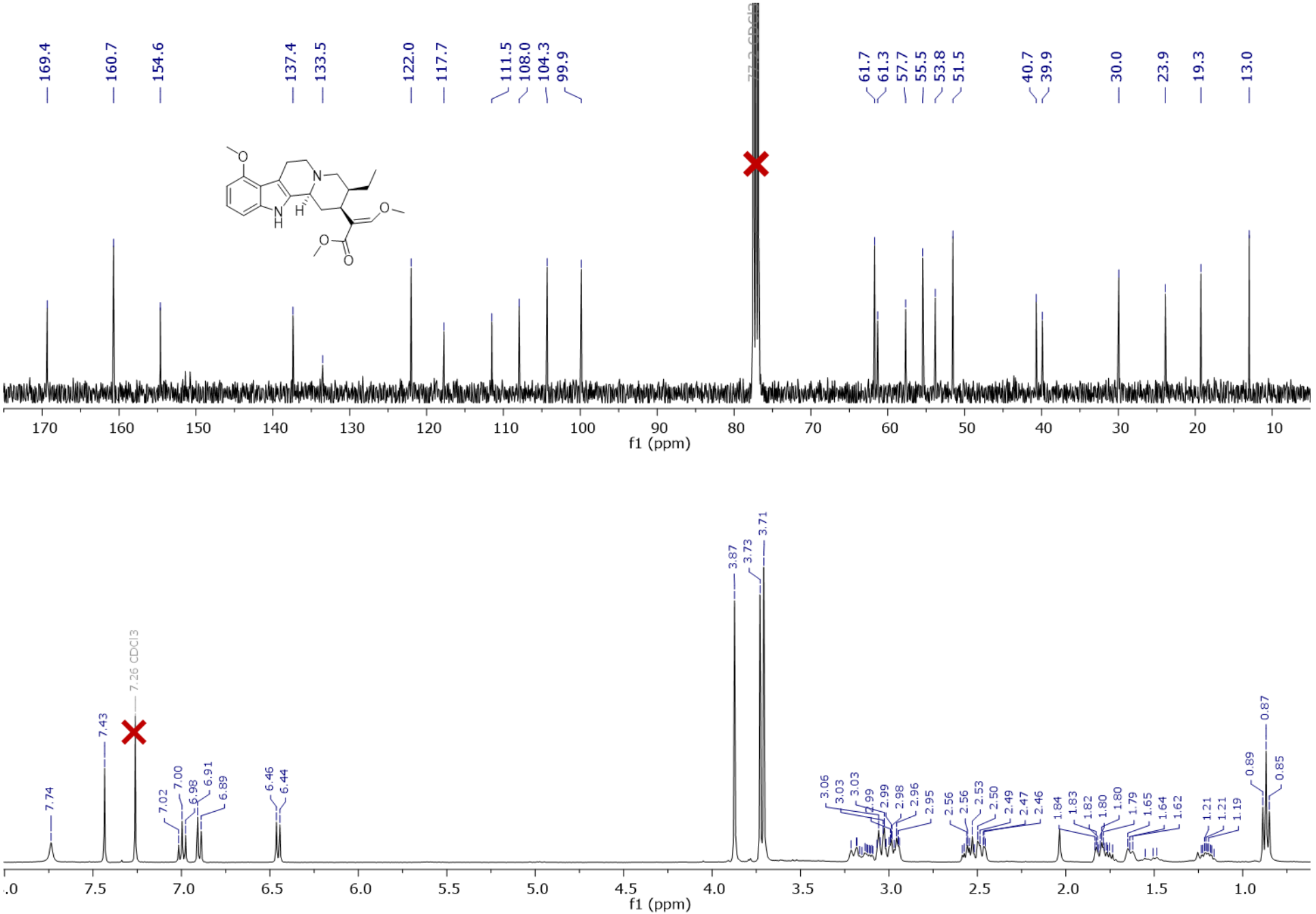

Figure S14. ^{1}H and ^{13}C NMR spectra for mitragynine (**1**) ($CDCl_3$, 400 MHz and 100 MHz, respectively).

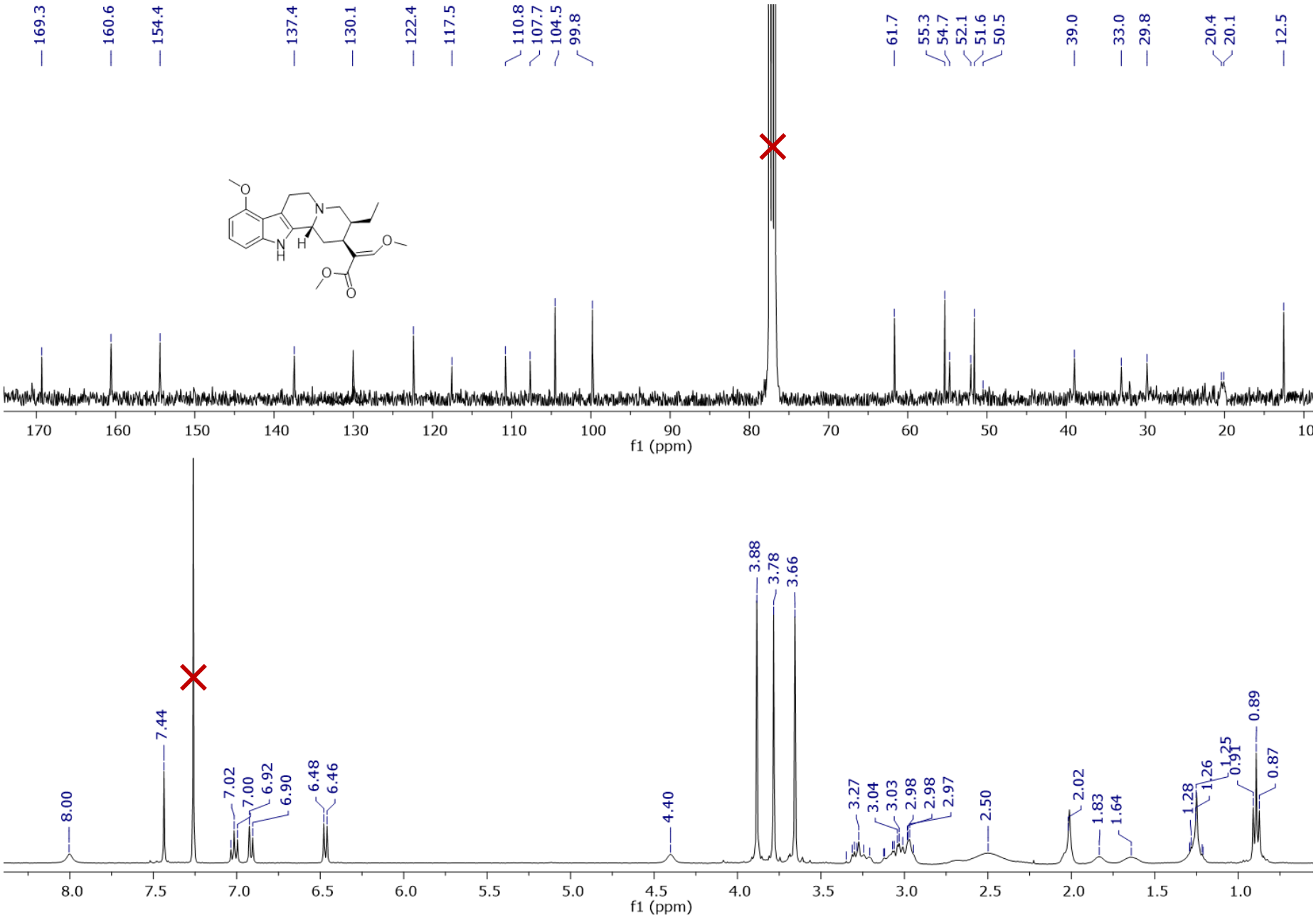

Figure S15. ^{1}H and ^{13}C NMR spectra for speciociliatine (**2**) ($CDCl_3$, 400 MHz and 100 MHz, respectively).

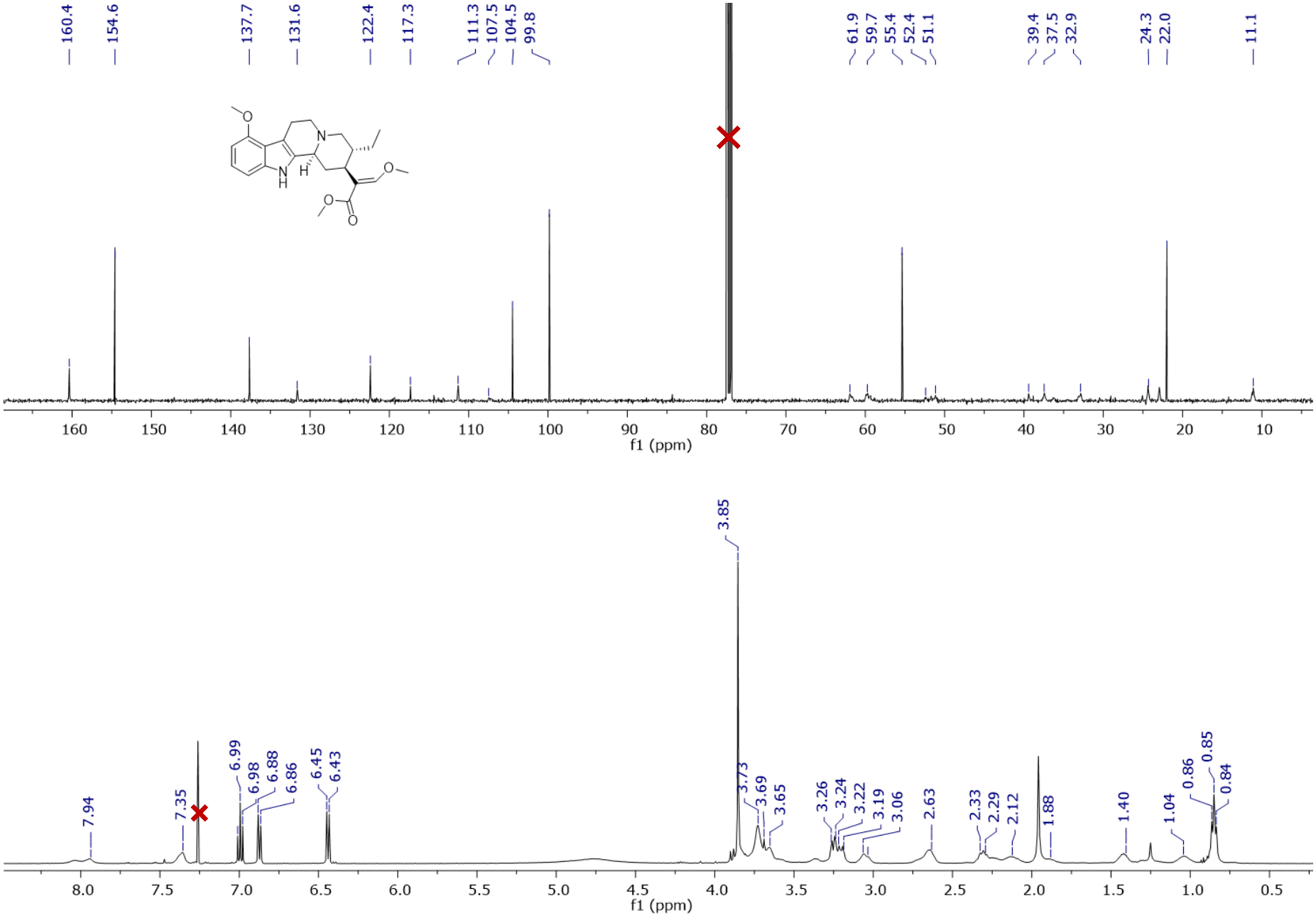

Figure S16. ^{1}H and ^{13}C NMR spectra for speciogynine (**3**) ($CDCl_3$, 400 MHz and 100 MHz, respectively).

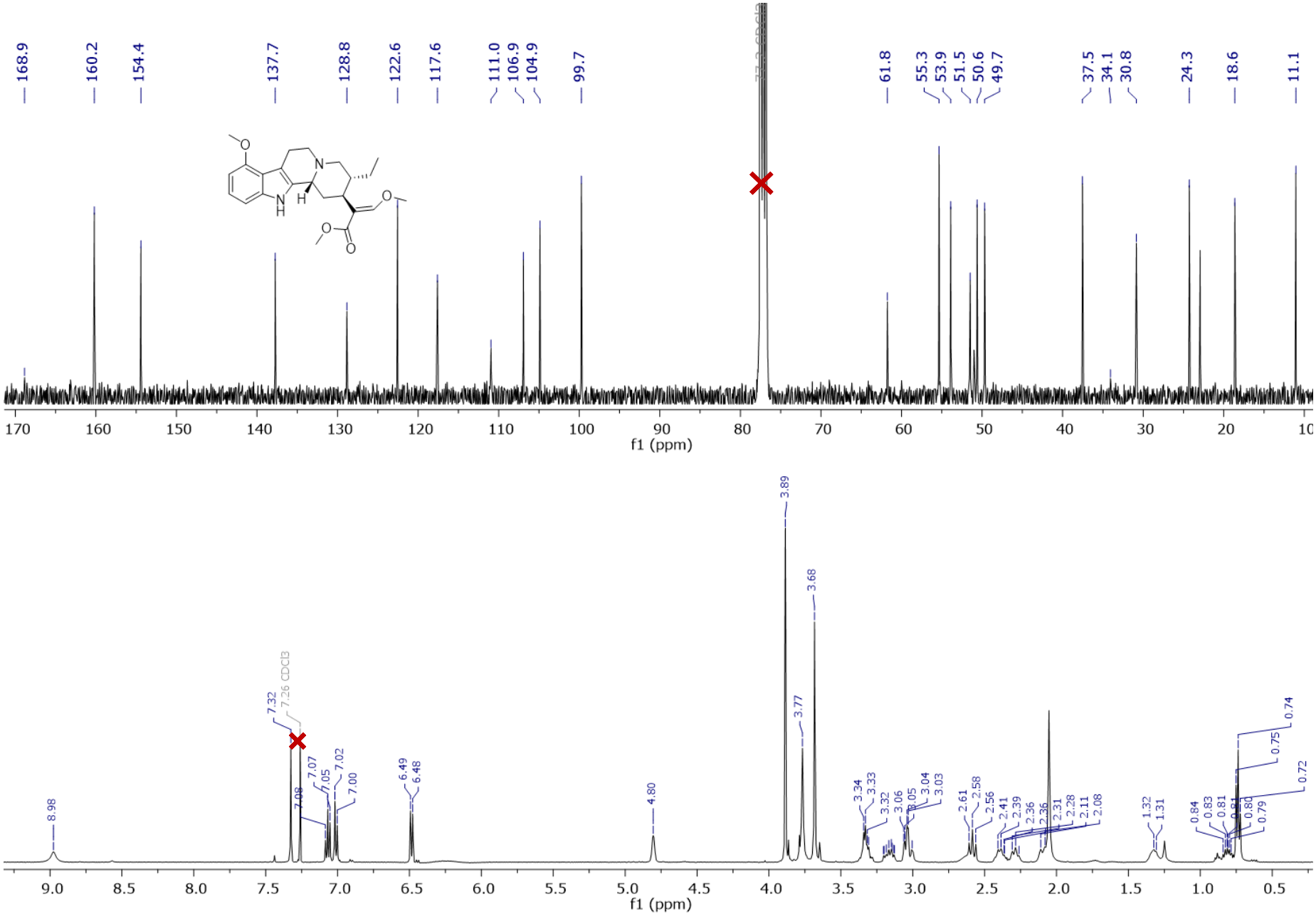

Figure S17. ^{1}H and ^{13}C NMR spectra for mitraciliatine (**4**) ($CDCl_3$, 400 MHz and 100 MHz, respectively).

Table S4. Comparison of NMR Data for Compounds 1-4 ($CDCl_3$, 100 MHz and 400 MHz).

			mitragynine (**1**)			speciociliatine (**2**)			speciogynine (**3**)			mitraciliatine (**4**)
position	δ_C	type	δ_H (*J* in Hz)	δ_C	type	δ_H (*J* in Hz)	δ_C	type	δ_H (*J* in Hz)	δ_C	type	δ_H (*J* in Hz)
2	133.5	C		130.1	C		131.6	C		128.8	C	
3	61.3	CH	3.20, d (8.4)	54.7	CH	4.40, bs	61.9	CH	3.21, m	53.9	CH	4.80, s
5	53.8	CH_2	2.97, m	52.1	CH_2	3.23, m	52.4[a]	CH_2	3.20, m	50.6	CH_2	3.32, m
			2.55, m			3.04, m			2.68, m			
6	23.9	CH_2	3.11, m	20.4	CH_2	3.31, m	22.0	CH_2	3.19, m	18.6	CH_2	3.20, m
			2.97, m			2.89, m			3.06, m			3.02, m
7	108.0	C		107.7	C		107.5[a]	C		106.9	C	
8	117.7	C		117.5	C		117.3	C		117.6	C	
9	154.6	C		154.4	C		154.6	C		154.4	C	
10	99.9	CH	6.45, d (7.7)	99.8	CH	6.47, d (7.7)	99.8	CH	6.44, d (7.8)	99.7	CH	6.49, d (7.6)
11	122.0	CH	7.00, t (7.9)	122.4	CH	7.02, t (8.0)	122.4	CH	6.99, t (7.9)	122.6	CH	7.07, t (7.9)
12	104.3	CH	6.90, d (8.1)	104.5	CH	6.91, d (8.1)	104.5	CH	6.87, d (8.0)	104.9	CH	7.01, d (8.0)
13	137.4	C		137.4	C		137.7	C		137.7	C	
14	30.0	CH_2	2.55, m	29.8	CH_2	2.50, m	32.9	CH_2	2.17, m	30.8	CH_2	2.60, t (11.5)
			1.81, m			2.02, m			1.95, m			2.10, bd (11.4)
15	39.9	CH	3.06, m	33.0	CH	2.97, m	39.4	CH	2.63, m	34.1	CH	2.28, m
16	111.5	C		110.8	C		111.3	C		111.0	C	
17	160.7	CH	7.43, s	160.6	CH	7.44, s	160.4	CH	7.35, bs	160.2	CH	7.32, s
18	13.0	CH_3	0.87, t (7.3)	12.5	CH_3	0.89, t (7.9)	11.1	CH_3	0.85, t (7.2)	11.1	CH_3	0.74, t (7.0)
19	19.3	CH_2	1.75, m	20.1	CH_2	1.64, m	24.3	CH_2	1.40, m	24.3	CH_2	1.32, m
			1.19, qd (7.4, 2.7)			1.25, m			1.04, m			0.84, m
20	40.7	CH	1.64, dt (11.5, 2.6)	39.0	CH	1.83, m	37.5	CH	2.31, m	37.5	CH	2.40, m
21	57.7	CH_2	3.00, m	50.5	CH_2	3.27, m	59.7	CH_2	3.26, m	49.7	CH_2	3.05, m
			2.44, m			2.89, m			2.21, m			2.57, m
22	169.4	C		169.3	C		170.2[a]	C		168.9	C	
9-OCH_3	55.5	CH_3	3.87, s	55.3	CH_3	3.88, s	55.4	CH_3	3.85, s	55.3	CH_3	3.89, s
17-OCH_3	61.7	CH_3	3.73, s	61.7	CH_3	3.78, s	61.9	CH_3	3.72, s	61.8	CH_3	3.77, s
22-OCH_3	51.5	CH_3	3.71, s	51.6	CH_3	3.66, s	51.1	CH_3	3.72, s	51.5	CH_3	3.68, s
NH			7.74, bs			8.00, bs			7.94, bs			8.98, bs

[a]Signals observed by 2D experiments

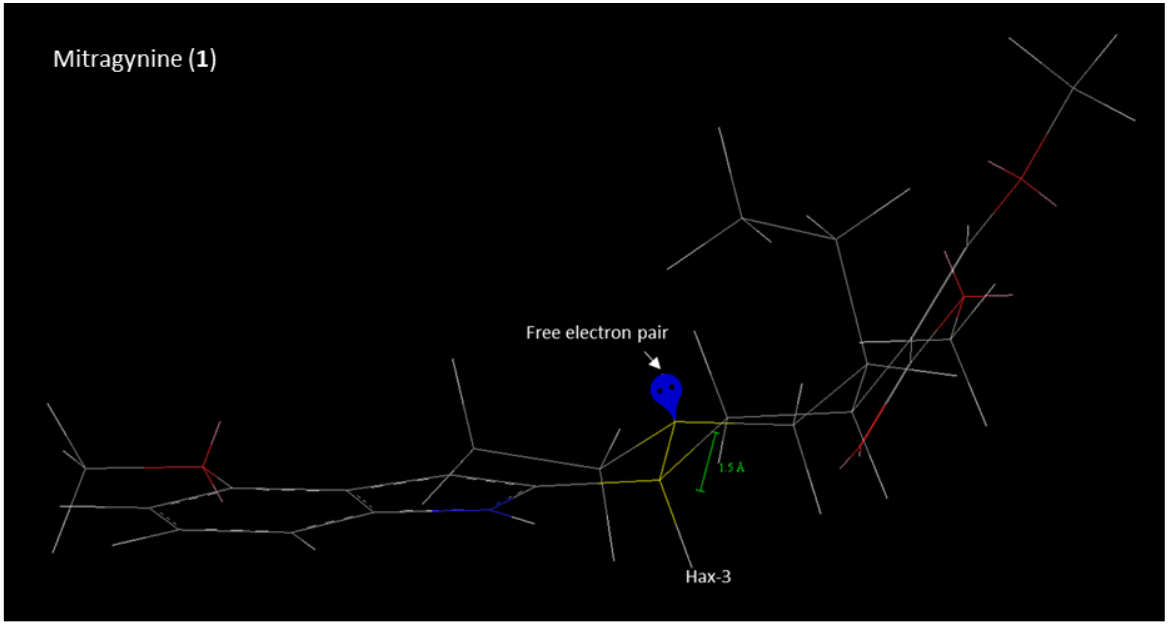

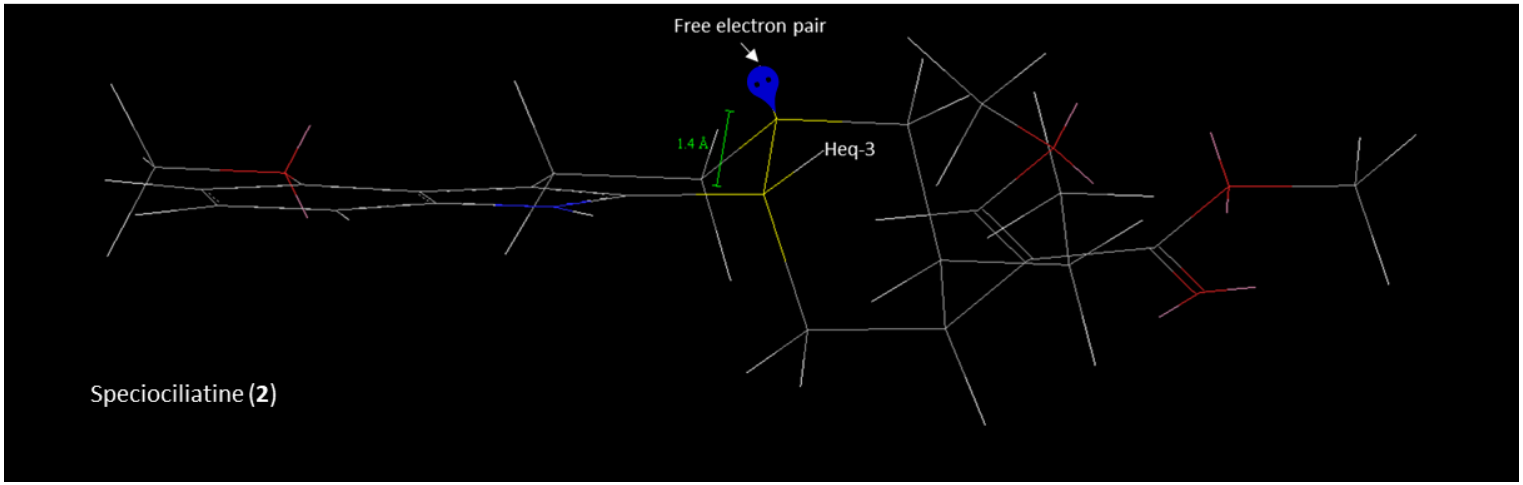

Figure S18. Representation for the different orientations of H-3 with respect to the nitrogen non-bonding electron pair for the most stable conformation of mitragynine (**1**) and speciociliatine (**2**).

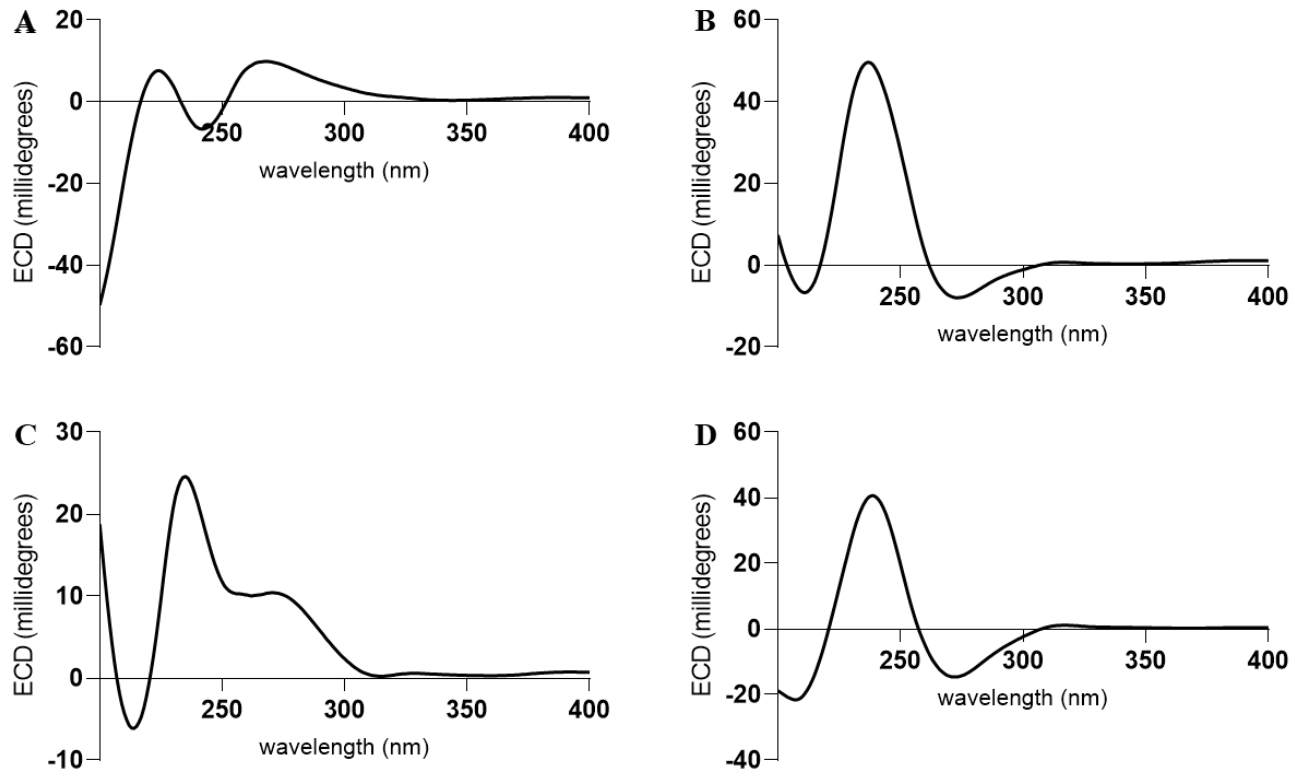

Figure S19. Comparison of the ECD spectra acquired in CH_3OH for A) mitragynine (**1**), B) speciociliatine (**2**), C) speciogynine (**3**), and D) mitraciliatine (**4**).

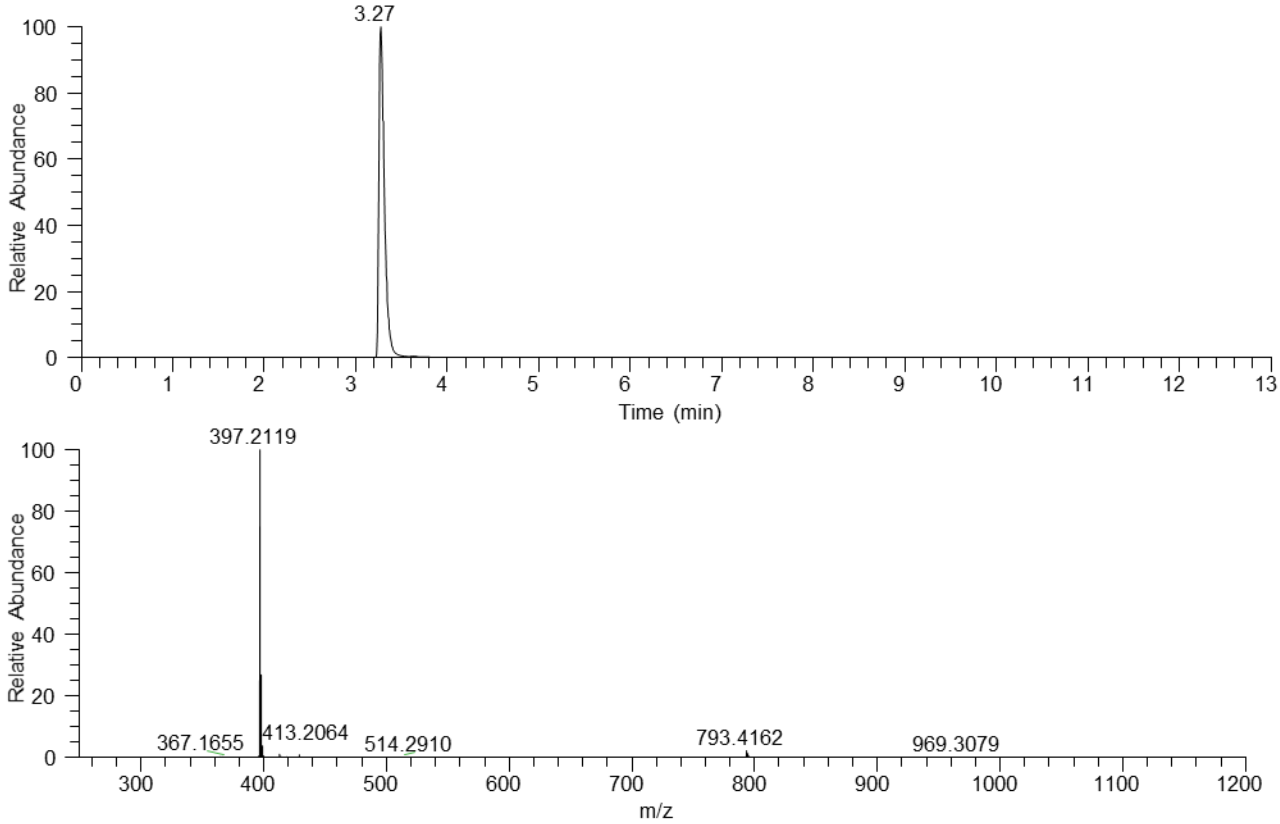

Figure S20. UPLC-HRESIMS data for paynantheine (**5**).

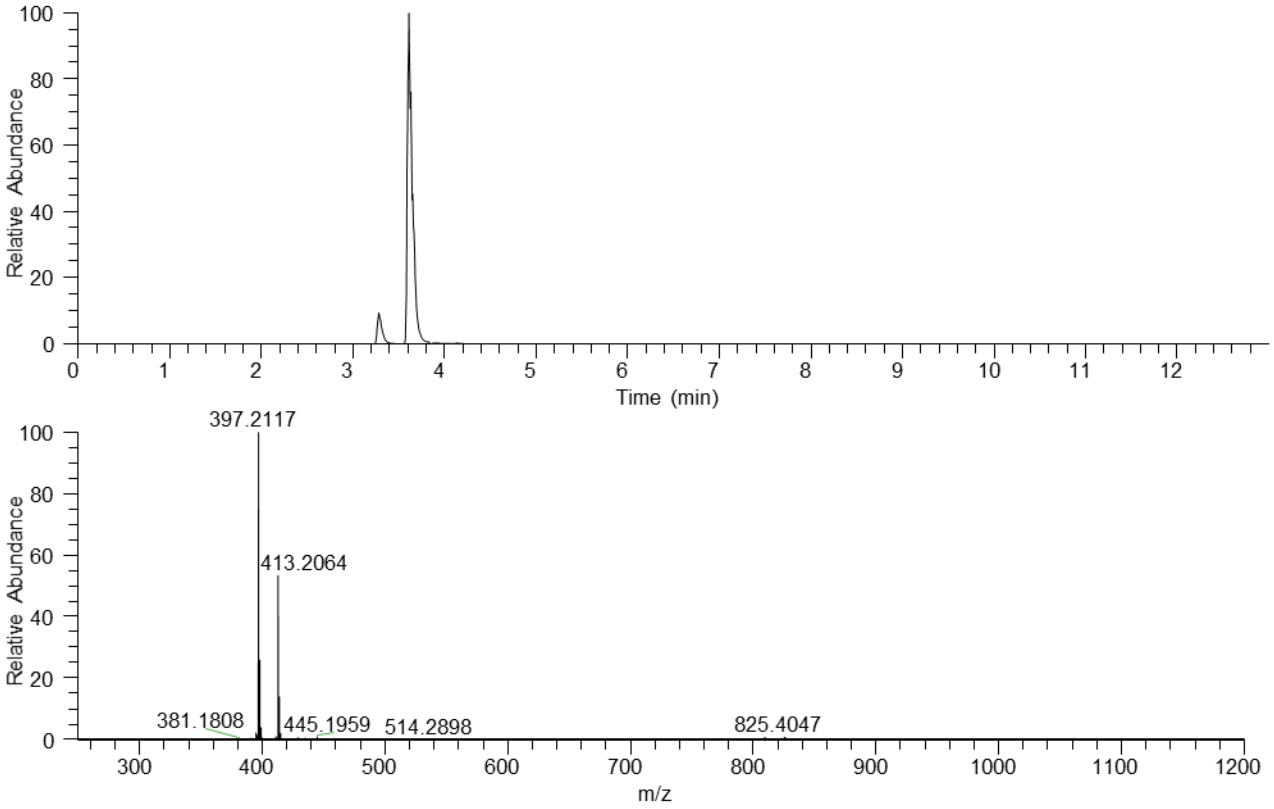

Figure S21. UPLC-HRESIMS data for isopaynantheine (**6**).

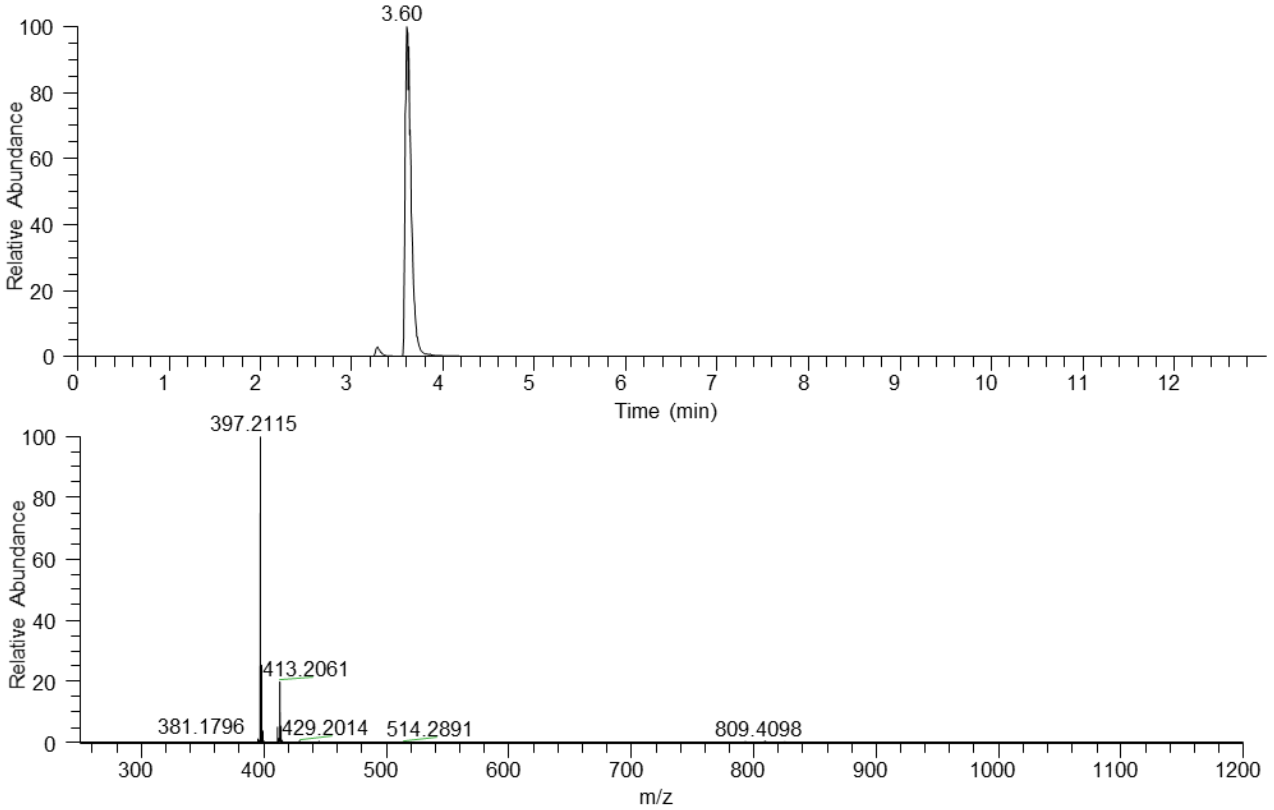

Figure S22. UPLC-HRESIMS data for epiallo-isopaynantheine (**7**).

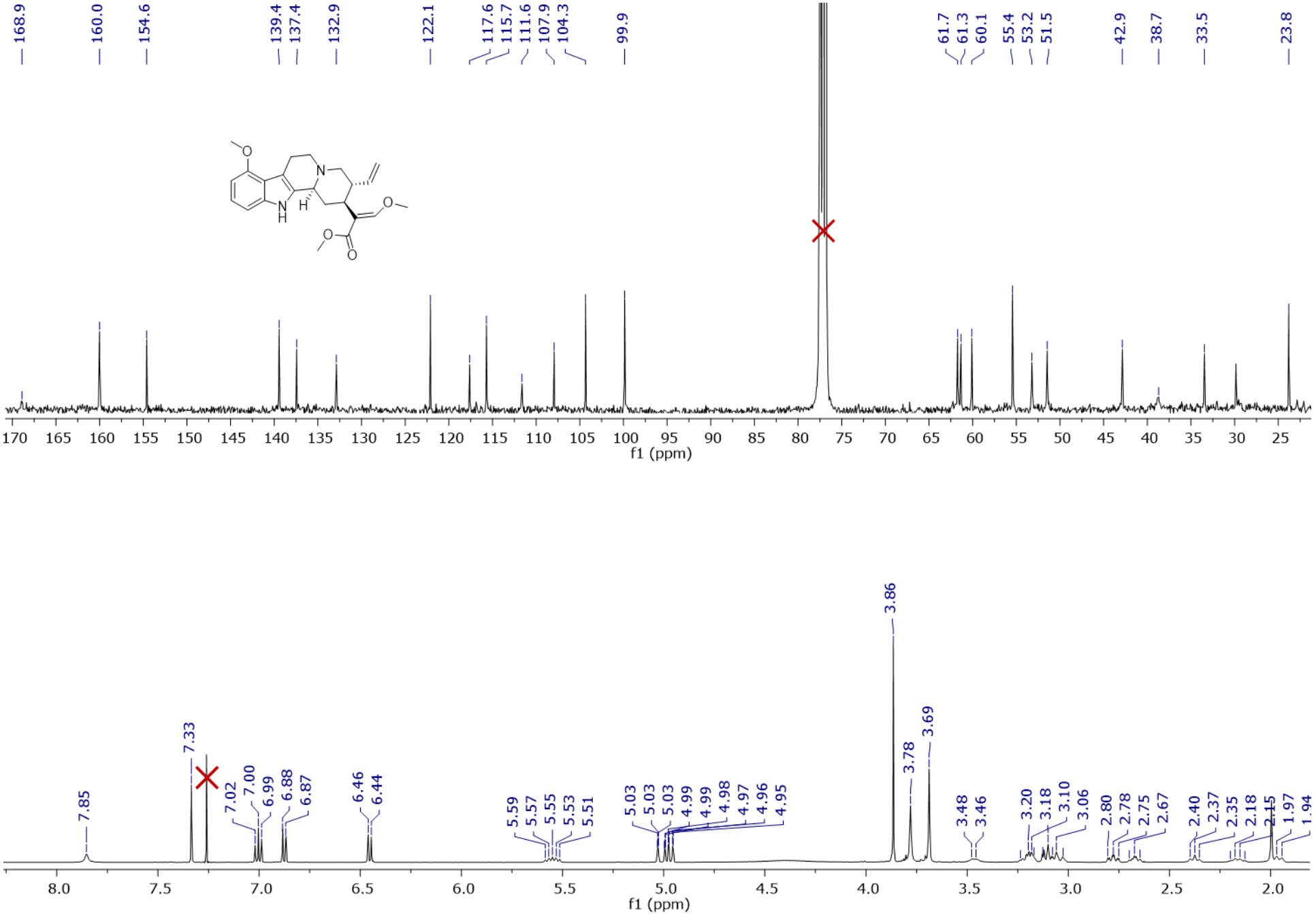

Figure S23. ^{1}H and ^{13}C NMR spectra for paynantheine (**5**) ($CDCl_3$, 400 MHz and 100 MHz, respectively).

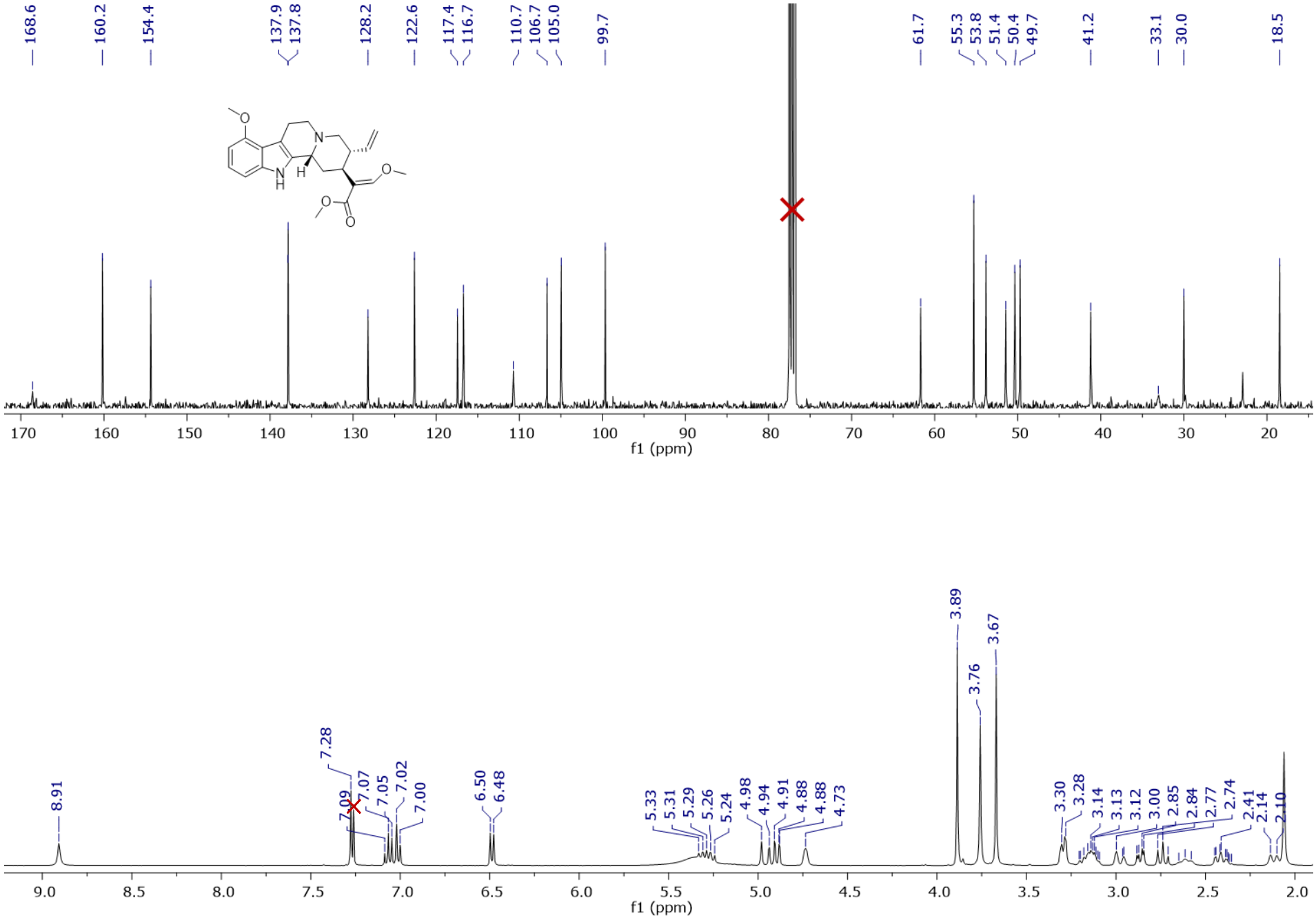

Figure S24. ^{1}H and ^{13}C NMR spectra for isopaynantheine (**6**) ($CDCl_3$, 400 MHz and 100 MHz, respectively).

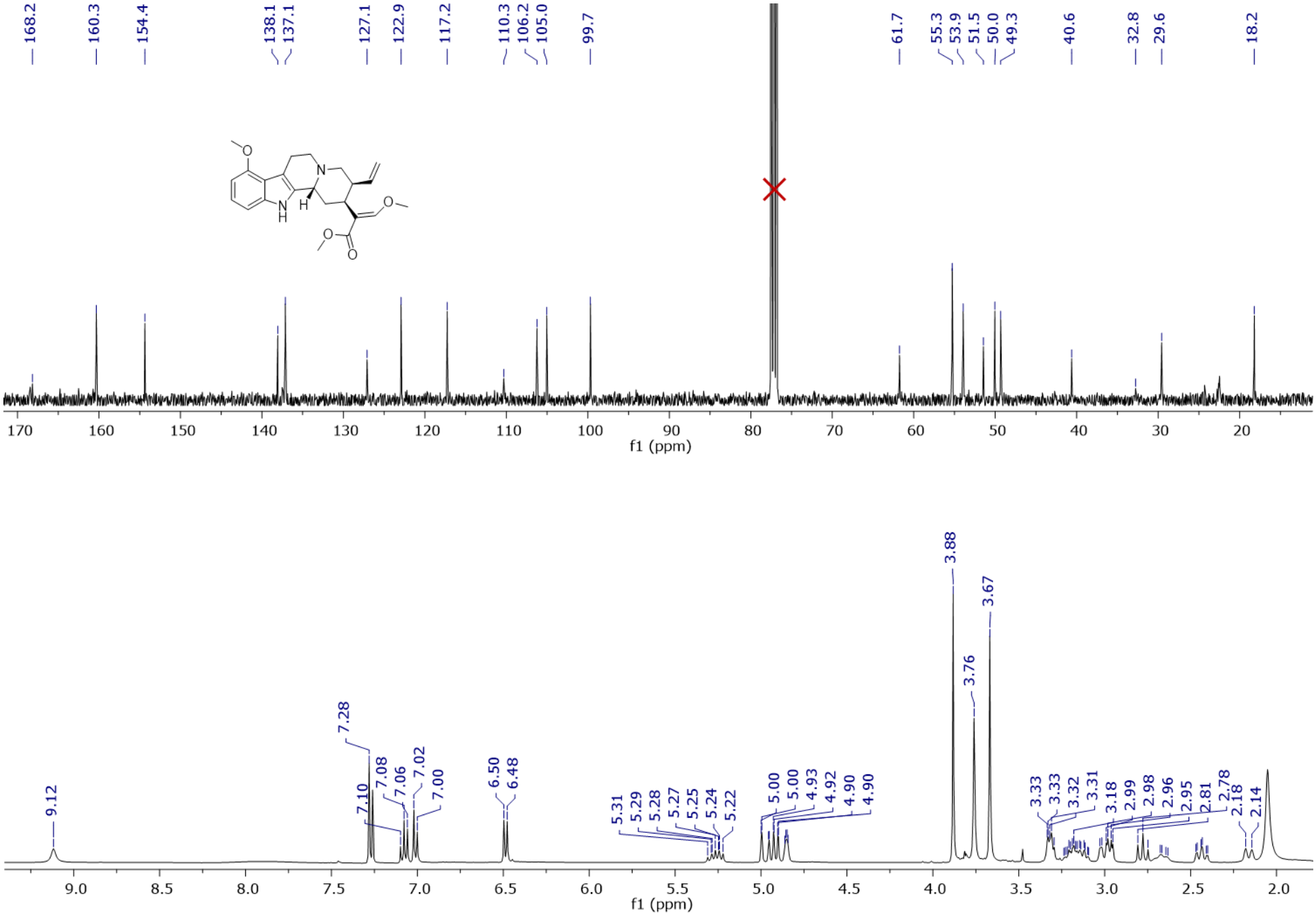

Figure S25. ^{1}H and ^{13}C NMR spectra for epiallo-isopaynantheine (**7**) ($CDCl_3$, 400 MHz and 100 MHz, respectively).

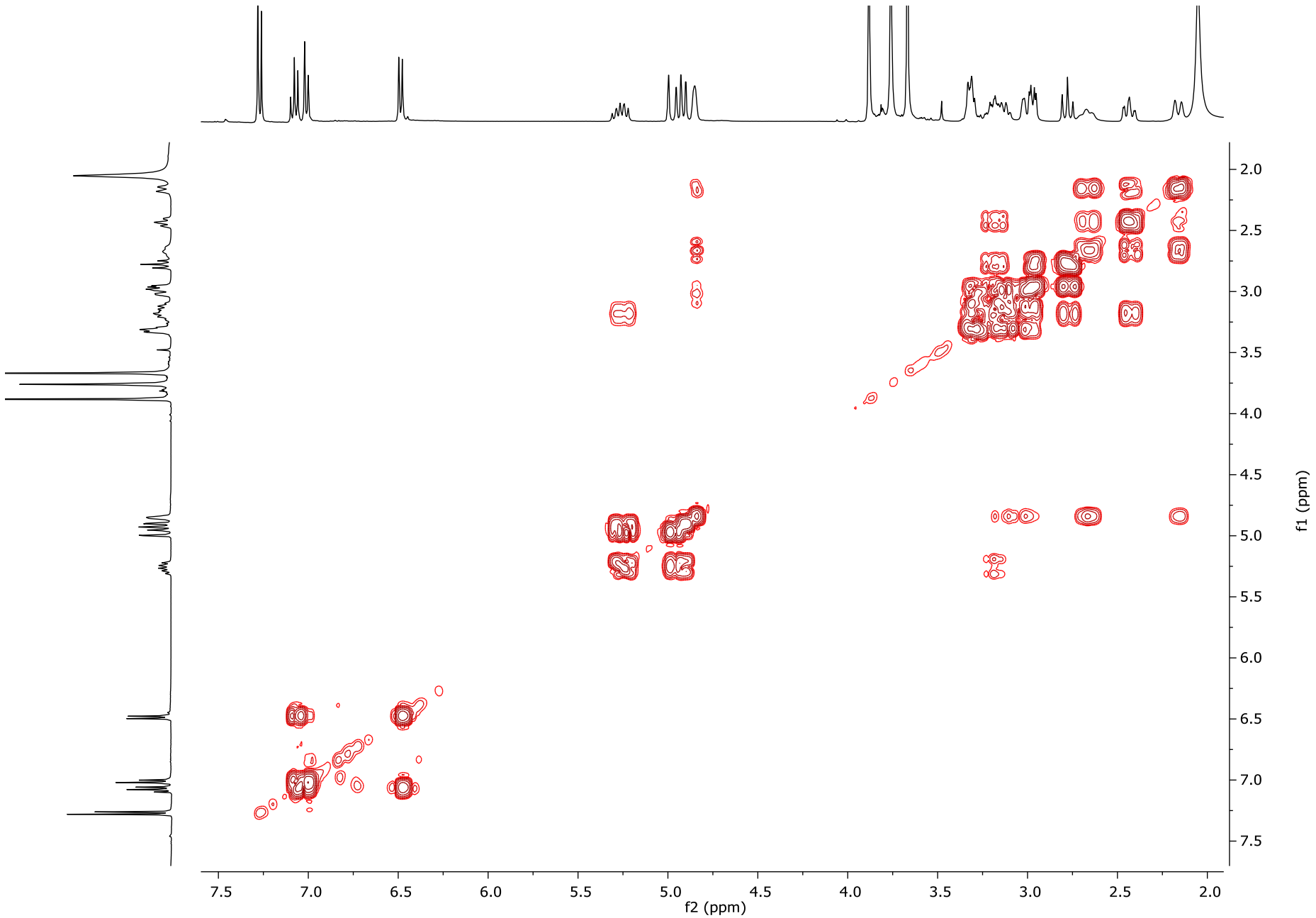

Figure S26. COSY spectrum for epiallo-isopaynantheine (**7**) ($CDCl_3$, 400 MHz).

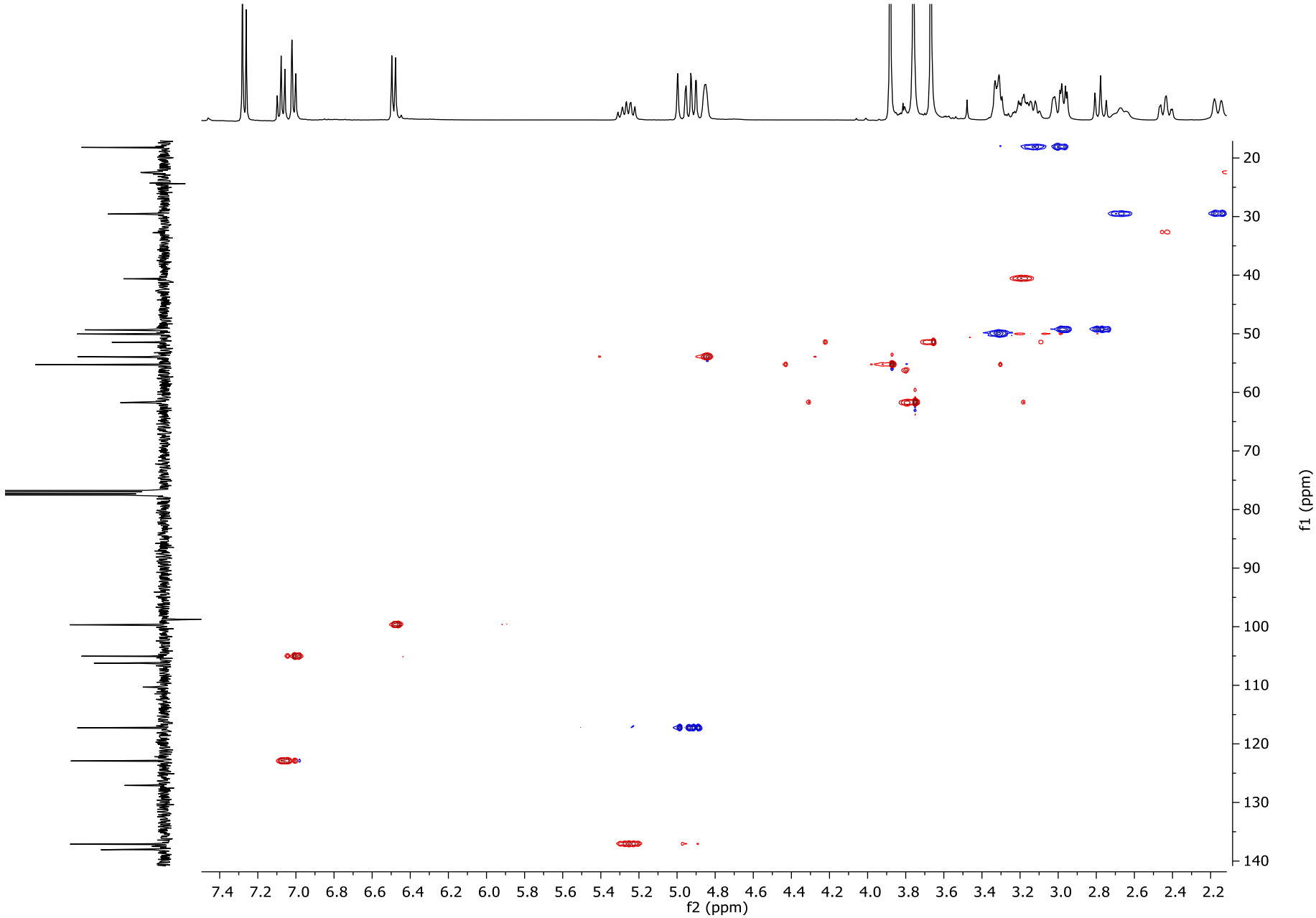

Figure S27. HSQC spectrum for epiallo-isopaynantheine (**7**) ($CDCl_3$, 400 MHz).

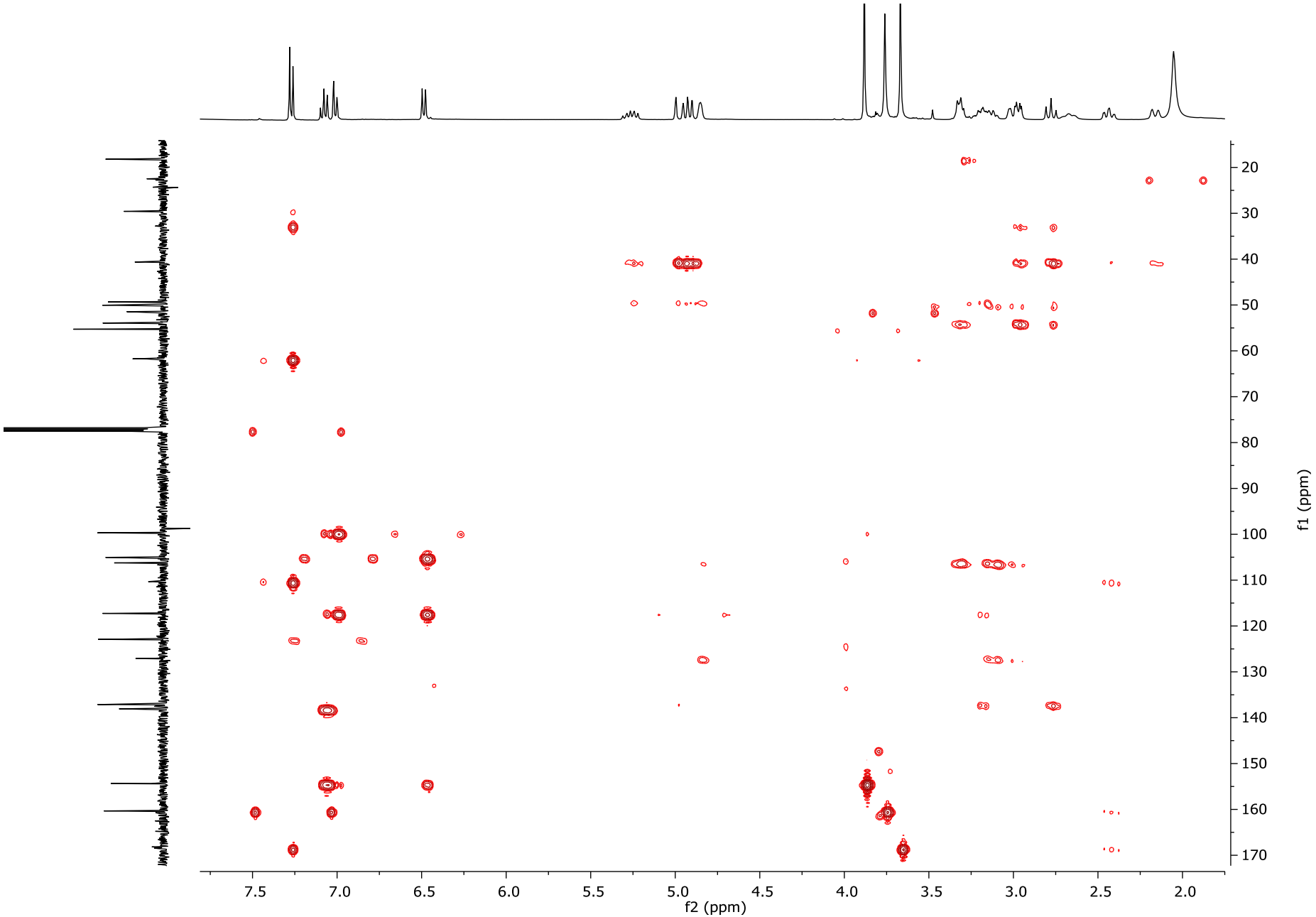

Figure S28. HMBC spectrum for epiallo-isopaynantheine (**7**) ($CDCl_3$, 400 MHz).

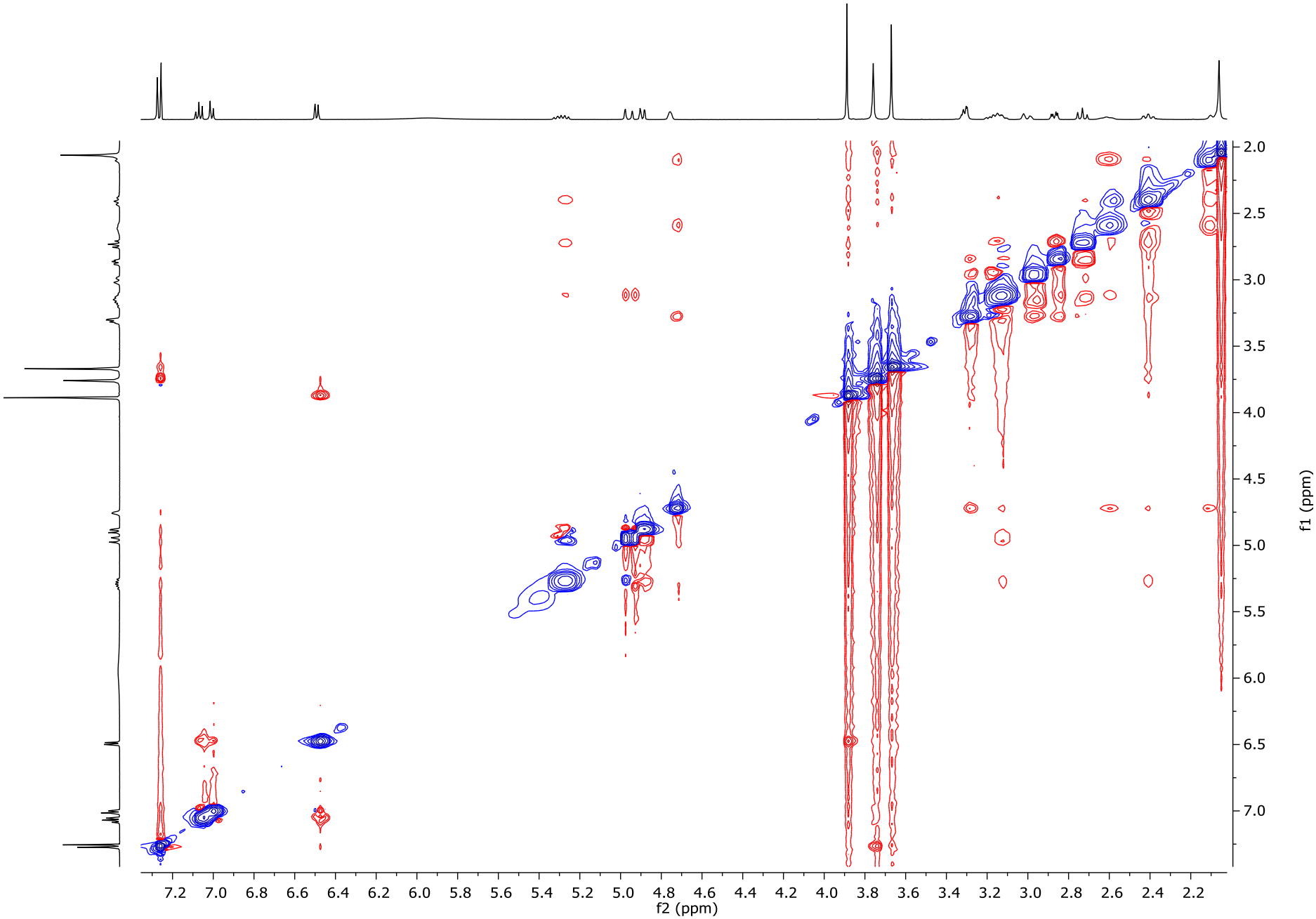

Figure S29. NOESY spectrum for isopaynantheine (**6**) ($CDCl_3$, 400 MHz).

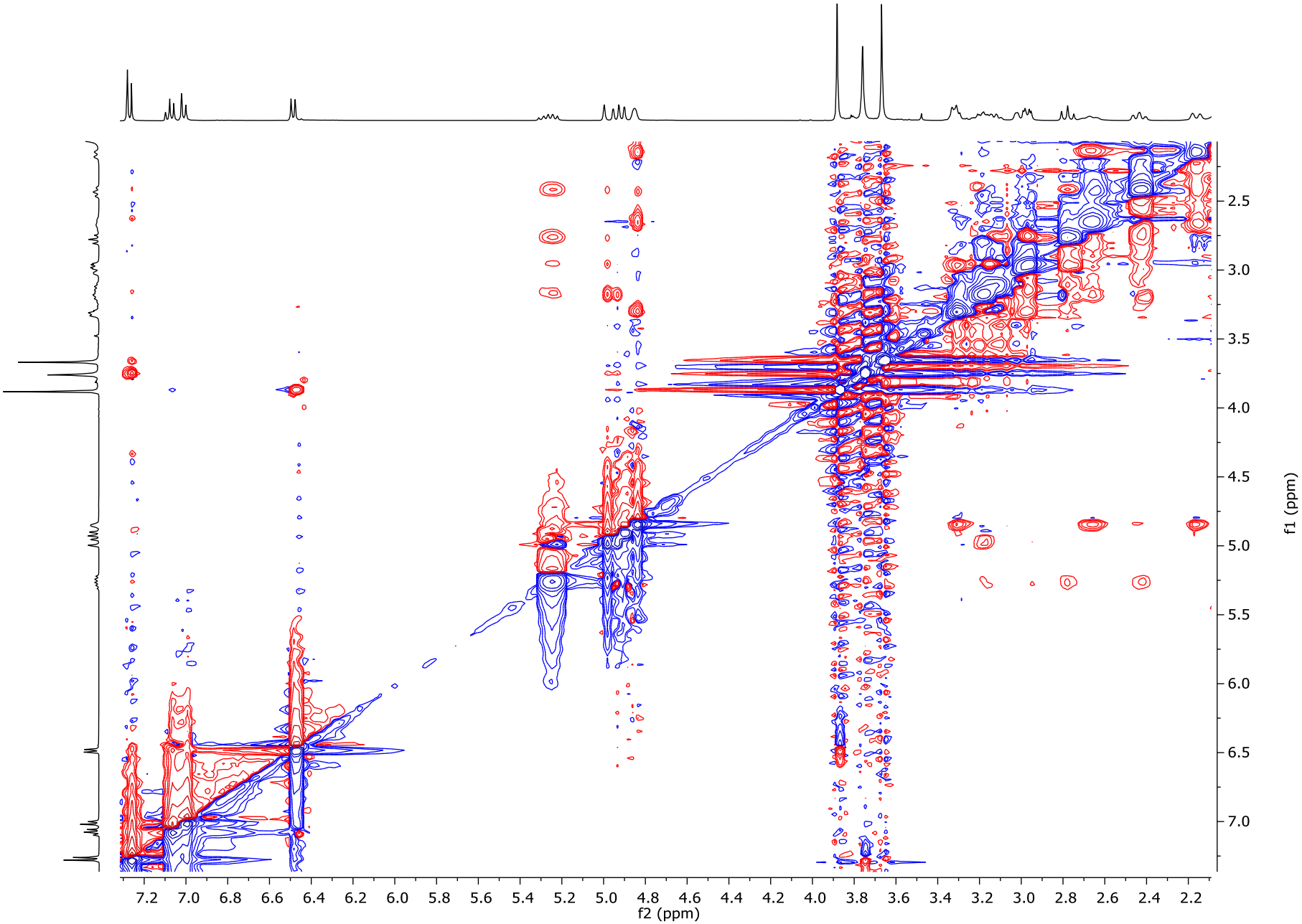

Figure S30. NOESY spectrum for epiallo-isopaynantheine (**7**) ($CDCl_3$, 400 MHz).

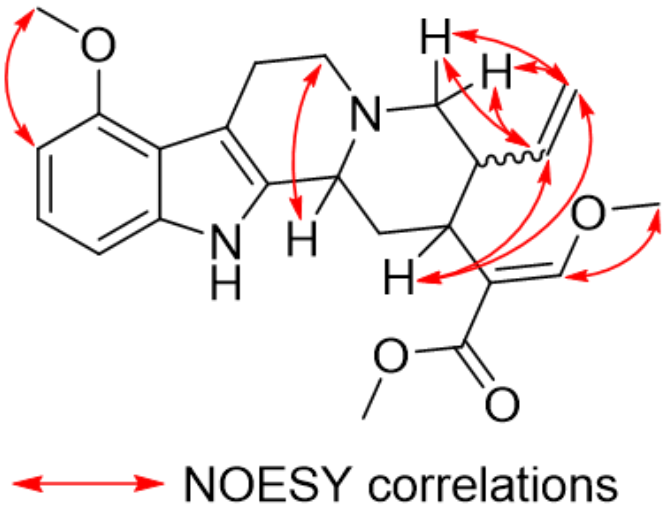

Compound	Distances (Å)	
	$H_{15} \rightarrow H_{18}$	$H_{15} \rightarrow H_{19}$
Isopaynantheine (**6**)	2.6	4.6
Epiallo-isopaynantheine (**7**)	3.6	2.8

Figure S31. Observed NOESY correlations for compounds **6** and **7**, and the distances for the key positions in the diastereoisomers.

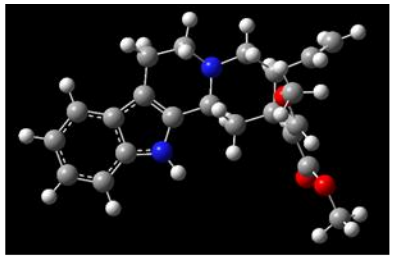

7a (ΔG 0.000 kcal/mol; P = 23.33%)

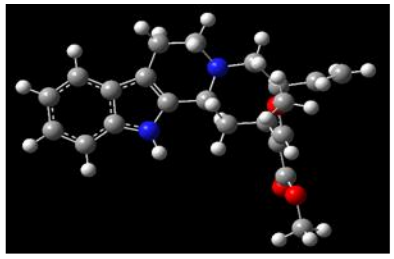

7b (ΔG 0.003 kcal/mol; P = 23.23%)

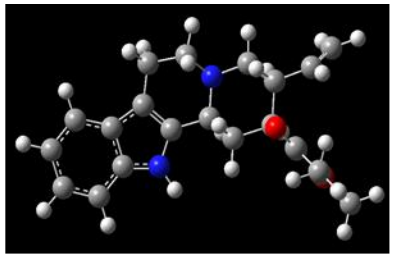

7c (ΔG 0.366 kcal/mol; P = 12.56%)

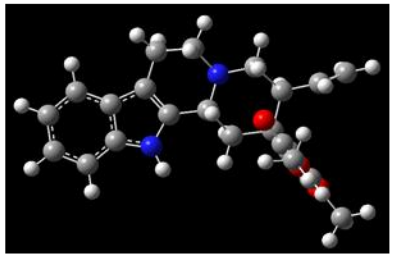

7d (ΔG 0.336 kcal/mol; P = 12.56%)

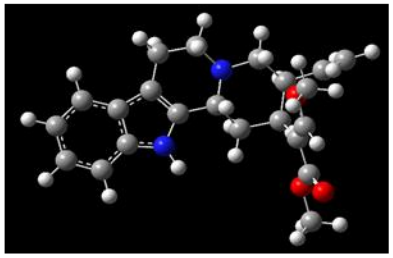

7e (ΔG 0.470 kcal/mol; P = 10.53%)

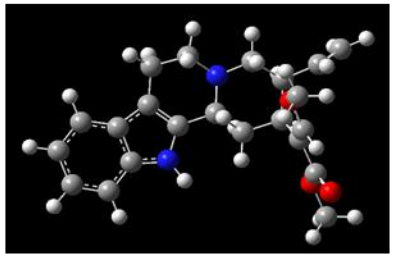

7f (ΔG 0.470 kcal/mol; P = 10.53%)

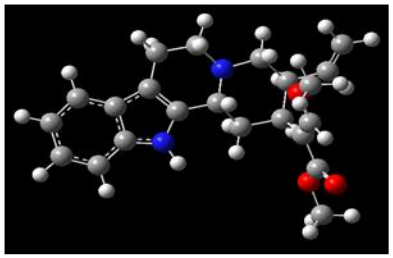

7g (ΔG 1.293 kcal/mol; P = 2.63%)

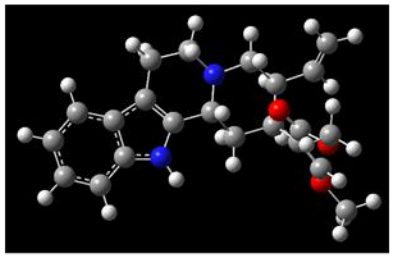

7h (ΔG 1.364 kcal/mol; P = 2.33%)

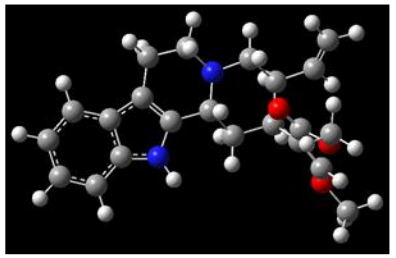

7i (ΔG 1.373 kcal/mol; P = 2.29%)

Figure S32. Nine conformers for the prediction of the ECD spectrum for **7**. The Boltzmann distributions are expressed as a percentage of population (P); the number of excited states considered for the calculation was n = 30.

Table S5. Comparison of NMR Data for Compounds 5-7 ($CDCl_3$, 100 MHz and 400 MHz)

	paynantheine (**5**)			isopaynantheine (**6**)			epiallo-isopaynantheine (**7**)		
Position	δ_C	type	δ_H (*J* in Hz)	δ_C	type	δ_H (*J* in Hz)	δ_C	type	δ_H (*J* in Hz)
2	132.9	C		128.2	C		127.1	C	
3	60.1	CH	3.20, m	53.8	CH	4.73, bs	53.9	CH	4.85, bs
5	53.2	CH_2	3.47, m	50.4	CH_2	3.29, m	50.0	CH_2	3.32, m
			2.67, m						
6	23.8	CH_2	3.18, m	18.5	CH_2	3.18, m	18.2	CH_2	3.10, m
			2.80, m			3.00, m			3.02, m
7	107.9	C		106.7	C		106.2	C	
8	117.6	C		117.4	C		117.2	C	
9	154.6	C		154.4	C		154.4	C	
10	99.9	CH	6.45, d (7.8)	99.7	CH	6.49, d (7.6)	99.7	CH	6.49, d (7.8)
11	122.1	CH	7.00, t (7.9)	122.6	CH	7.07, t (7.9)	122.9	CH	7.08, t (7.9)
12	104.3	CH	6.88, d (8.0)	105.0	CH	7.02, d (8.1)	105.0	CH	7.01, d (8.1)
13	137.4	CH		137.8	CH		138.1	CH	
14	33.5	CH_2	2.16, dd (12.5, 12.00)	30.0	CH_2	2.61, t (14.0)	29.6	CH_2	2.65, m
			1.96, d (13.2)			2.11, d (14.3)			2.16, d (14.5)
15	38.7	CH	2.78, td (11.8, 3.7)	33.1	CH	2.40, td (12.8, 3.1)	32.8	CH	2.44, td (12.1, 3.0)
16	111.6	C		110.7	C		110.3	C	
17	160.0	CH	7.33, s	160.2	CH	7.28, s	160.3	CH	7.28, s
18	115.7	CH_2	5.01, dd (17.3, 2.0)	116.7	CH_2	4.96, dd (17.2, 1.8)	117.2	CH_2	4.98, dd (17.3, 1.7)
			4.96, dd (10.4, 2.1)			4.89, dd (10.2, 1.8)			4.91, dd (10.3, 1.8)
19	139.4	CH	5.55, dt (17.9, 9.3)	137.9	CH	5.29, ddd (18.0, 10.3, 8.3)	137.1	CH	5.27, ddd (18.0, 10.3, 8.3)
20	42.9	CH	3.08, m	41.2	CH	3.13, m	40.6	CH	3.19, m
21	61.3	CH_2	3.03, m	49.7	CH_2	2.86, dd (11.6, 3.9)	49.3	CH_2	2.97, dd (11.7, 3.8)
			2.37, m			2.74, t (11.6)			2.78, t (11.8)
22	168.9	C		168.6	C		168.2	C	
9-OCH_3	55.4	CH_3	3.86, s	55.3	CH_3	3.89, s	55.3	CH_3	3.88, s
17-OCH_3	61.7	CH_3	3.78, s	61.7	CH_3	3.76, s	61.7	CH_3	3.76, s
22-OCH_3	51.5	CH_3	3.69, s	51.4	CH_3	3.67, s	51.5	CH_3	3.67, s
NH			7.85, s			8.91, s			9.12, s

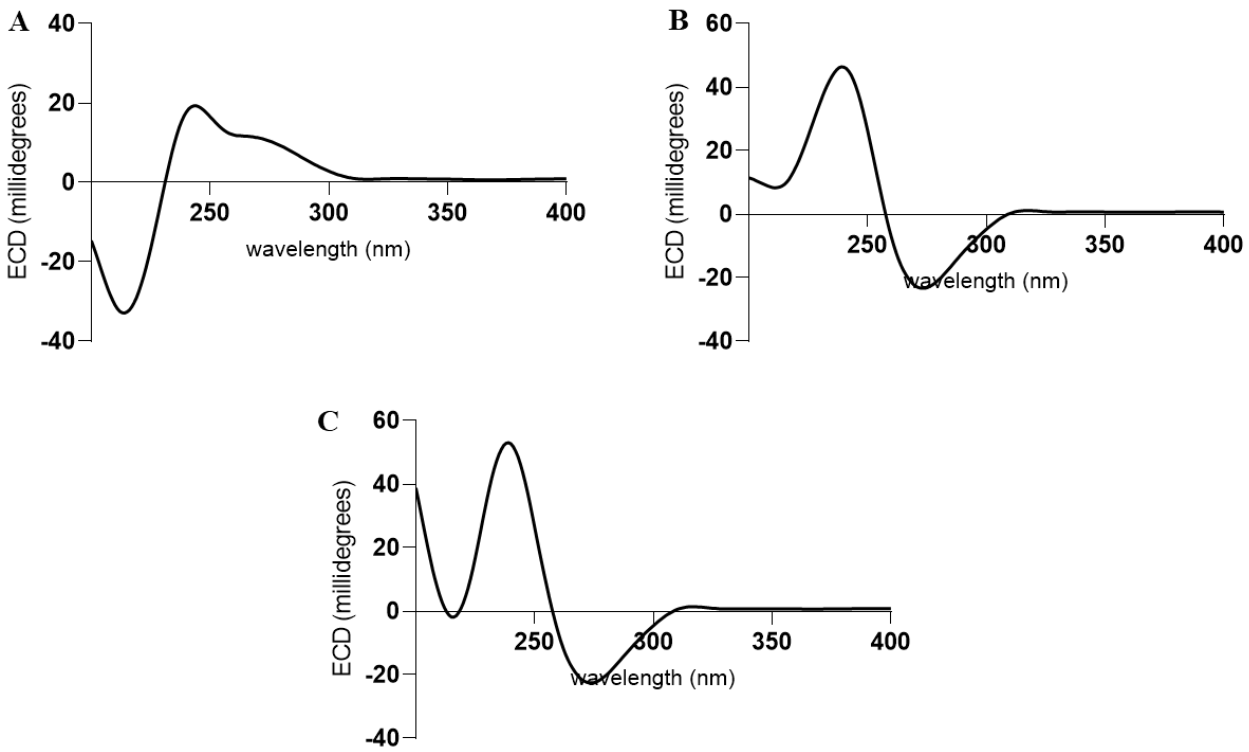

Figure S33. Comparison of the ECD spectra acquired in CH_3OH for A) paynantheine (**5**), B) isopaynantheine (**6**), and C) epiallo-isopaynantheine (**7**).

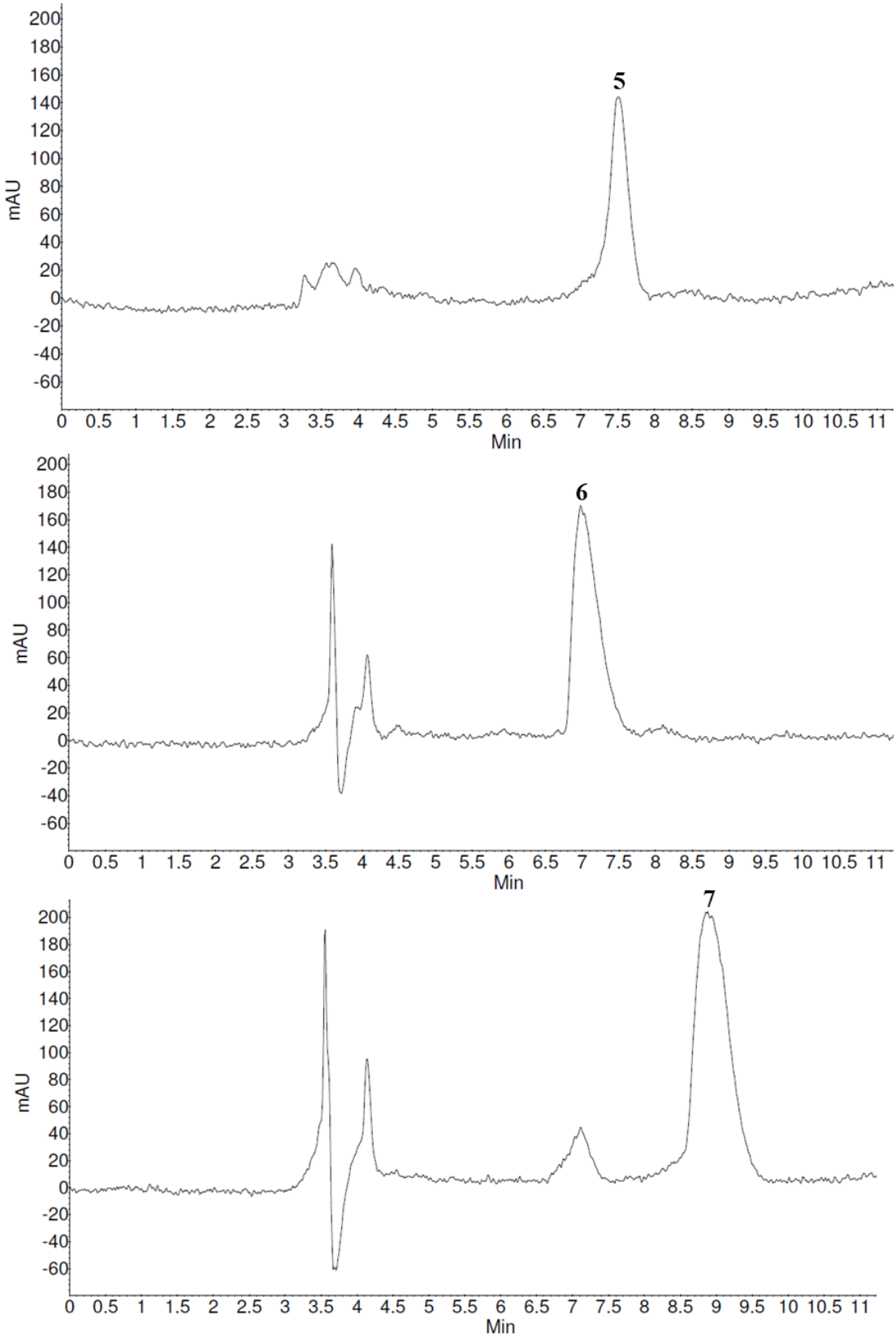

Figure S34. NP-HPLC chromatograms for compounds **5**, **6**, and **7**. These data were acquired using a Luna Silica column (Phenomenex, 250 x 4.6 mm) via isocratic conditions using a mixture of $CHCl_3$-MeOH (95:5) with a flow rate of 1 mL/min and UV set at 250 nm.

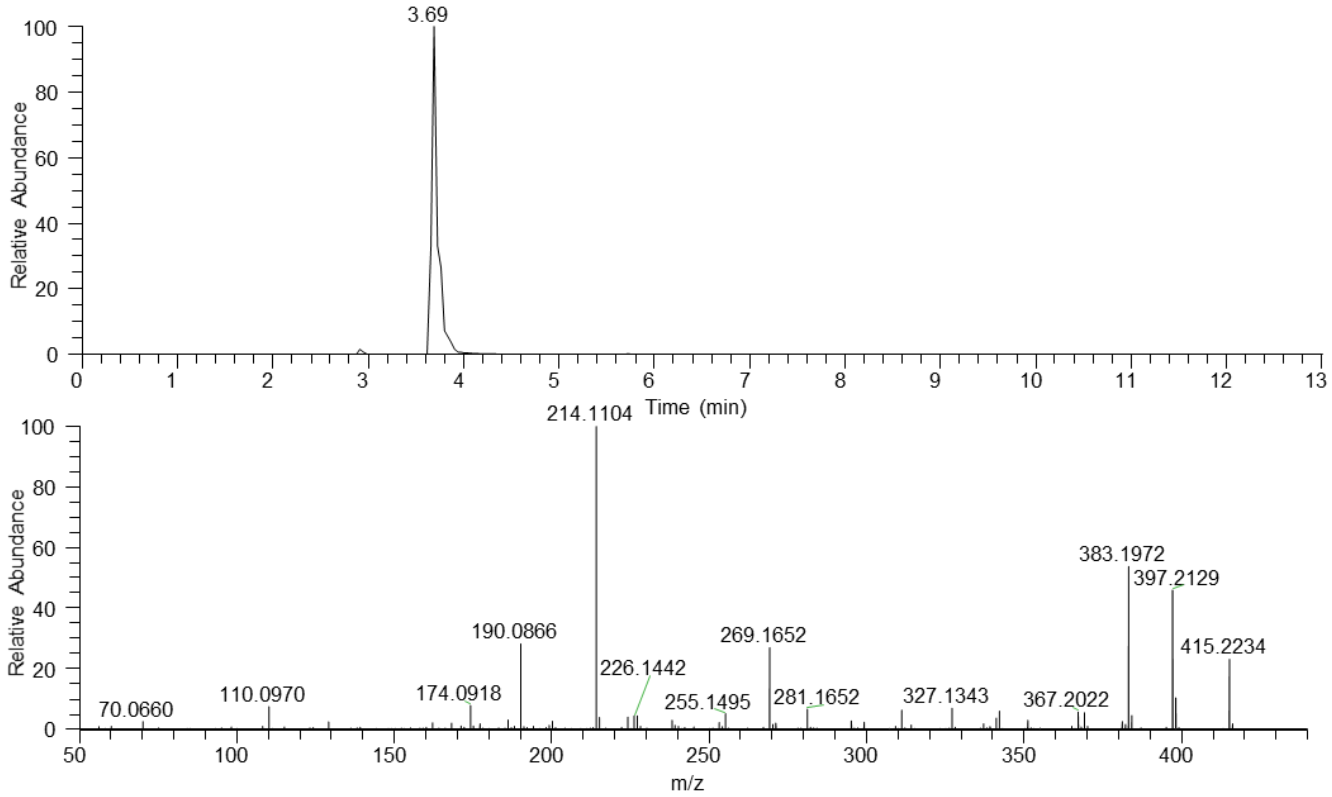

Figure S35. UPLC-HRESIMS data for mitragynine-*N*(4)-oxide (**8**).

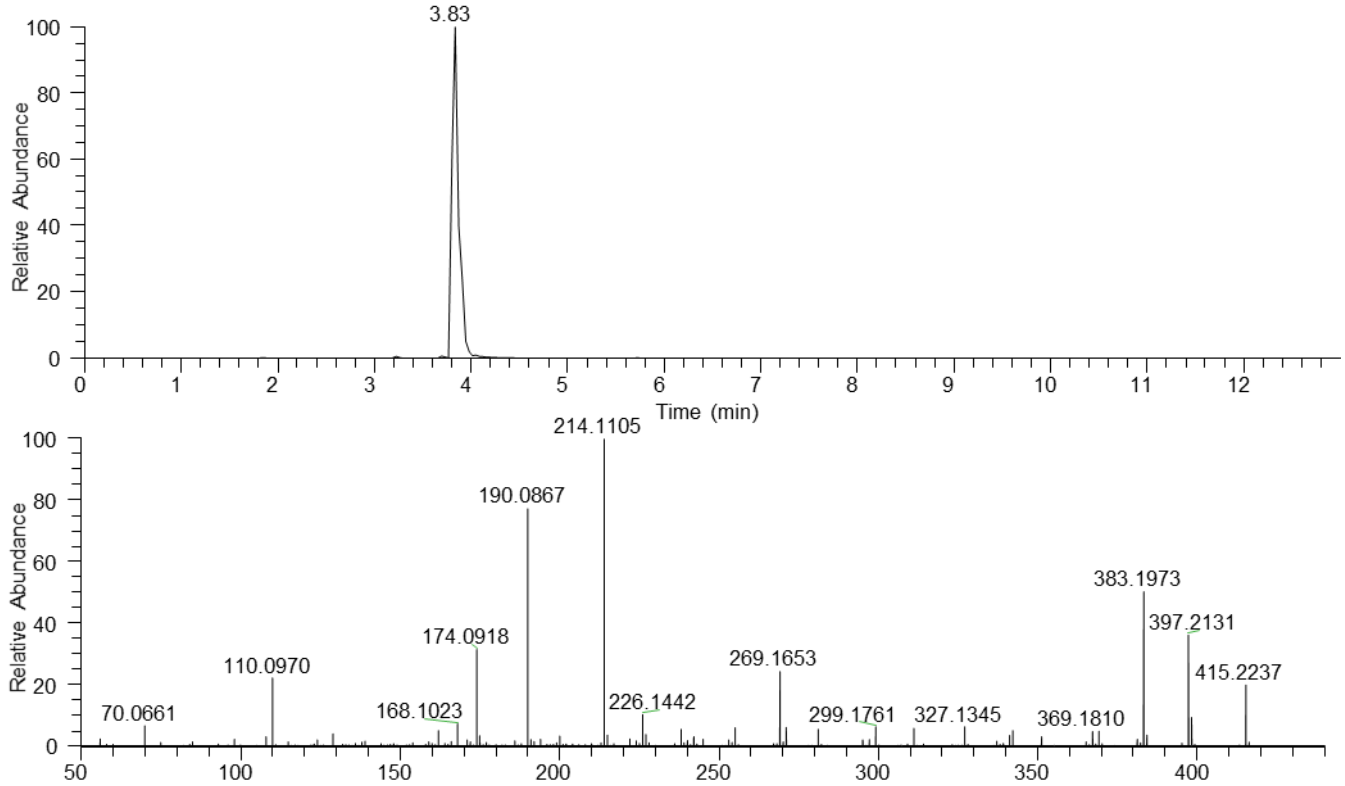

Figure S36. UPLC-HRESIMS data for speciociliatine-*N*(4)-oxide (**9**).

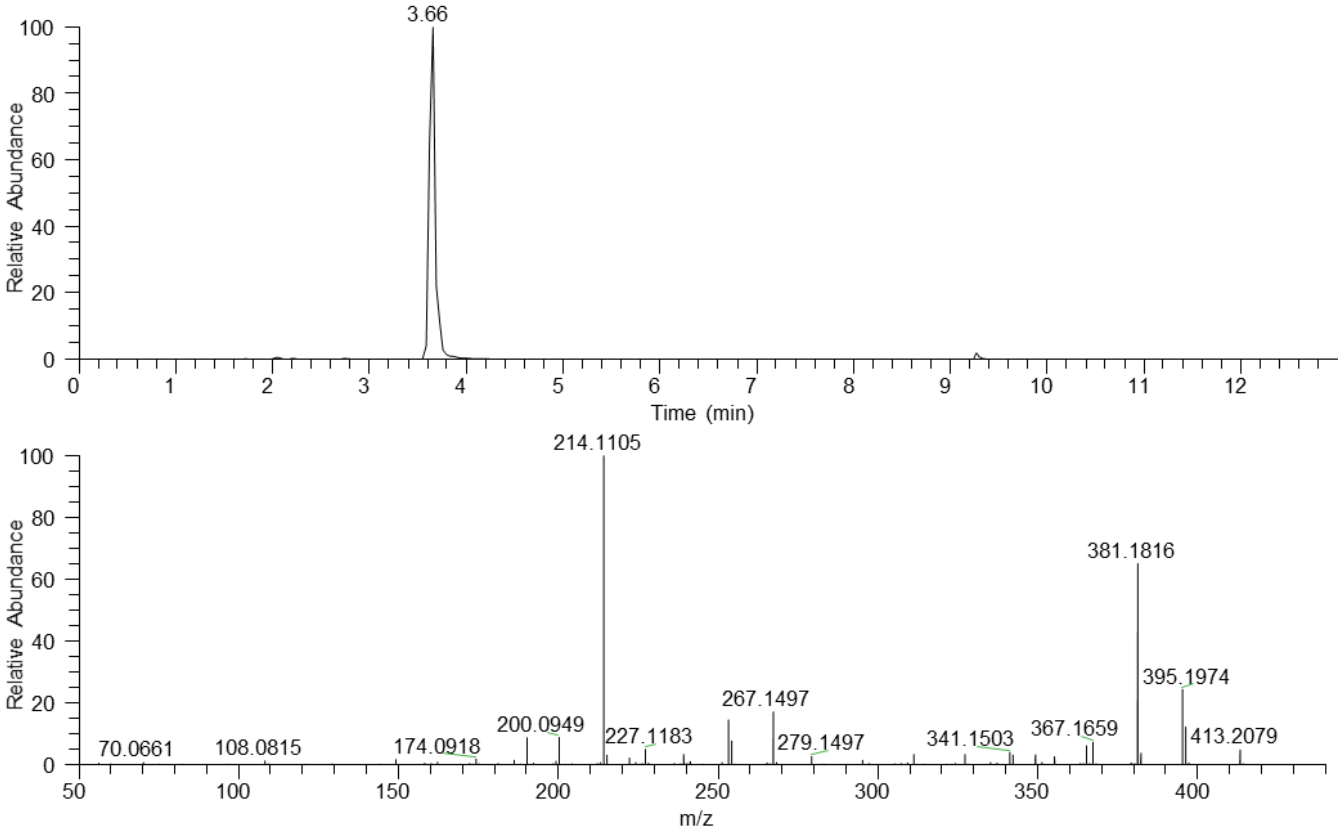

Figure S37. UPLC-HRESIMS data for isopaynantheine-*N*(4)-oxide (**10**).

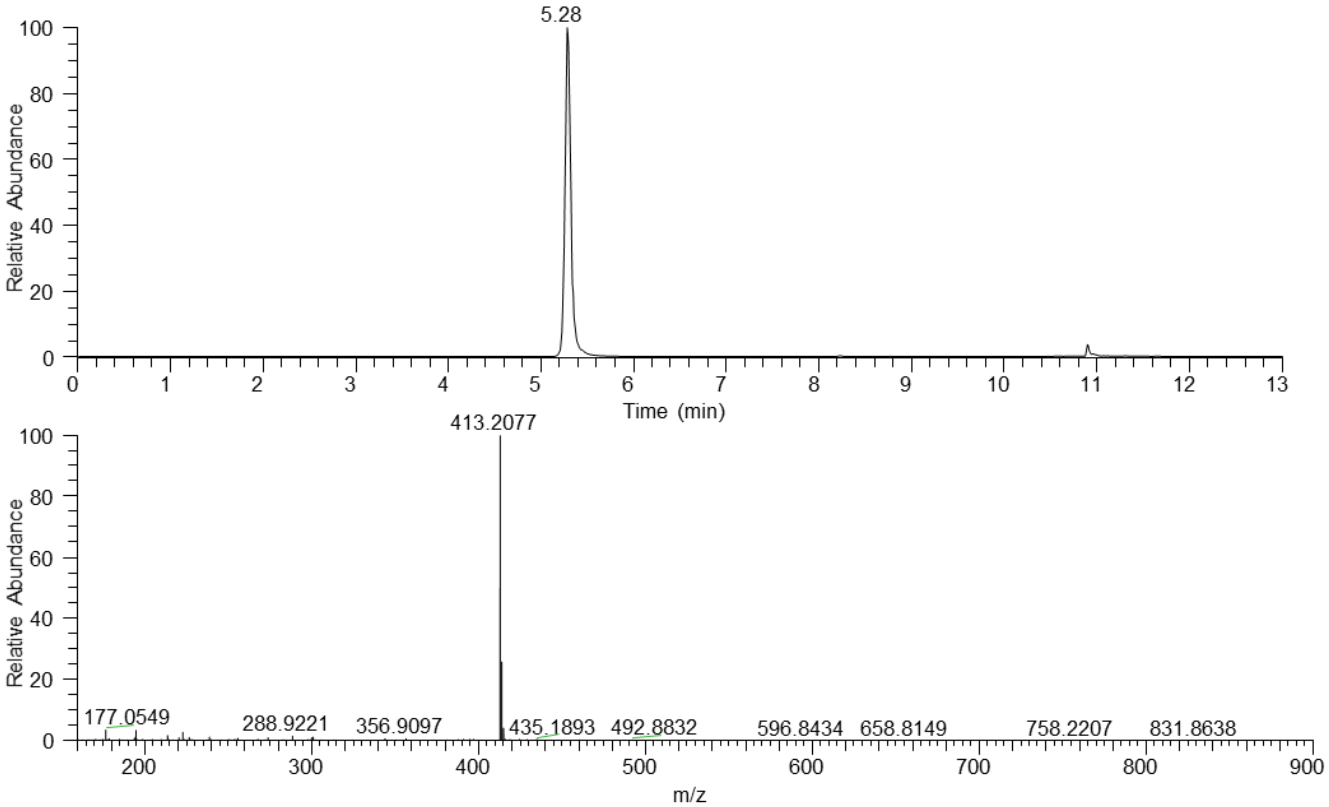

Figure S38. UPLC-HRESIMS data for epiallo-isopaynantheine-*N*(4)-oxide (**11**)

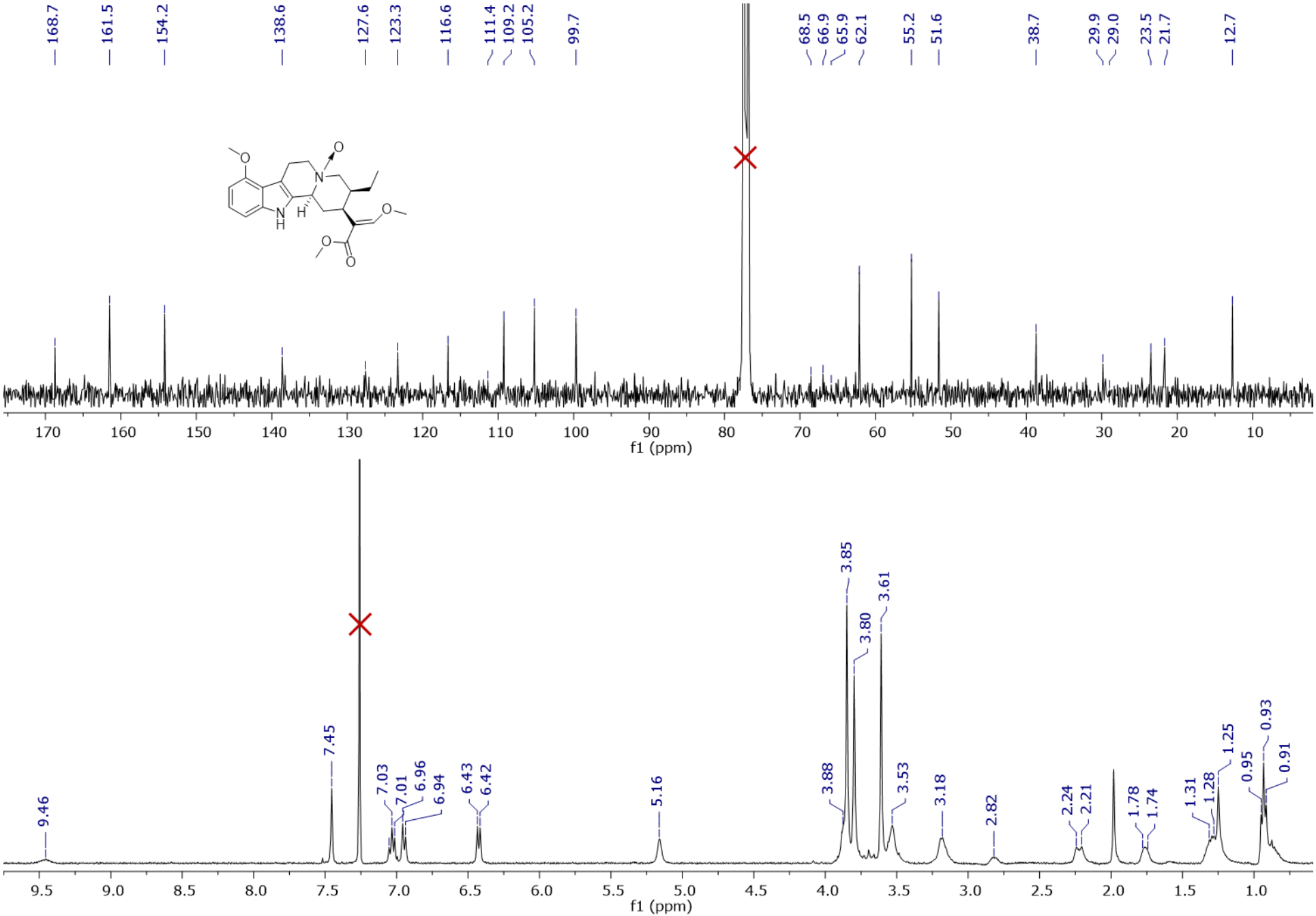

Figure S39. ^{1}H and ^{13}C NMR spectra for mitragynine-*N*(4)-oxide (**8**) ($CDCl_3$, 400 MHz and 100 MHz, respectively).

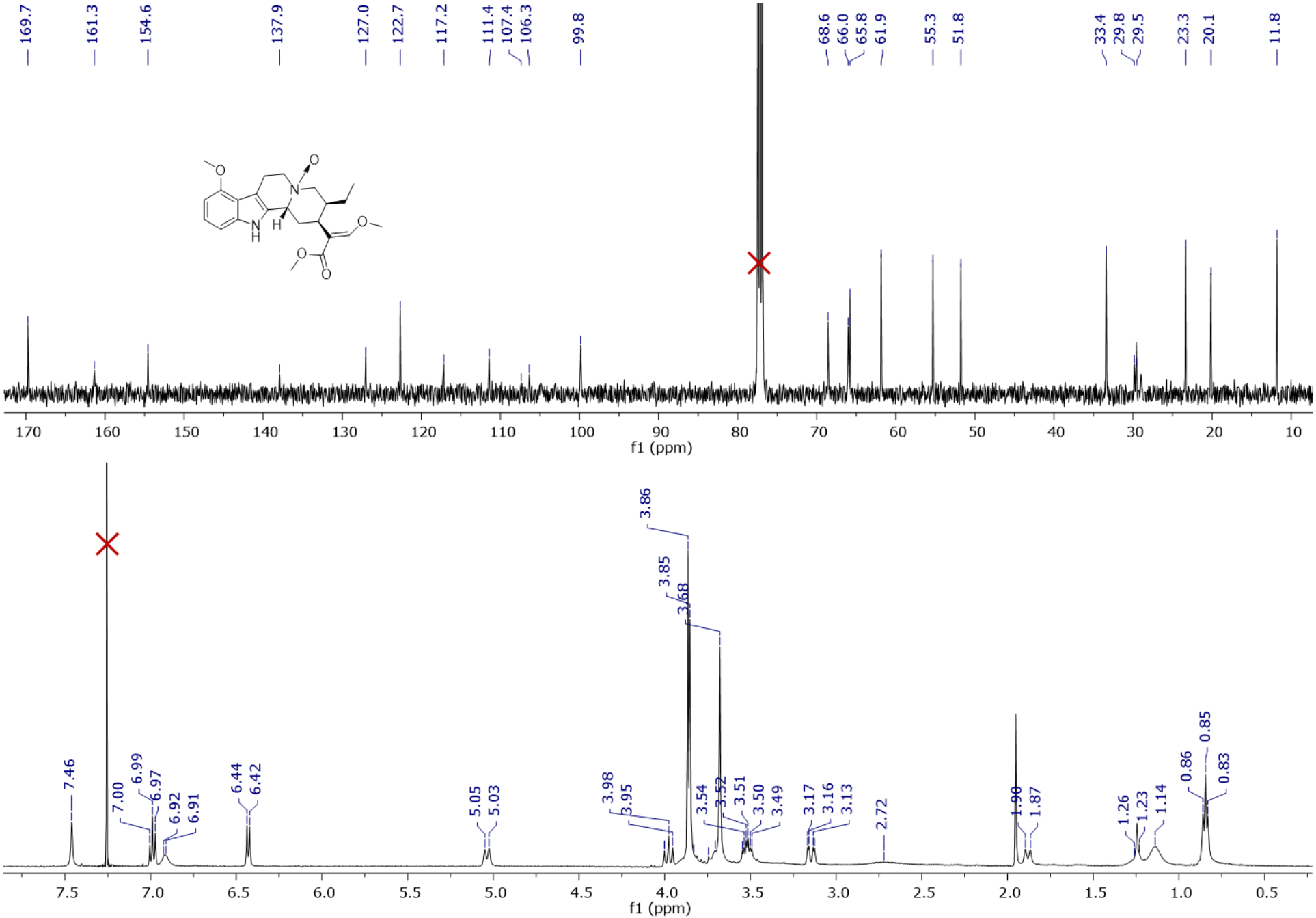

Figure S40. ^{1}H and ^{13}C NMR spectra for speciociliatine-*N*(4)-oxide (**9**) ($CDCl_3$, 400 MHz and 100 MHz, respectively).

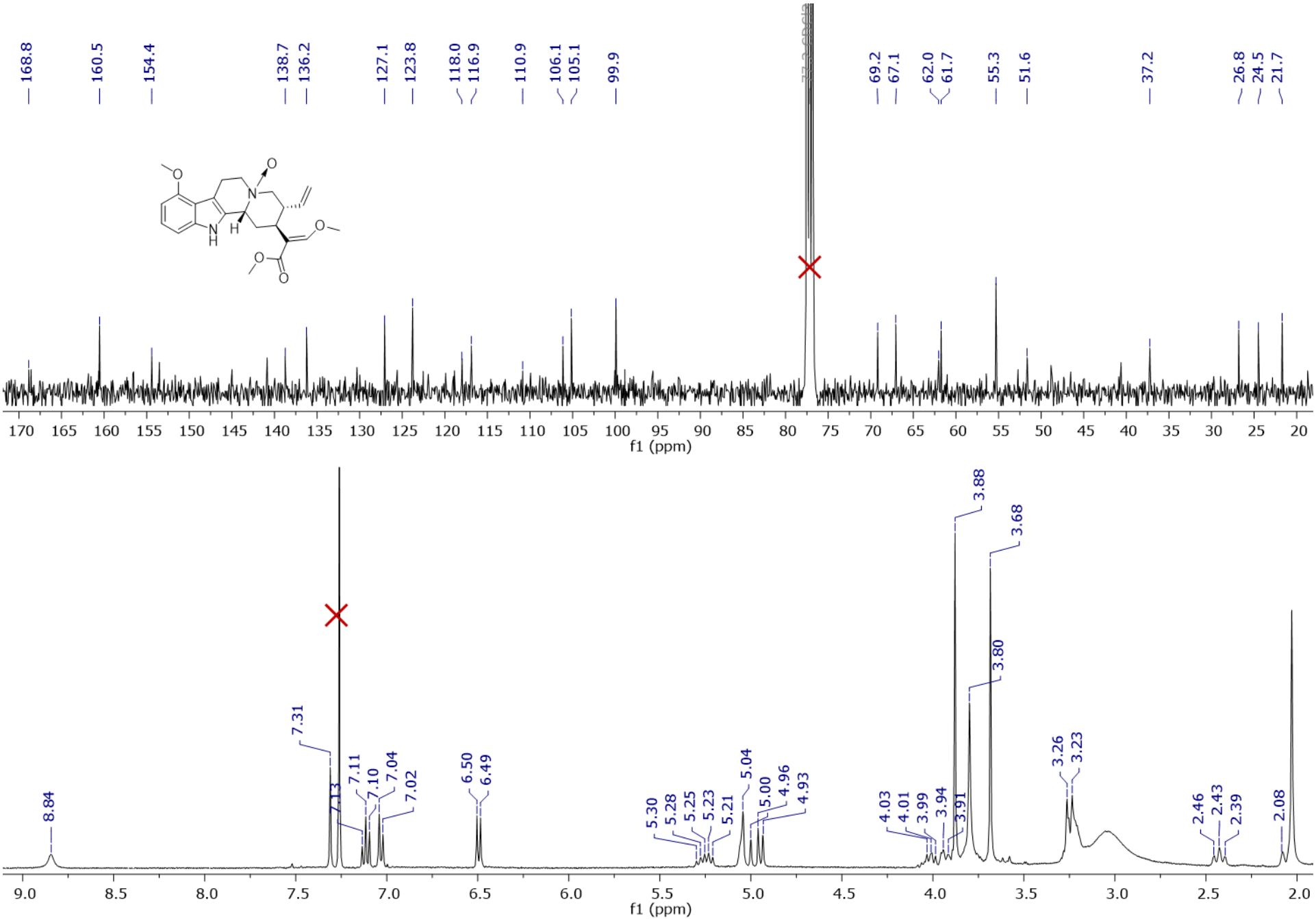

Figure S41. ^{1}H and ^{13}C NMR spectra for isopaynantheine-*N*(4)-oxide (**10**) ($CDCl_3$, 400 MHz and 100 MHz, respectively).

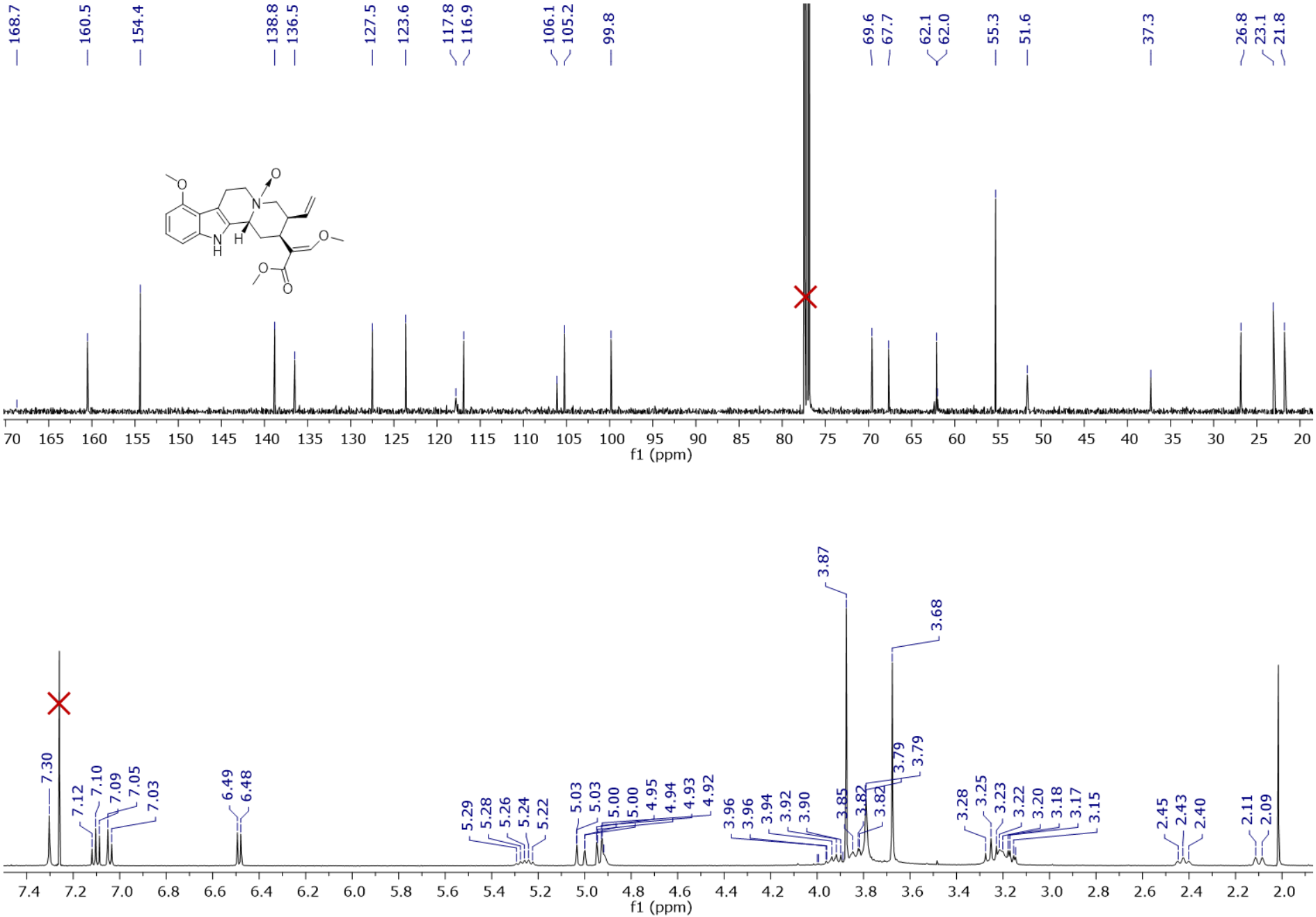

Figure S42. ^{1}H and ^{13}C NMR spectra for epiallo-isopaynantheine-*N*(4)-oxide (**11**) ($CDCl_3$, 400 MHz and 100 MHz, respectively).

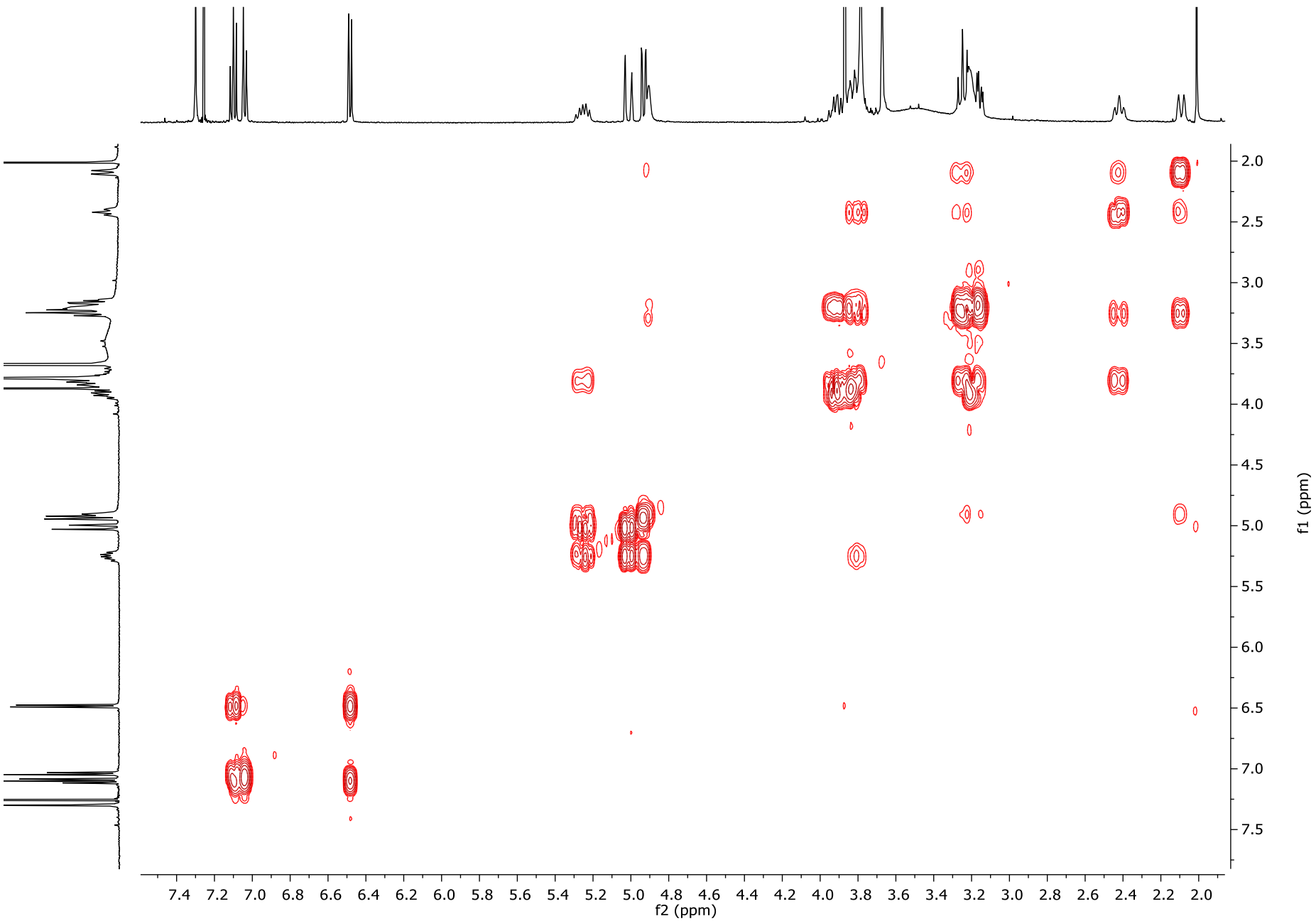

Figure S43. COSY spectrum for epiallo-isopaynantheine-*N*(4)-oxide (**11**) ($CDCl_3$, 400 MHz).

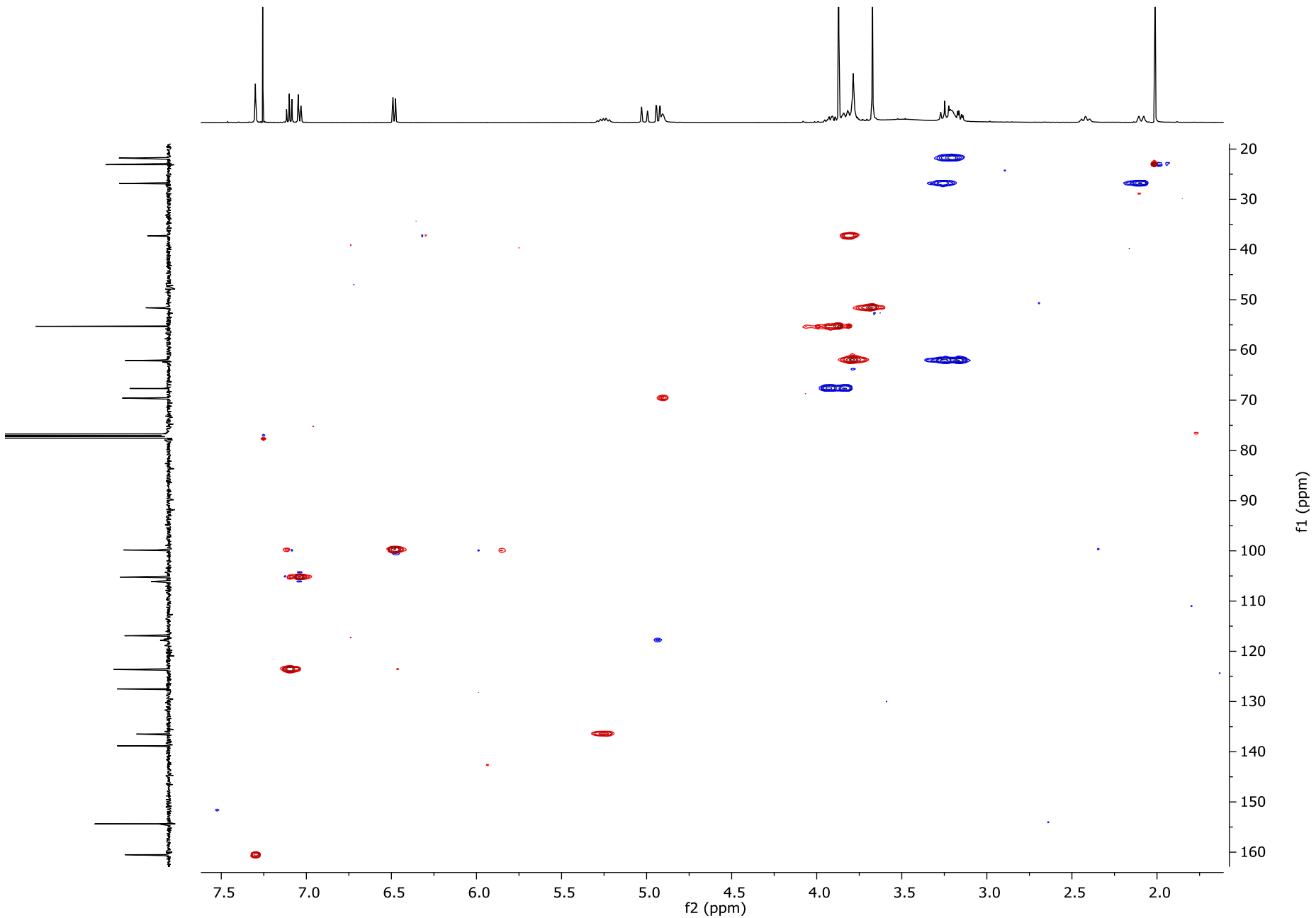

Figure S44. HSQC spectrum for epiallo-isopaynantheine-*N*(4)-oxide (**11**) ($CDCl_3$, 400 MHz).

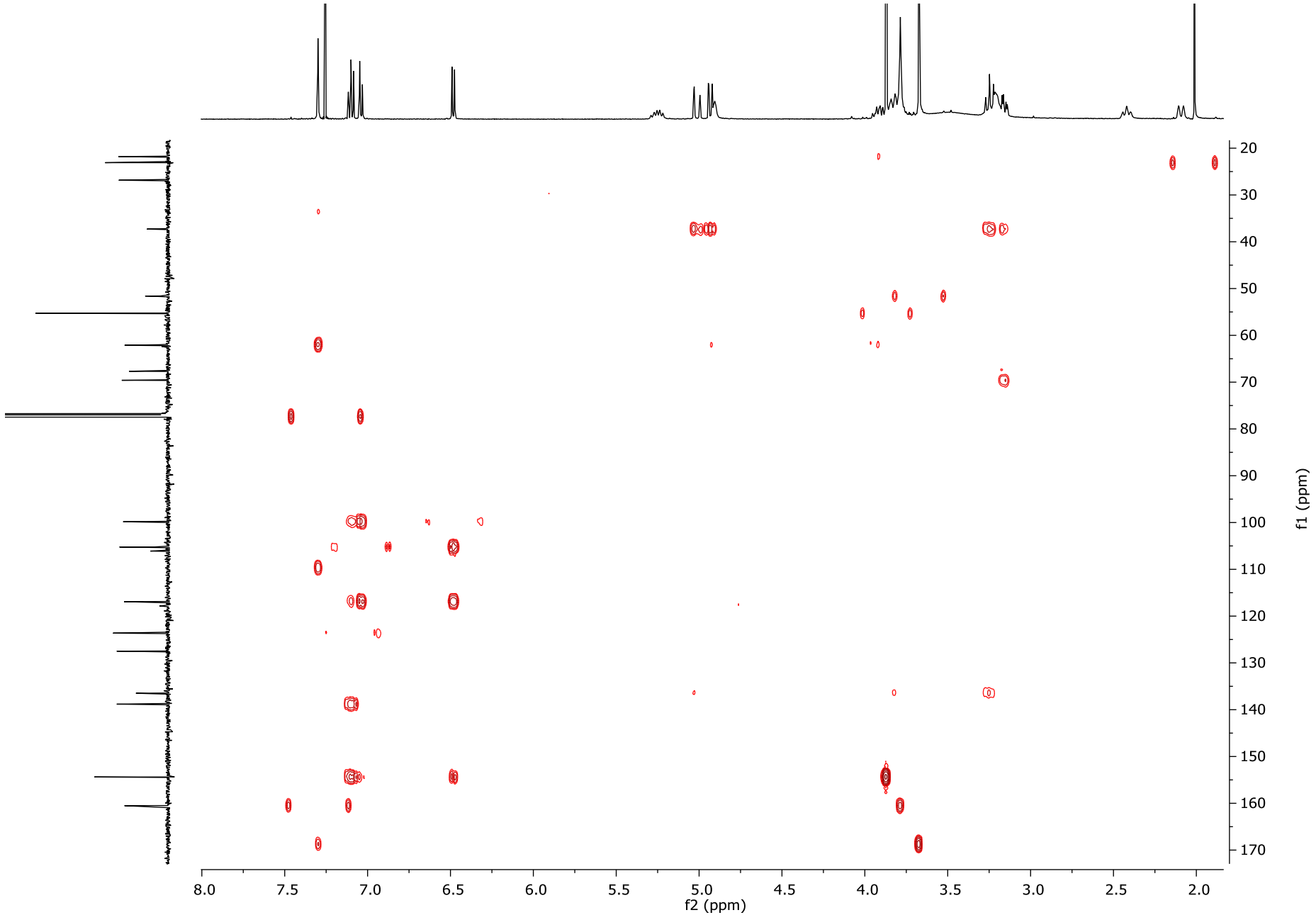

Figure S45. HMBC spectrum for epiallo-isopaynantheine-*N*(4)-oxide (**11**) ($CDCl_3$, 400 MHz).

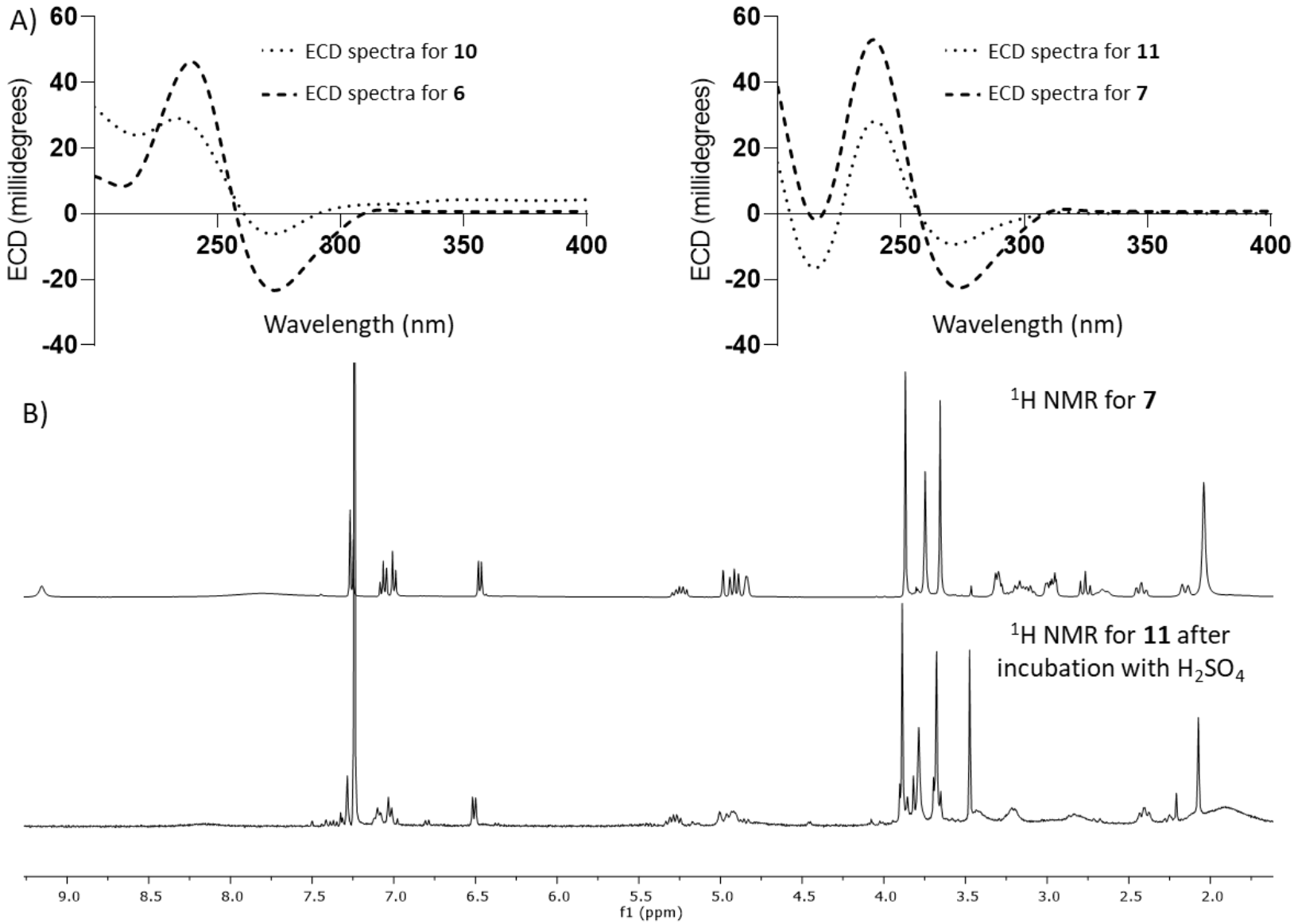

Figure S46. A) Comparison of the ECD spectra for *N*-oxides (**10** and **11**), and indole alkaloids (**6** and **7**); B) Comparison of the ^{1}H NMR of **7**, and that of **11** after incubation with sulfuric acid.

Table S6. Comparison of NMR Data for Compounds 8-11 ($CDCl_3$, 100 MHz and 400 MHz)

	mitragynine-*N*(4)-oxide (**8**)			speciociliatine-*N*(4)-oxide (**9**)			isopaynantheine-*N*(4)-oxide (**10**)			epiallo-isopaynantheine-*N*(4)-oxide (**11**)		
position	δ_C	type	δ_H (*J* in Hz)	δ_C	type	δ_H (*J* in Hz)	δ_C	type	δ_H (*J* in Hz)	δ_C	type	δ_H (*J* in Hz)
2	127.6	C		127.0	C		127.1	C		127.5	C	
3	66.9	CH	5.16, s	66.0	CH	5.04, d (12.5)	69.2	CH	5.04, bs	69.6	CH	4.91, bs
5	65.9	CH_2	3.88, m	65.8	CH_2	3.98, m	67.1	CH_2	3.81,m	67.7	CH_2	3.94, m
						3.51, td (11.7, 4.7)						3.83, m
6	21.7	CH_2	3.18, m	20.1	CH_2	3.15, dd (16.7, 4.5)	21.7	CH_2	3.25, m	21.8	CH_2	3.20, m
7	109.2	C		107.4	C		106.1	C		106.1	C	
8	116.6	C		117.2	C		116.9	C		116.9	C	
9	154.2	C		154.6	C		154.4	C		154.4	C	
10	99.7	CH	6.43, d (7.7)	99.8	CH	6.43, d (7.7)	99.9	CH	6.49, d (7.8)	99.8	CH	6.48 d (7.7
11	123.3	CH	7.03, t (7.9)	122.7	CH	6.99, t (7.9)	123.8	CH	7.11, t (7.9)	123.6	CH	7.10, t (7.9)
12	105.2	CH	6.95, d (8.1)	106.3	CH	6.92, bs	105.1	CH	7.03, d (8.2)	105.2	CH	7.04, d (8.1)
13	138.6	C	-	137.9	C	-	138.7	C	-	138.8	C	
14	29.0	CH_2	2.23, d (15.0)	29.5	CH_2	1.25, m	26.8	CH_2	2.08, m	26.8	CH_2	2.10, d (13.8)
15	29.9	CH_2	2.82, bs	29.8	CH_2	1.88, d (14.7)	24.5	CH_2	2.43, t (12.3)	23.1	CH_2	2.42 t (11.4)
16	111.4	C	-	111.4	C	-	110.9	C	-	109.1[a]	C	
17	161.5	CH	7.45, s	161.3	CH	7.46, s	160.5	CH	7.31, s	160.5	CH	7.30, s
18	12.7	CH_3	0.93, t (7.2)	11.8	CH_3	0.85, t (7.4)	118.0	CH_2	5.02, dd (17.5, 1.0)	117.8	CH_2	5.02, d (17.2)
									4.95, dd (10.2, 1.7)			4.94, dd (10.3, 1.6)
19	23.5	CH_2	1.31, m	23.3	CH_2	1.14, m	136.2	CH	5.25, dt (17.5, 9.3)	136.5	CH	5.26, dt (17.5, 8.6)
			1.28, m									
20	38.7	CH	1.76, bs	33.4	CH	2.72, bs	37.2	CH	3.85, m	37.3	CH	3.81, m
21	68.5	CH_2	3.53, m	68.6	CH_2	3.72, m	61.7	CH_2	3.25, m	62.1	CH_2	3.25, t (11.7)
									3.10, m			3.17, m
22	168.7	C		169.7	C		168.8	C		168.7	C	
9-OCH_3	55.2	CH_3	3.85, s	55.3	CH_3	3.86, s	55.3	CH_3	3.88, s	55.3	CH_3	3.87, s
17-OCH_3	62.1	CH_3	3.80, s	61.9	CH_3	3.85, s	62.0	CH_3	3.80, s	62.0	CH_3	3.79, s
22-OCH_3	51.6	CH_3	3.61, s	51.8	CH_3	3.68, s	51.6	CH_3	3.68, s	51.6	CH_3	3.68, s
NH			9.46, s			-			8.84, s			-

[a]Signal observed by HMBC

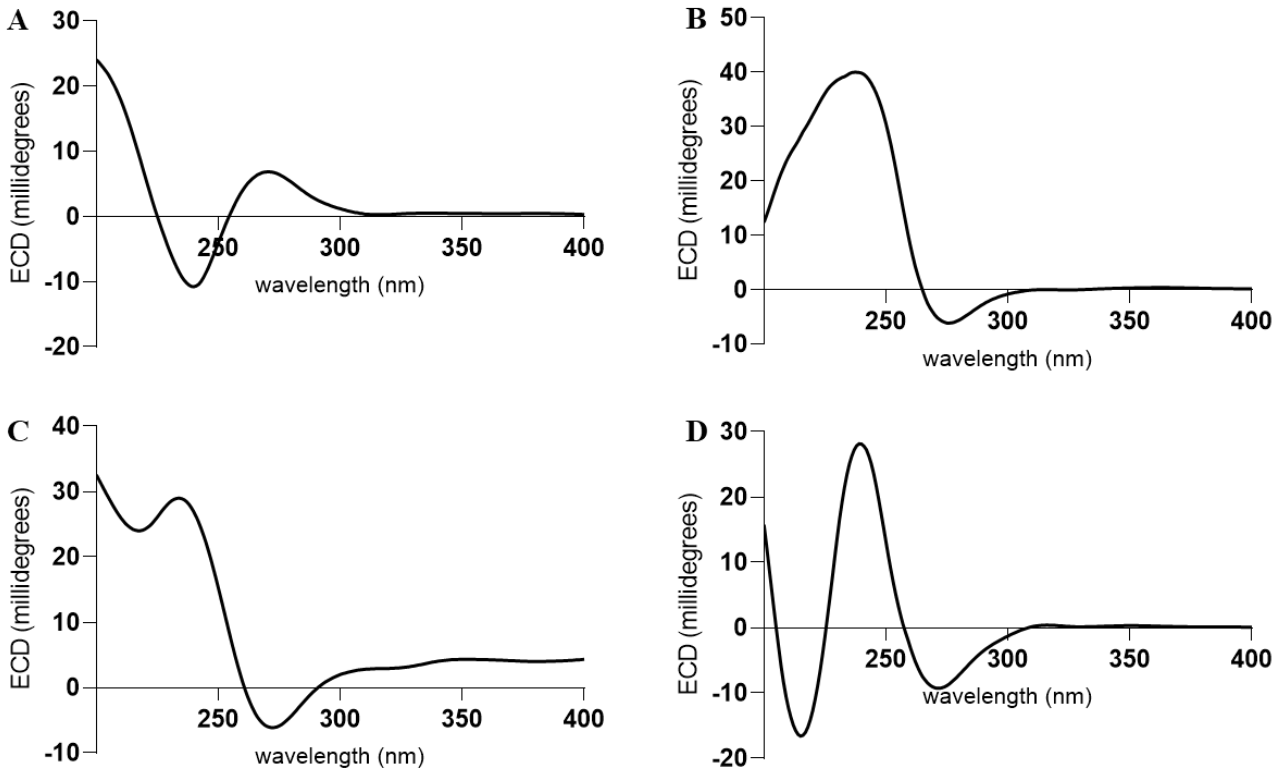

Figure S47. Comparison of the ECD spectra acquired in CH_3OH for A) mitragynine-*N*(4)-oxide (**8**), B) speciociliatine-*N*(4)-oxide (**9**), C) isopaynantheine-*N*(4)-oxide (**10**), and D) epiallo-isopaynantheine-*N*(4)-oxide (**11**).

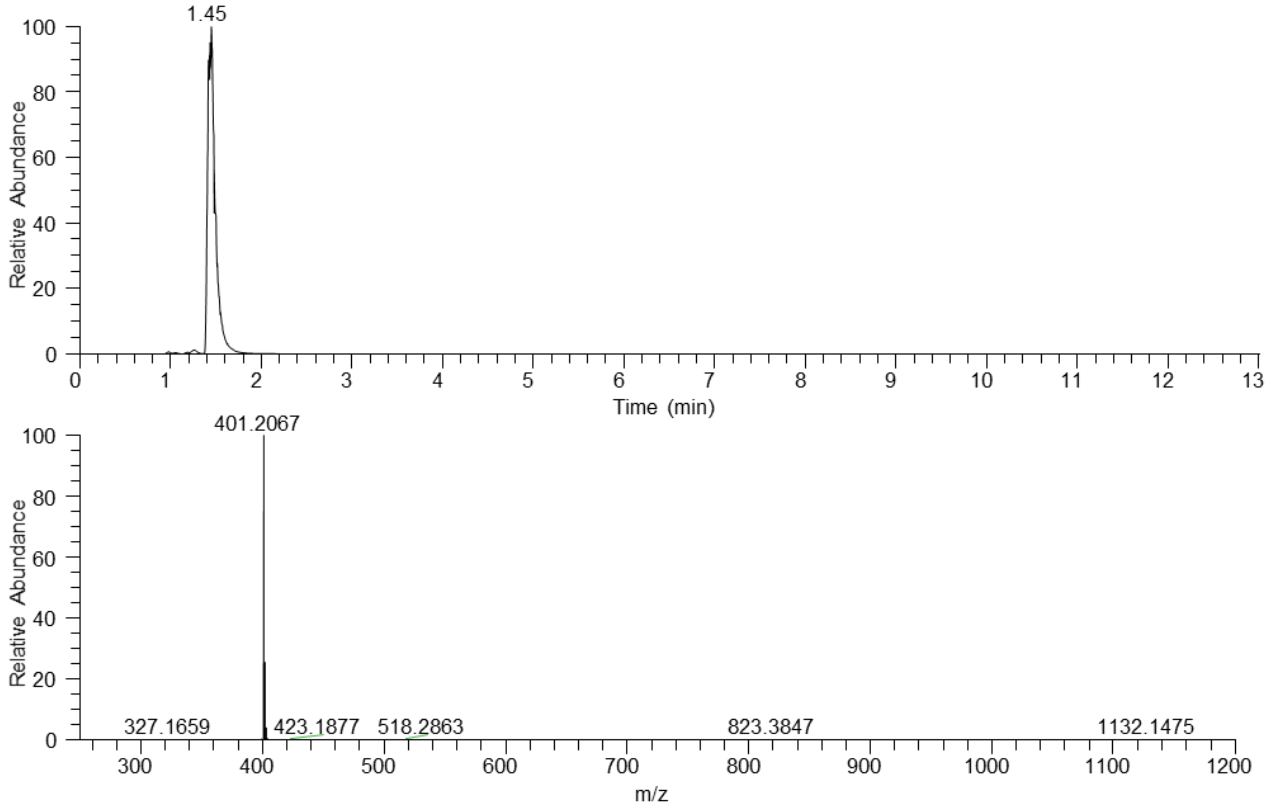

Figure S48. UPLC-HRESIMS data for speciofoline (**12**).

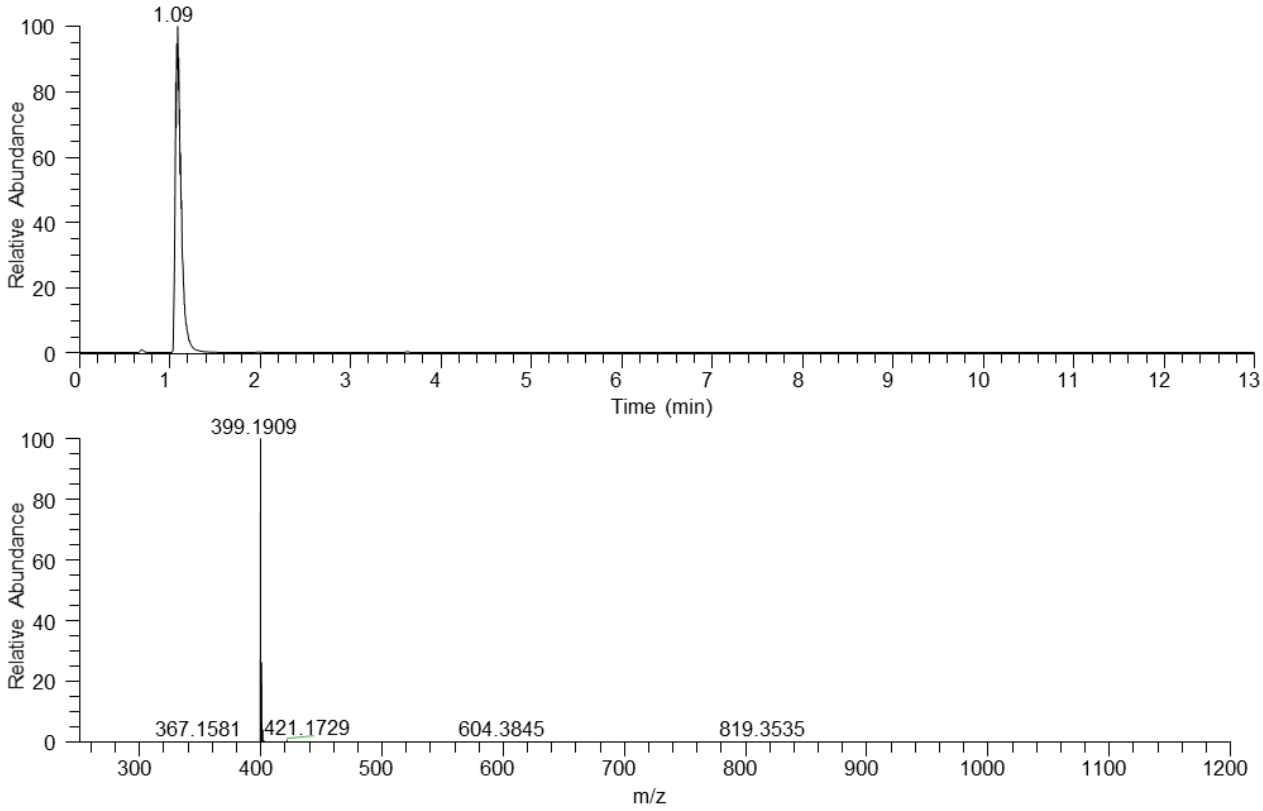

Figure S49. UPLC-HRESIMS data for isorotundifoleine (**13**).

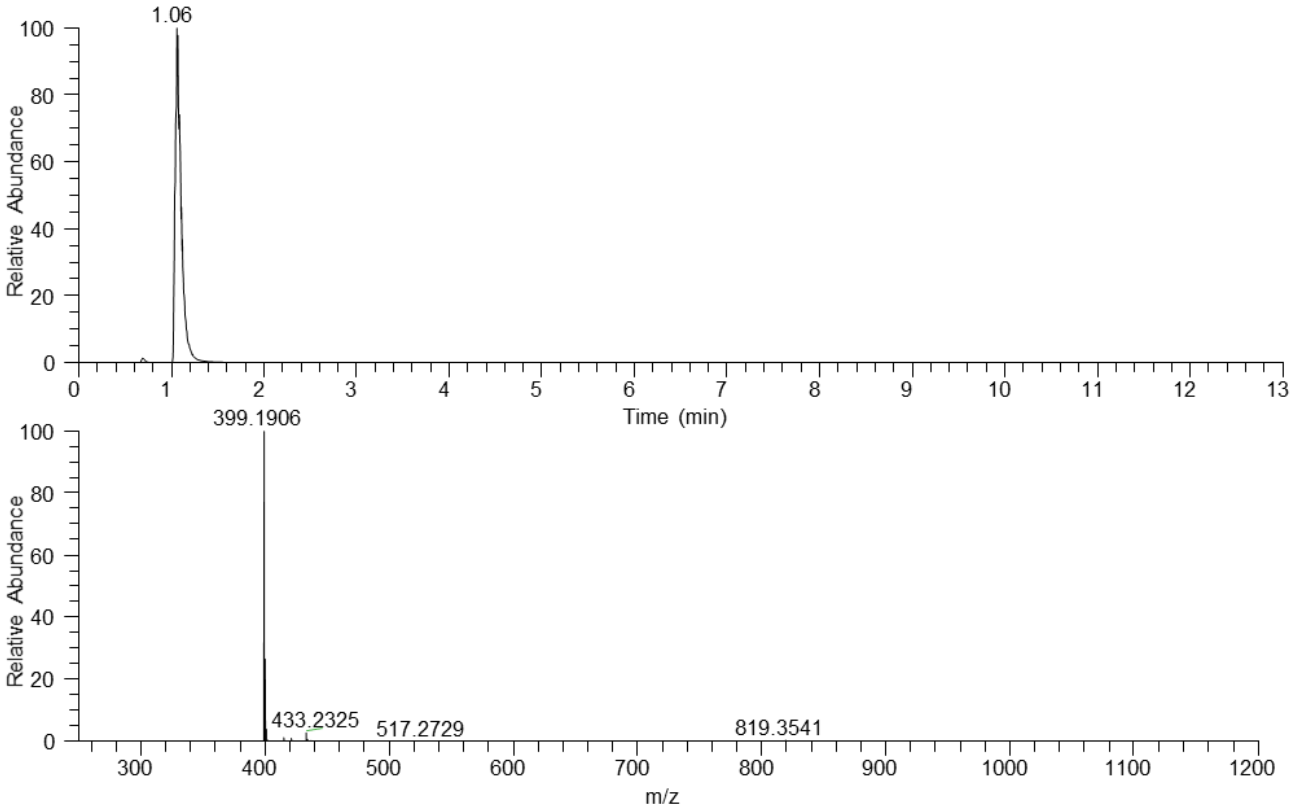

Figure S50. UPLC-HRESIMS data for isospeciofoleine (**14**).

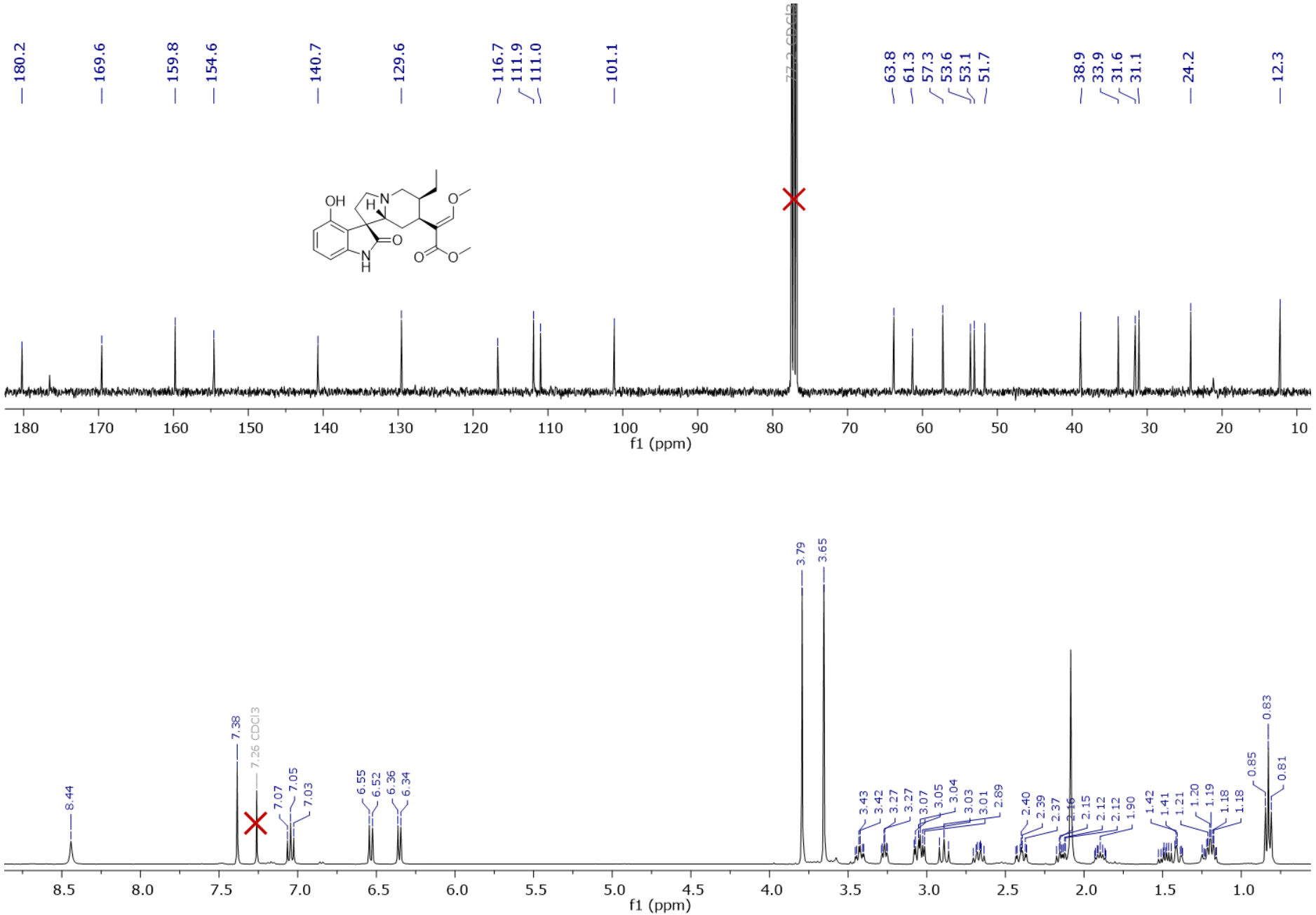

Figure S51. ^{1}H and ^{13}C NMR spectra for speciofoline (**12**) ($CDCl_3$, 400 MHz and 100 MHz, respectively).

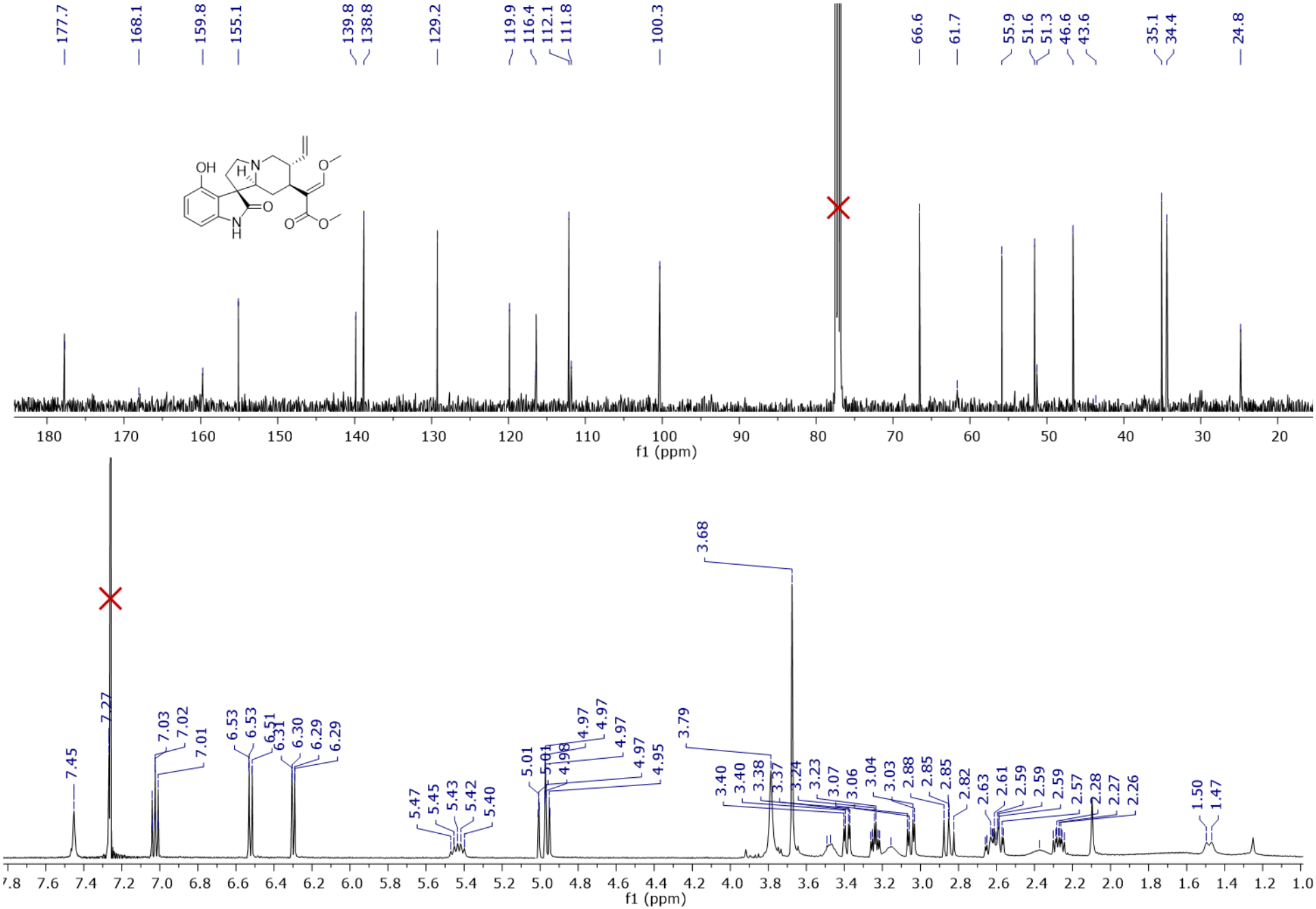

Figure S52. ^{1}H and ^{13}C NMR spectra for isorotundifoleine (**13**) ($CDCl_3$, 500 MHz and 125 MHz, respectively).

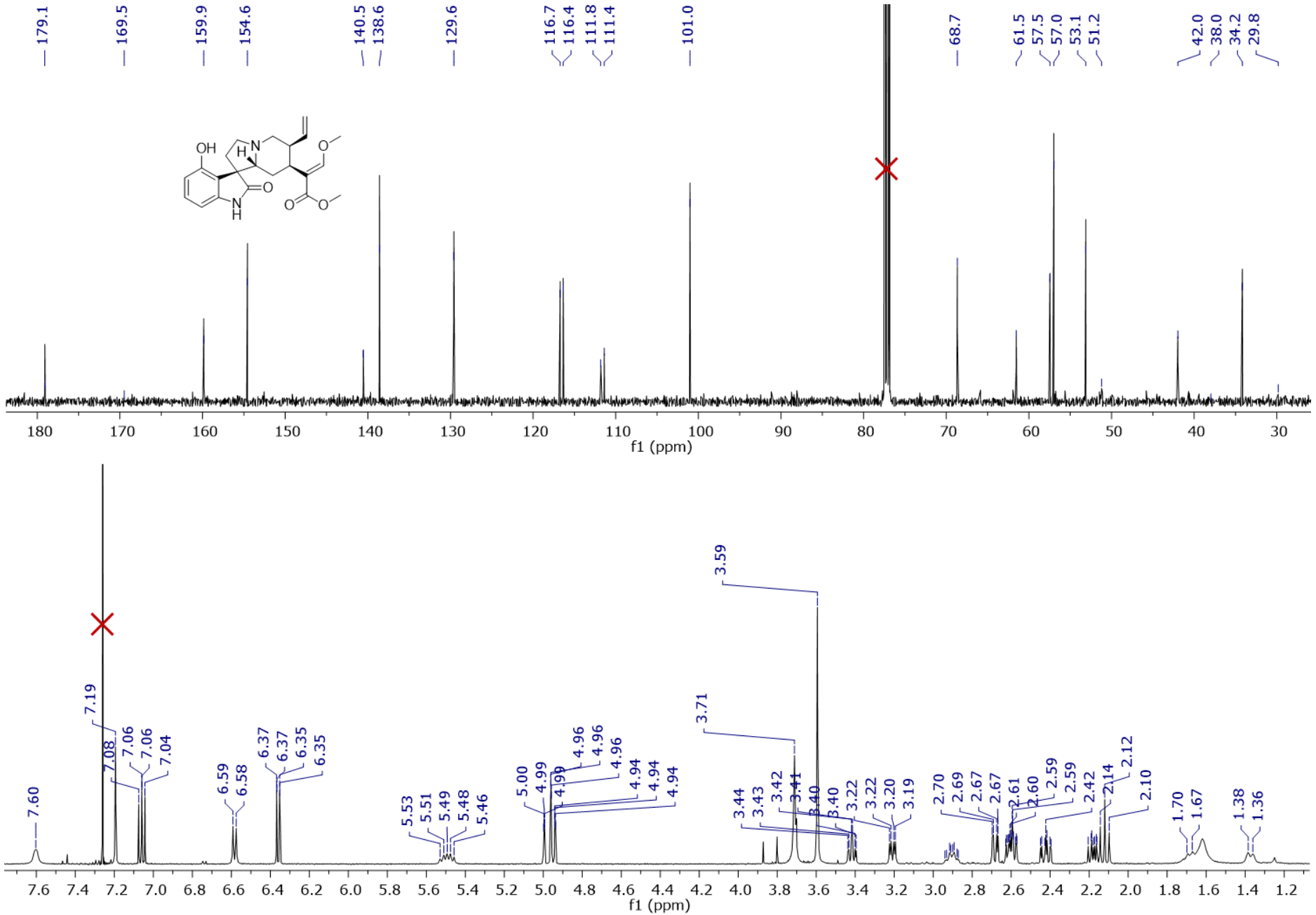

Figure S53. ^{1}H and ^{13}C NMR spectra for isospeciofoleine (**14**) ($CDCl_3$, 500 MHz and 125 MHz, respectively).

Table S7. Comparison of NMR Data for Compounds 12-14 ($CDCl_3$, 125 MHz and 500 MHz)

	speciofoline (**12**)			isorotundifoleine (**13**)			isospeciofoleine (**14**)		
Position	δ_C	type	δ_H (*J* in Hz)	δ_C	type	δ_H (*J* in Hz)	δ_C	type	δ_H (*J* in Hz)
2	180.2	C		177.7	C		179.1	C	
3	63.8	CH	3.06, dd (11.7, 3.6)	66.6	CH	3.39, dd (12.5, 3.6)	68.7	CH	2.68, dd (11.6, 3.2)
5	53.1	CH_2	3.43, td (9.2, 3.2)	46.6	CH_2	3.48, m	53.1	CH_2	3.42, td (9.2, 3.1)
			2.67, m			3.24, td (9.4, 4.1)			2.60, m
6	33.9	CH_2	2.40, ddd (13.8, 10.9, 3.3)	34.4	CH_2	2.61, m	34.2	CH_2	2.42, ddd (13.7, 10.7, 3.1)
			2.14, m			2.27, ddd (13.5, 9.3, 6.6)			2.18, m
7	57.3	C		55.9	C		57.5	C	
8	116.7	C		119.9	C		116.7	C	
9	154.6	C		155.1	C		154.6	C	
10	111.9	CH	6.35, d (7.6)	112.1	CH	6.30, dd (7.6, 0.8)	111.4	CH	6.36, dd (7.6, 0.7)
11	129.6	CH	7.05, t (8.0)	129.2	CH	7.02, dd (8.3, 7.7)	129.6	CH	7.06, dd (8.3, 7.7)
12	101.1	CH	6.53, d (8.3)	100.3	CH	6.52, dd (8.5, 0.8)	101.0	CH	6.58, d (8.3)
13	140.7	C		139.8	C		140.5	C	
14	31.6	CH_2	1.49, ddd (13.7, 12.1, 6.5)	24.8	CH_2	2.38, m	29.8	CH_2	1.68, d (13.4)
			1.40, m			1.48, d (14.0)			1.37, d (11.8)
15	31.1	CH	3.27, t (5.7)	43.6	CH	2.61, m	38.0	CH	2.60, m
16	111.0	C		111.8	C		111.8	C	
17	159.8	CH	7.38, s	159.8	CH	7.27, s	159.9	CH	7.19, s
18	12.3	CH_3	0.83, d (7.4)	116.4	CH_2	5.01, m	116.4	CH_2	4.97, m
						4.96, m			4.95, m
19	24.2	CH_2	1.21, dqd (14.0, 6.8, 2.8)	138.8	CH	5.43, dt (18.7, 9.1)	138.6	CH	5.49, dt (17.3, 9.5)
20	38.9	CH	1.90, dp (12.3, 7.1)	35.1	CH	3.16, m	42.0	CH	2.90, m
21	53.6	CH_2	3.06, dd (11.7, 3.6)	51.6	CH_2	3.05, dd (14.0, 4.2)	57.0	CH_2	3.21, dd (11.2, 3.9)
			2.89, t (11.6)			2.85, dd (13.8, 12.2)			2.12, t (11.3)
22	169.6	C		168.1	C		169.5	C	
17-OCH_3	61.3	CH_3	3.79, s	61.7	CH_3	3.79, s	61.5	CH_3	3.71, s
22-OCH_3	51.7	CH_3	3.65, s	51.3	CH_3	3.68, s	51.2	CH_3	3.59, s
NH			8.44, s			7.45,s			7.60, s

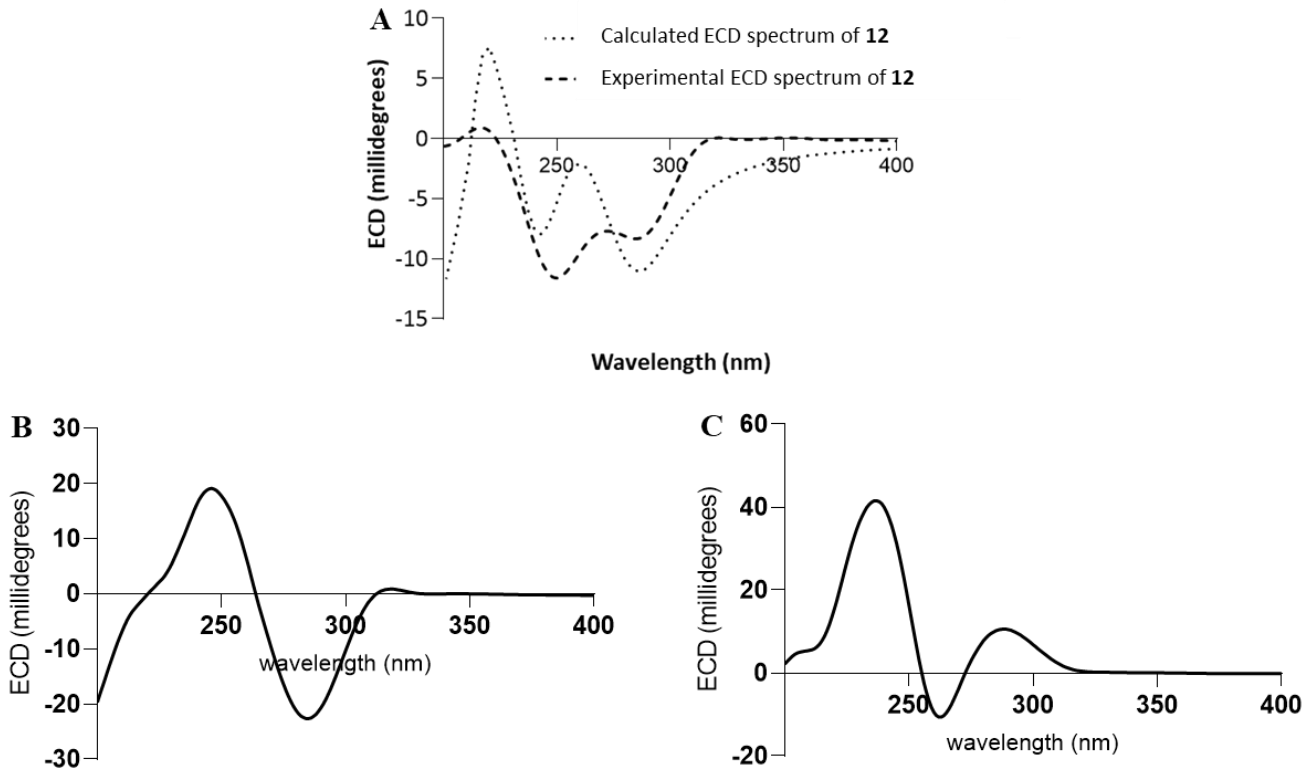

Figure S54. Comparison of the ECD spectra acquired in CH_3OH for A) speciofoline (**12**), B) isorotundifoleine (**13**), and C) isospeciofoleine (**14**).

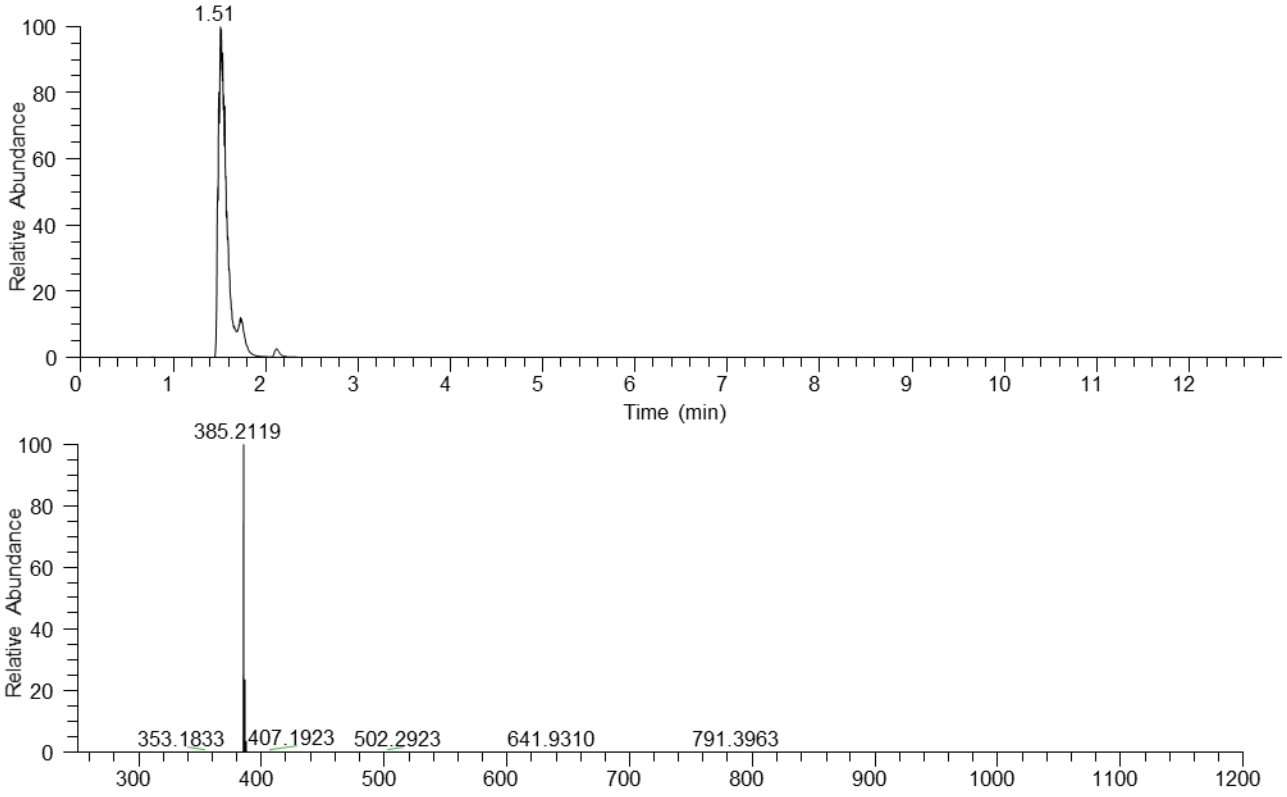

Figure S55. UPLC-HRESIMS data for corynoxine A (**15**).

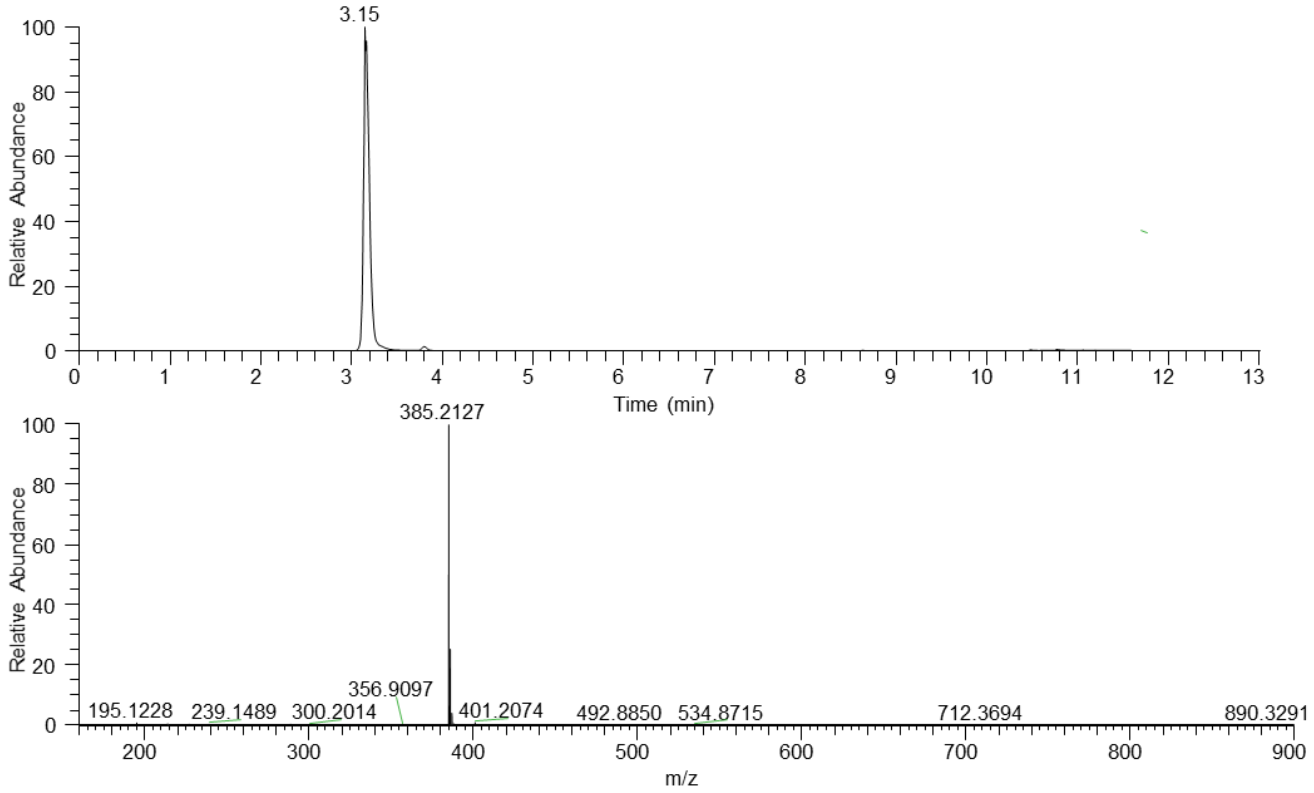

Figure S56. UPLC-HRESIMS data for corynoxine B (**16**).

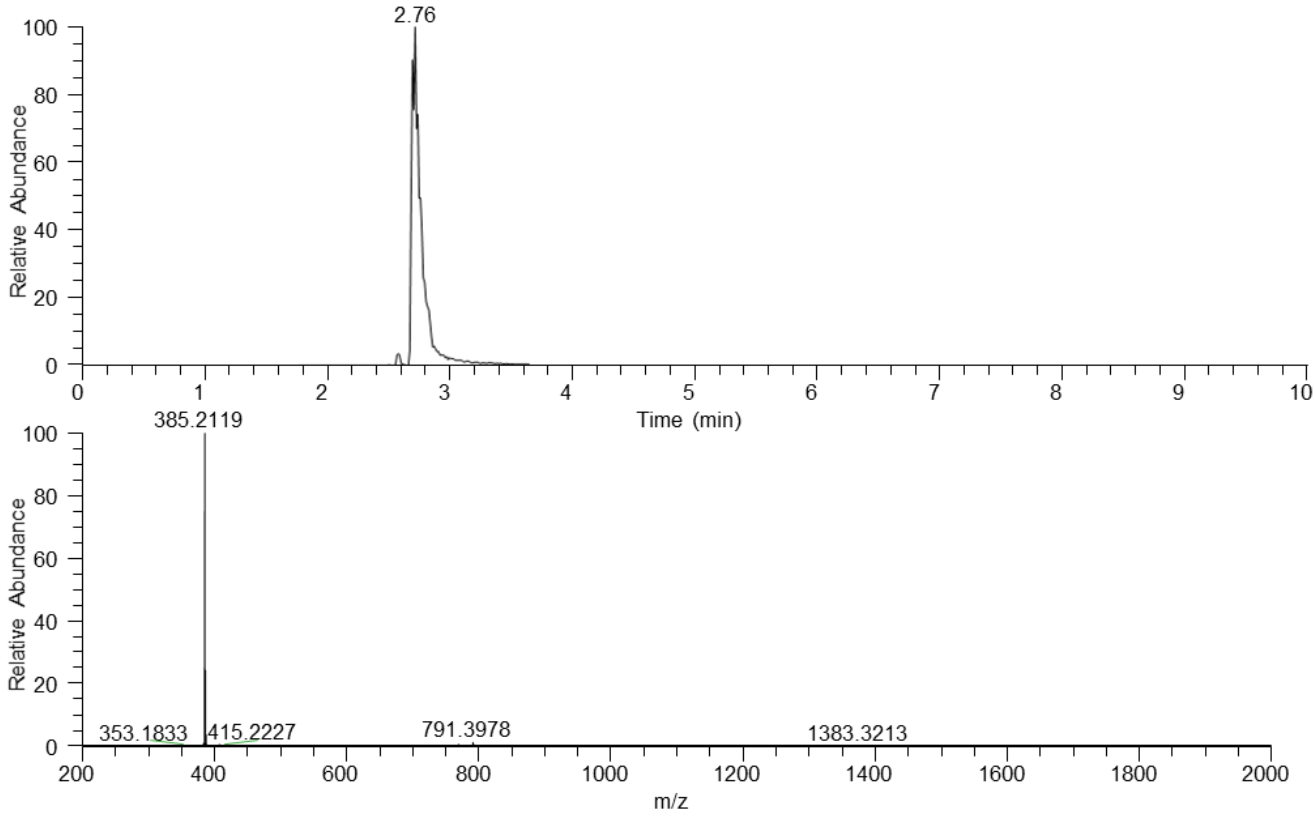

Figure S57. UPLC-HRESIMS data for 3-epirhynchophylline (**17**).

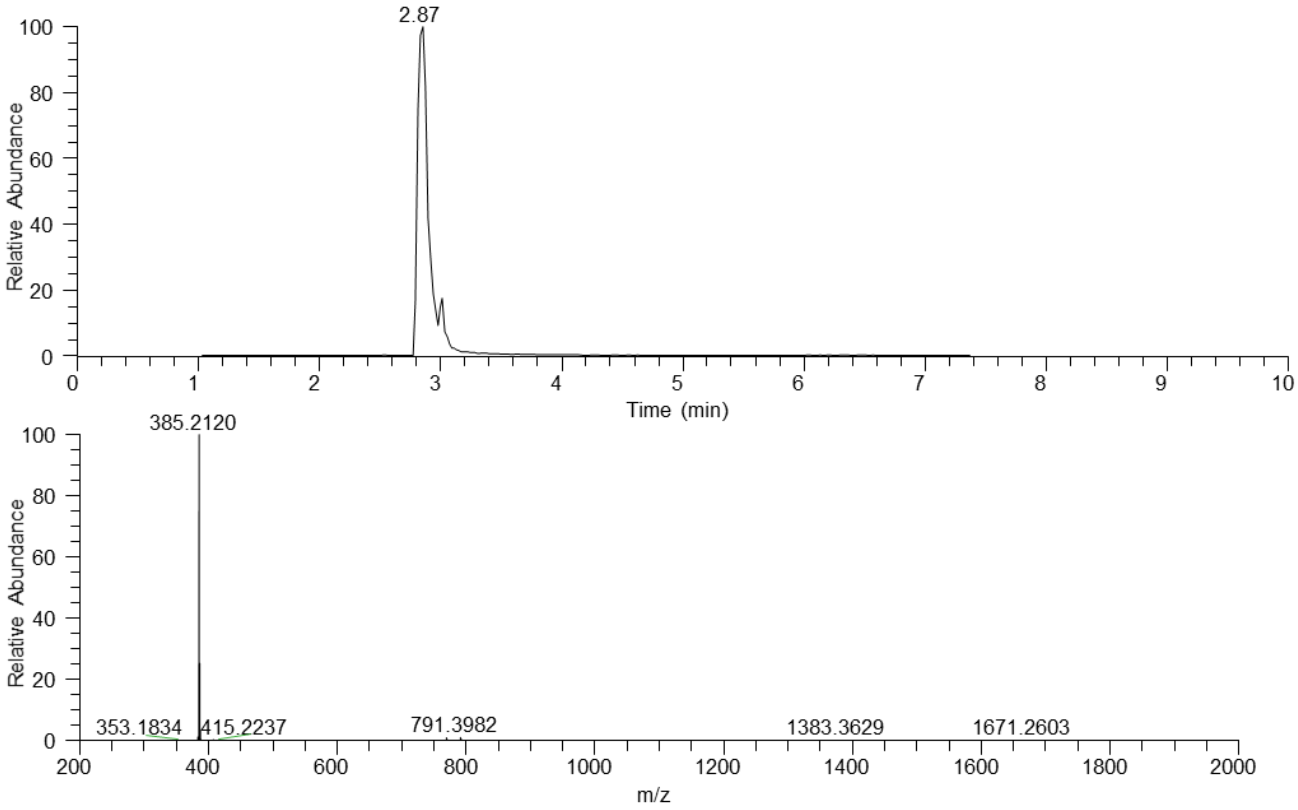

Figure S58. UPLC-HRESIMS data for 3-epicorynoxine B (**18**).

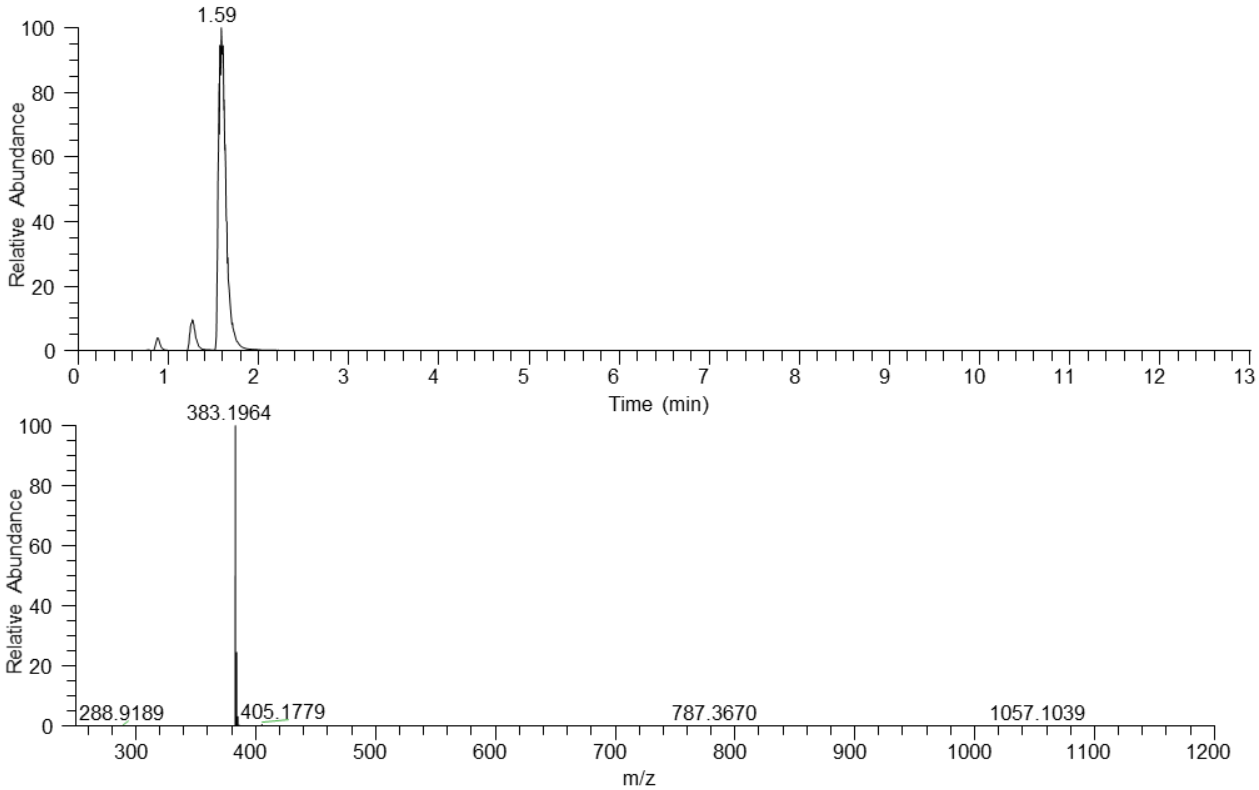

Figure S59. UPLC-HRESIMS data for corynoxeine (**19**)

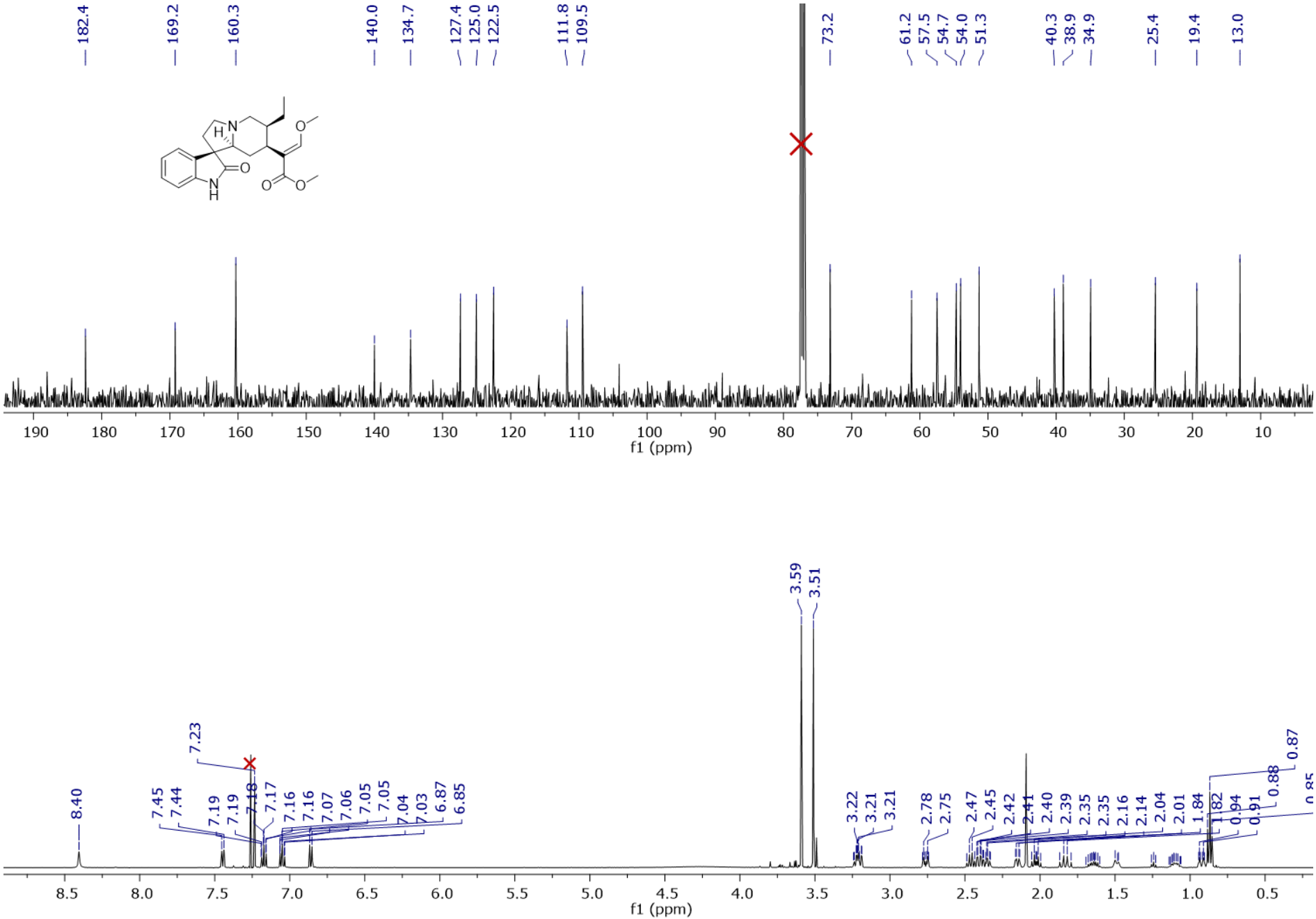

Figure S60. ^{1}H and ^{13}C NMR spectra for corynoxine A (**15**) ($CDCl_3$, 500 MHz and 125 MHz, respectively).

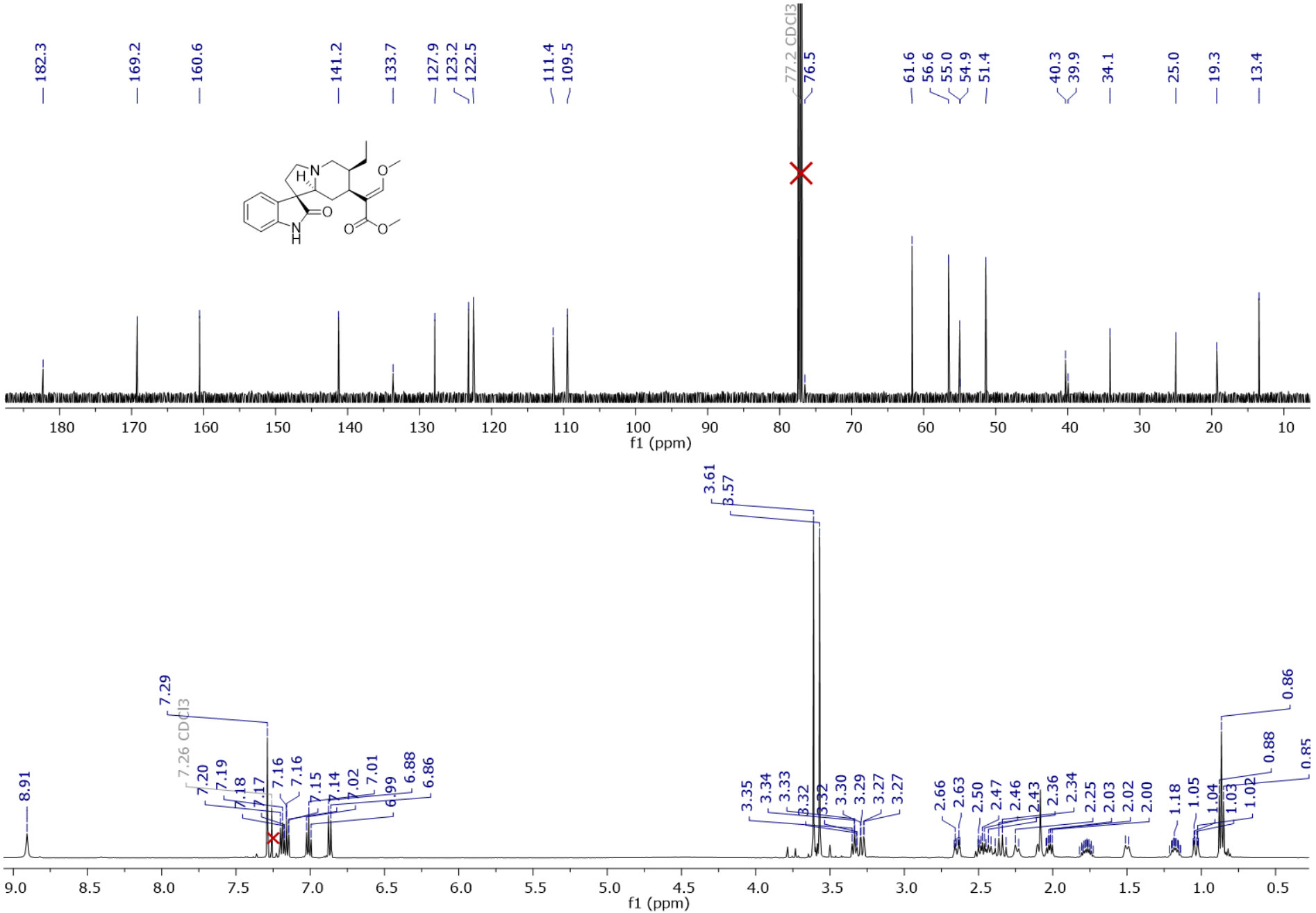

Figure S61. ^{1}H and ^{13}C NMR spectra for corynoxine B (**16**) ($CDCl_3$, 500 MHz and 125 MHz, respectively).

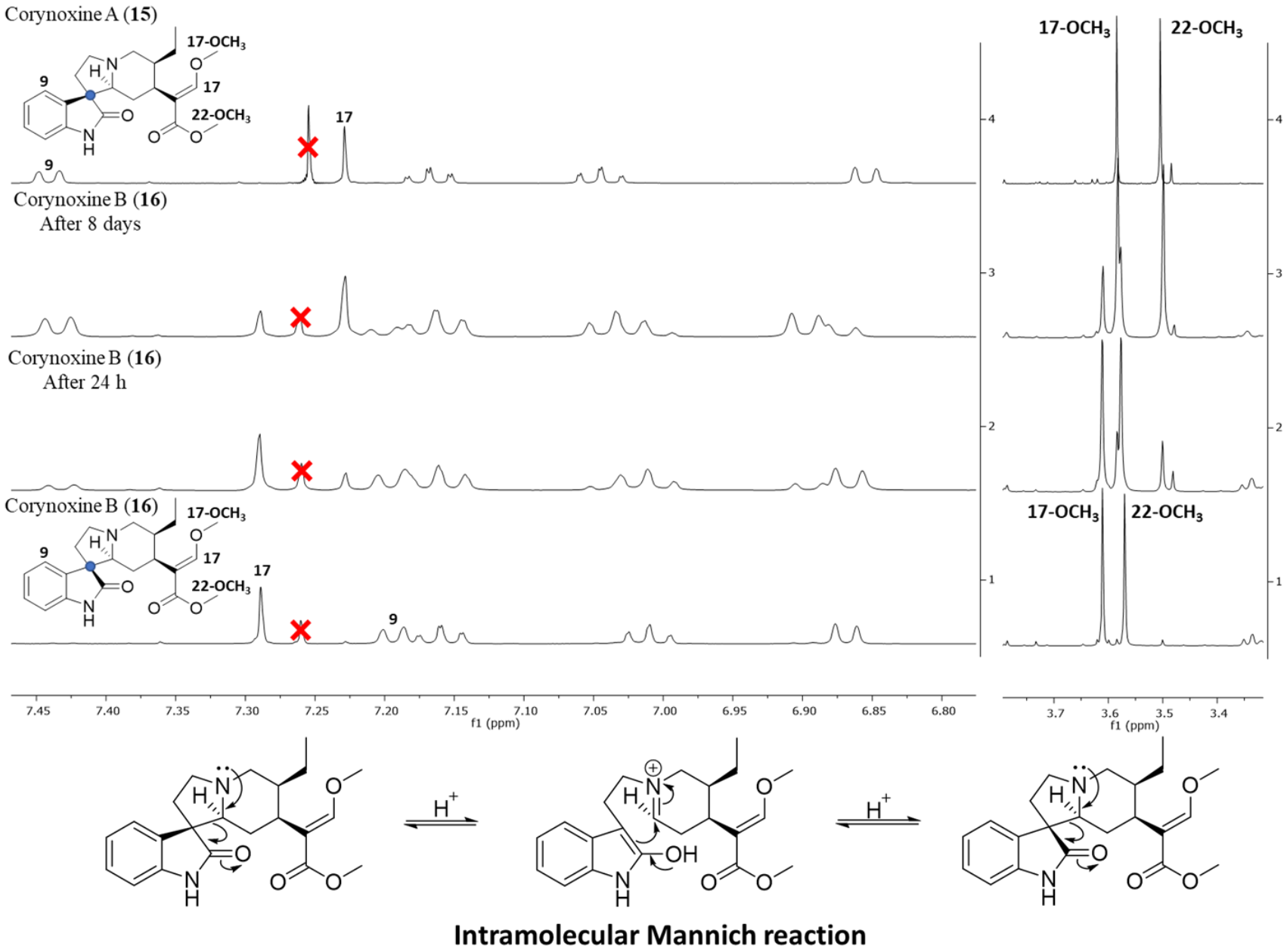

Figure S62. Monitoring the epimerization of corynoxine B (**16**) to corynoxine A (**15**) by ^{1}H NMR ($CDCl_3$, 500 MHz), and the proposed mechanism of epimerization via an intramolecular Mannich reaction.

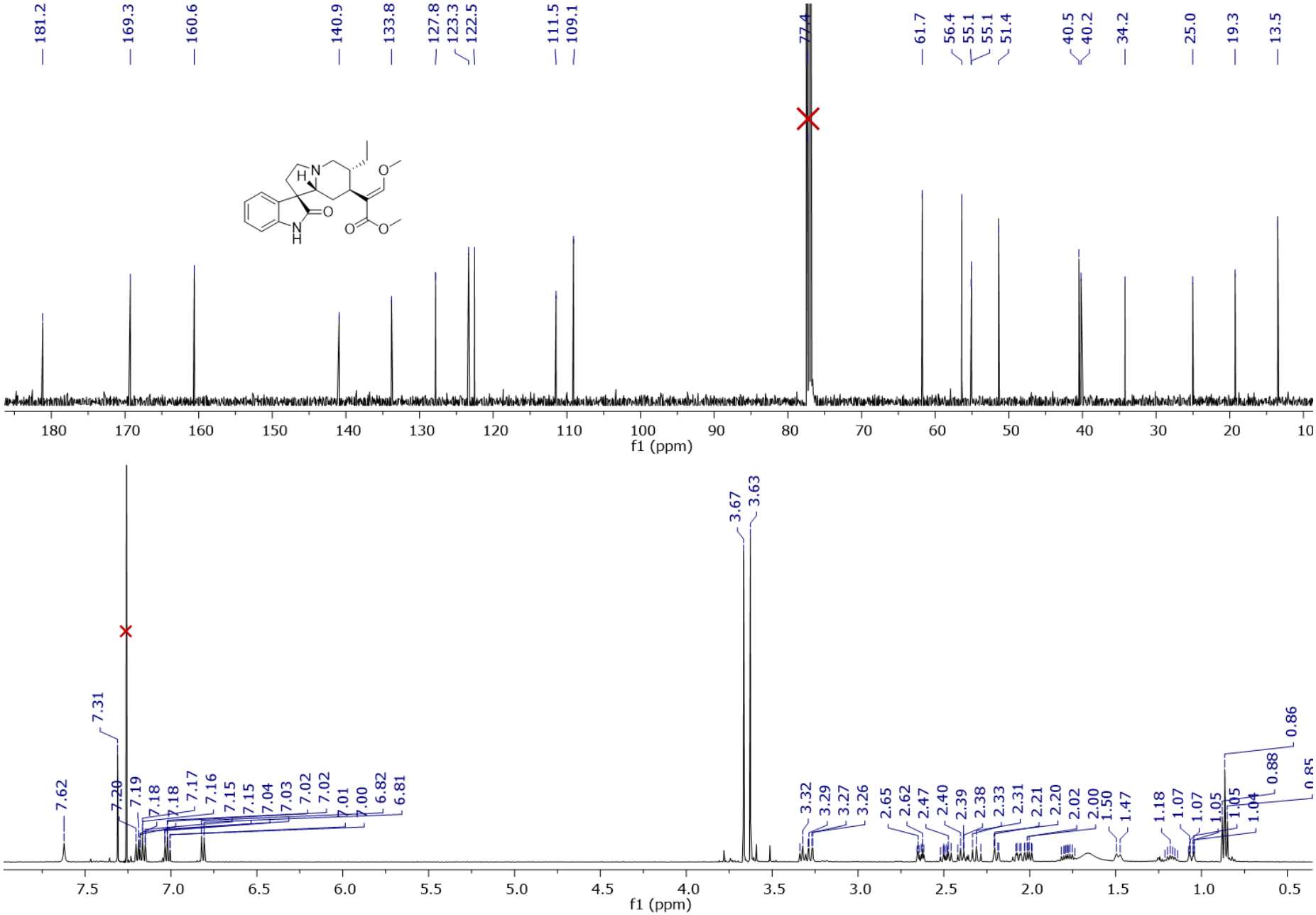

Figure S63. ^{1}H and ^{13}C NMR spectra for 3-epirhynchophylline (**17**) ($CDCl_3$, 500 MHz and 125 MHz, respectively).

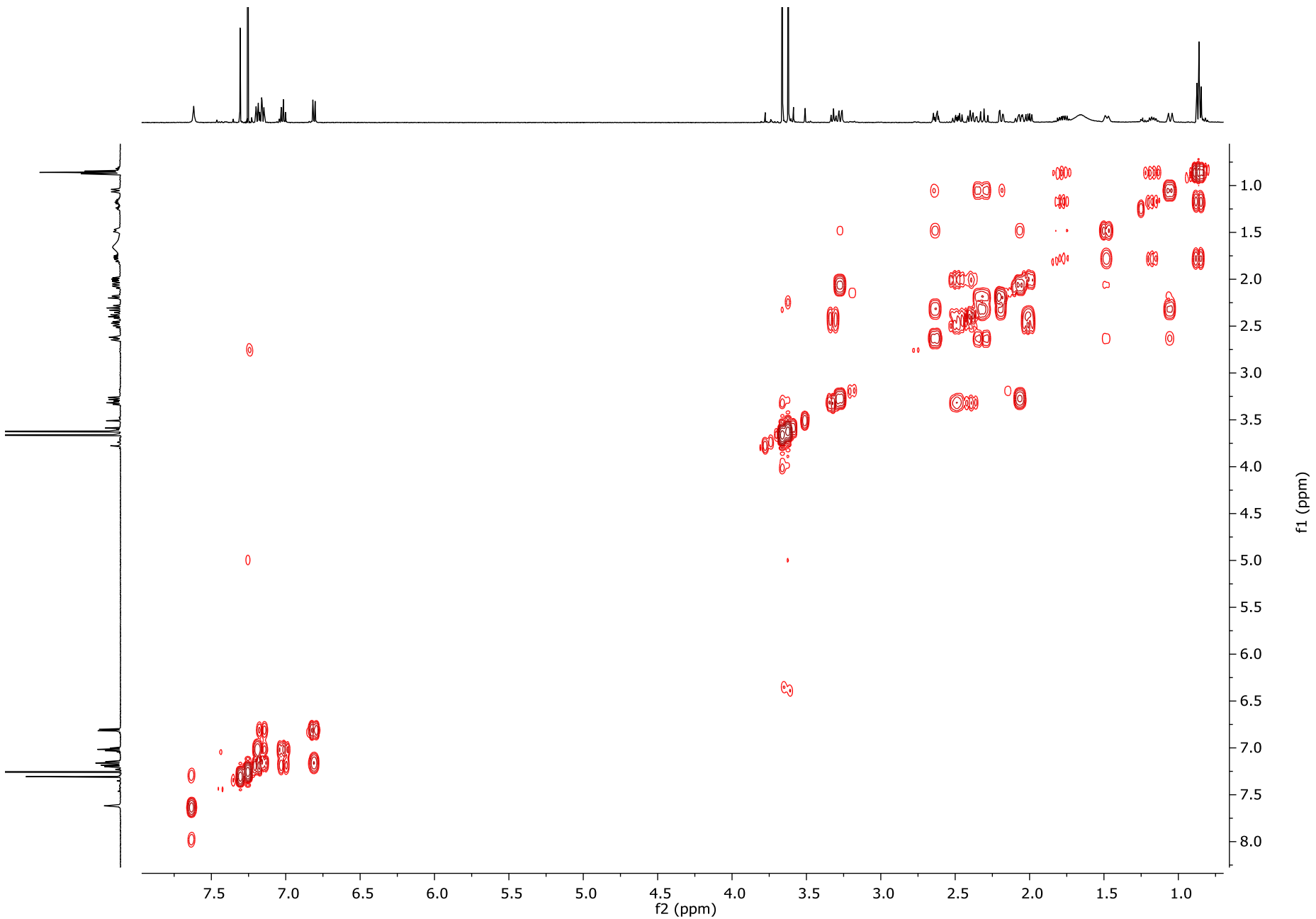

Figure S64. COSY spectrum for 3-epirhynchophylline (**17**) ($CDCl_3$, 500 MHz).

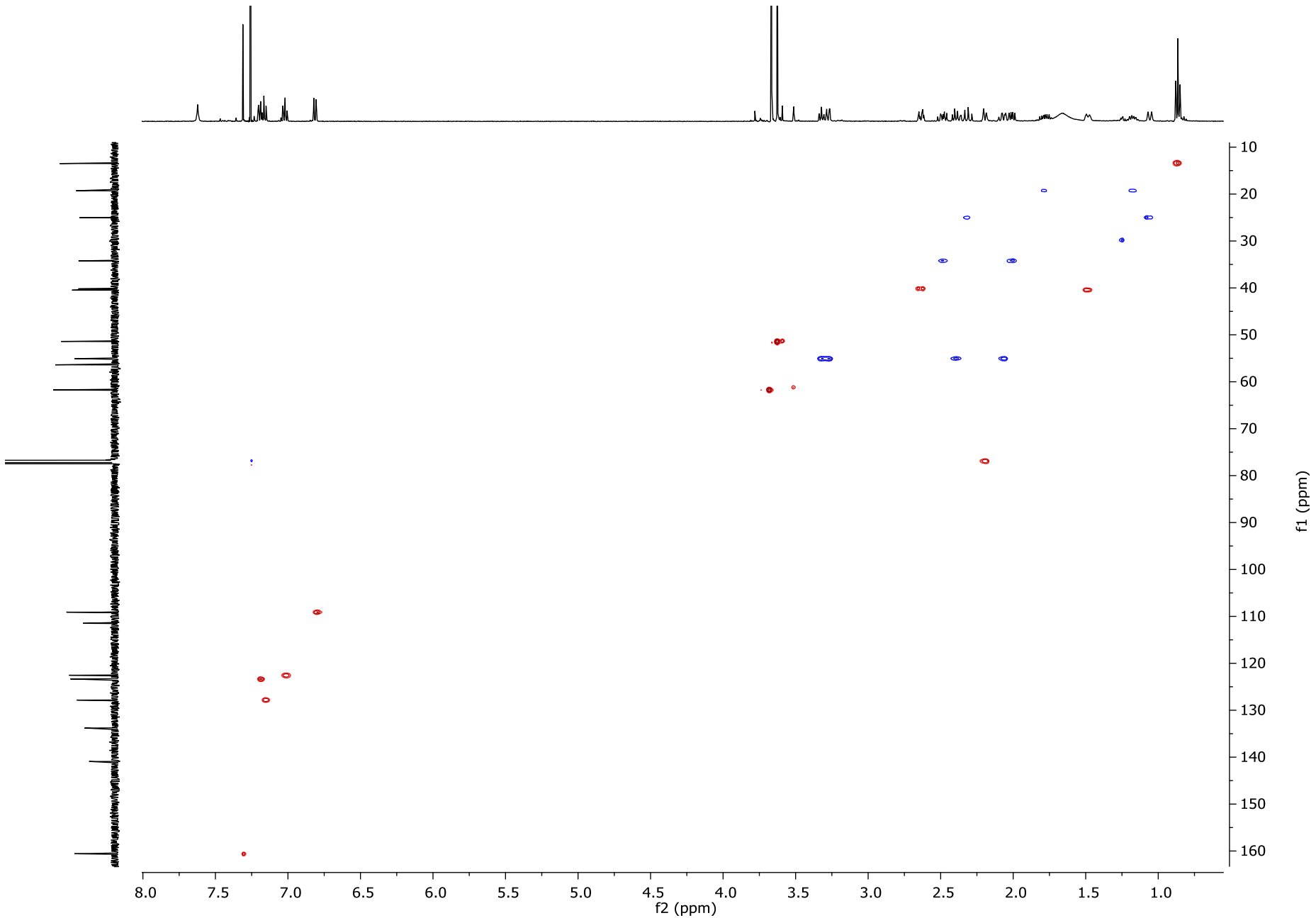

Figure S65. HSQC spectrum for 3-epirhynchophylline (**17**) ($CDCl_3$, 500 MHz).

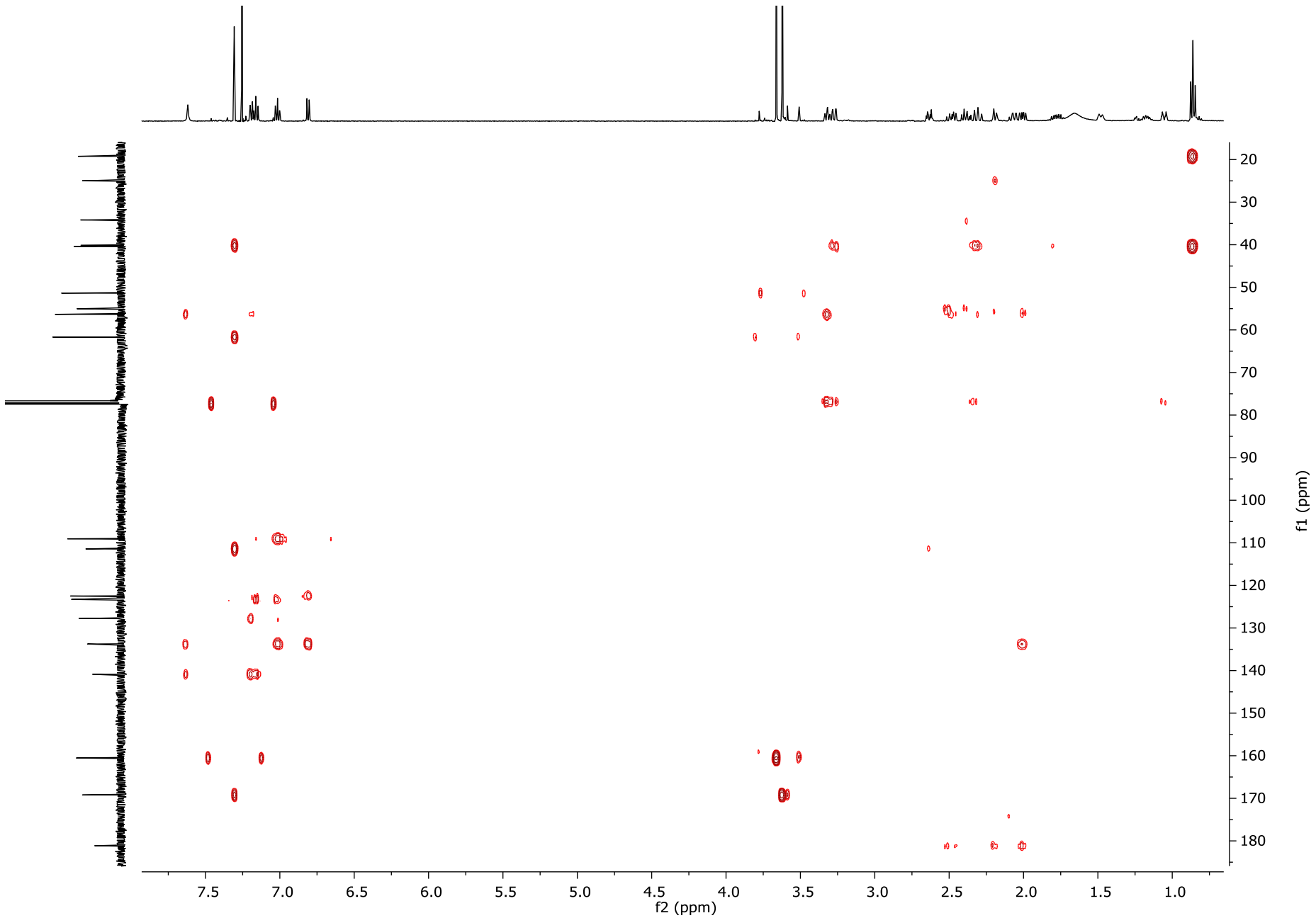

Figure S66. HMBC spectrum for 3-epirhynchophylline (**17**) ($CDCl_3$, 500 MHz).

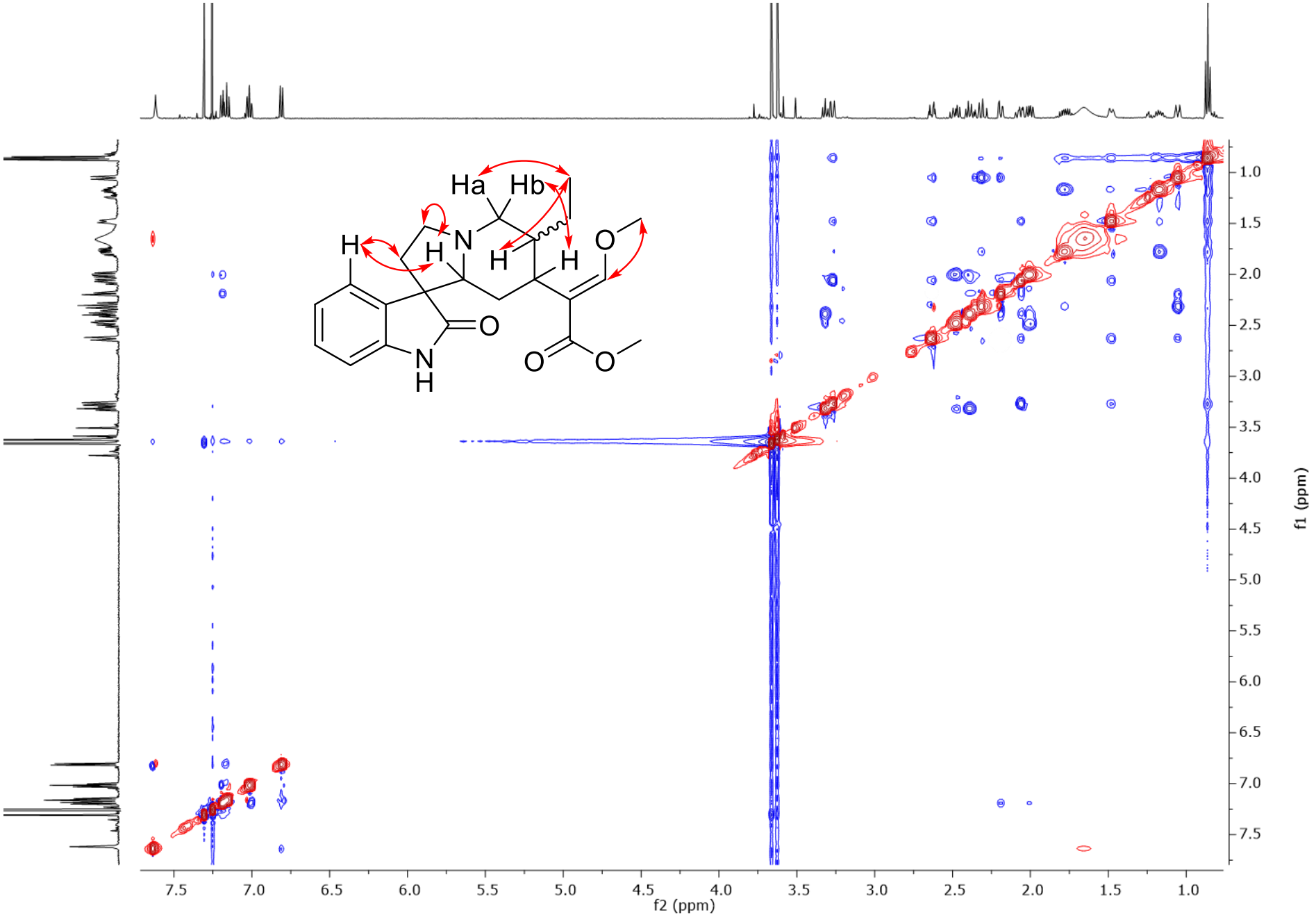

Figure S67. NOESY spectrum for 3-epirhynchophylline (**17**) ($CDCl_3$, 500 MHz).

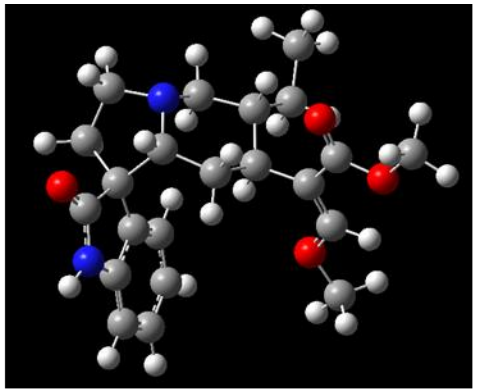

17a (ΔG 0.000 kcal/mol; P = 25.16%)

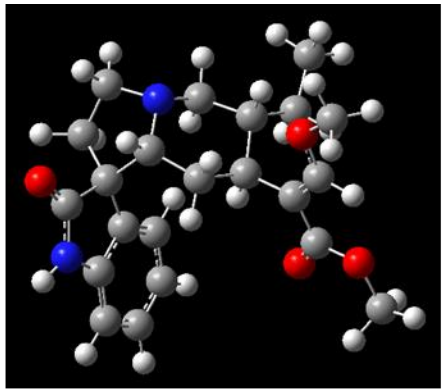

17b (ΔG 0.131 kcal/mol; P = 20.14%)

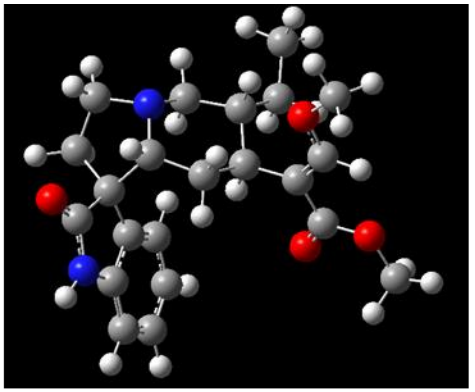

17c (ΔG 0.132 kcal/mol; P = 20.12%)

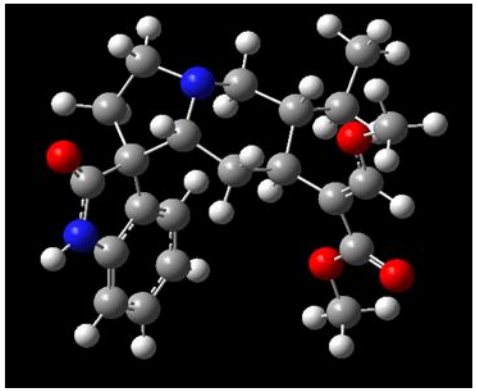

17d (ΔG 0.553 kcal/mol; P = 9.88%)

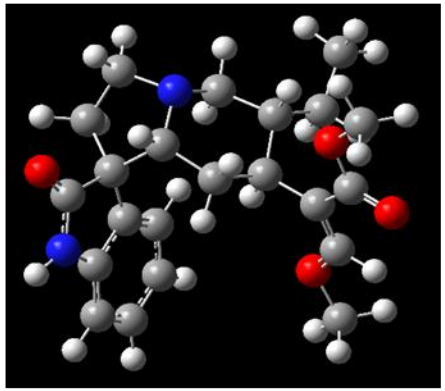

17e (ΔG 0.556 kcal/mol; P = 9.84%)

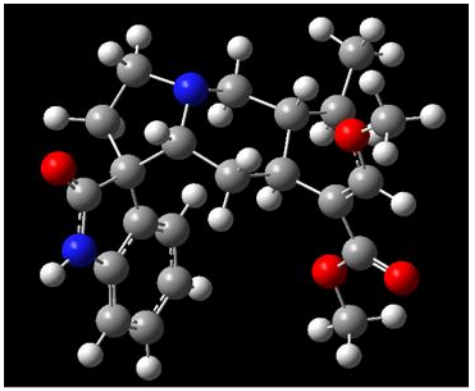

17f (ΔG 0.557 kcal/mol; P = 9.82%)

Figure S68. Six conformers used for the prediction of the ECD spectrum for **17**. The Boltzmann distributions are expressed as a percentage of population (P); the number of excited states considered for the calculation was n = 30.

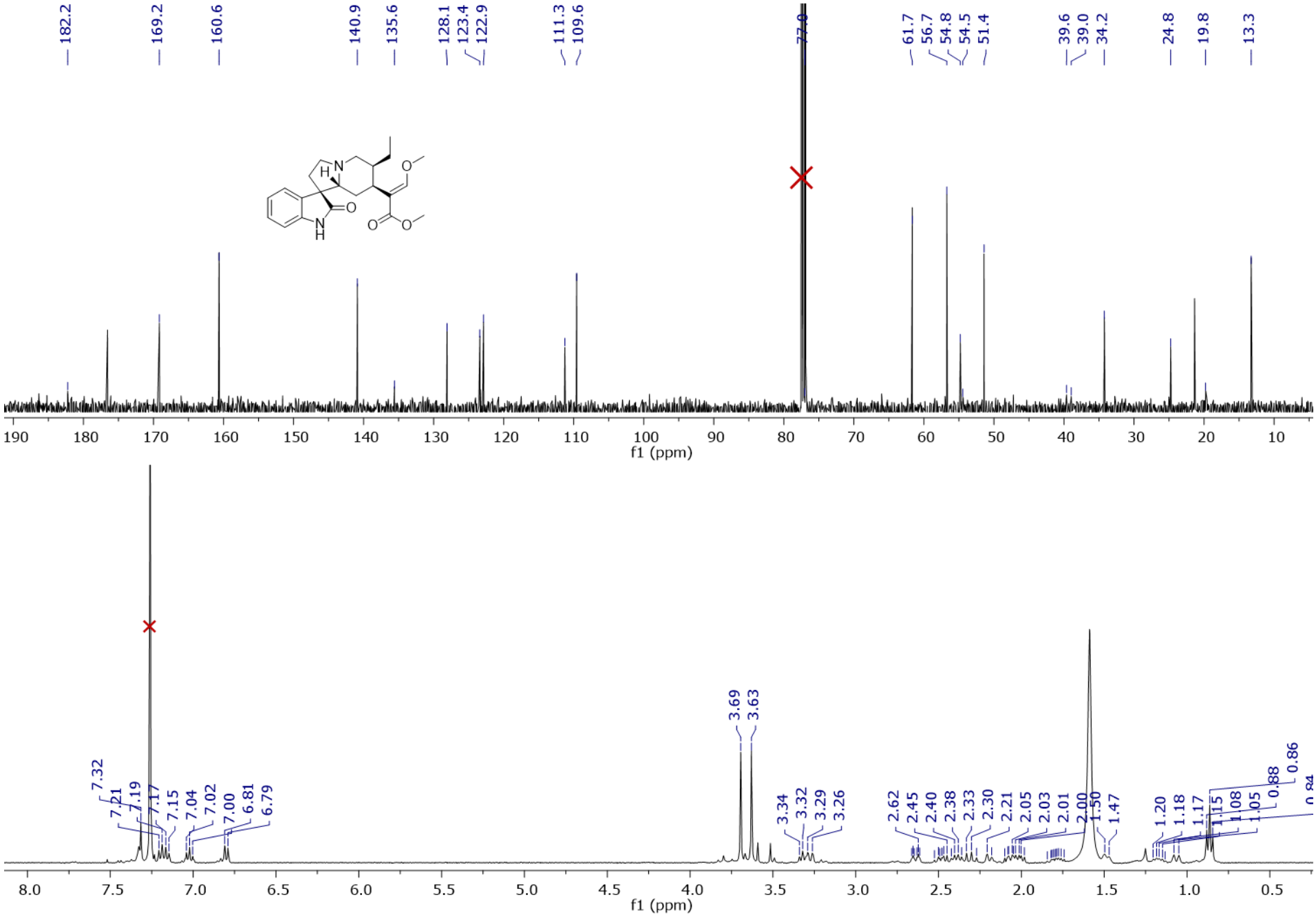

Figure S69. ^{1}H and ^{13}C NMR spectra for 3-epicorynoxine B (**18**) ($CDCl_3$, 500 MHz and 125 MHz, respectively).

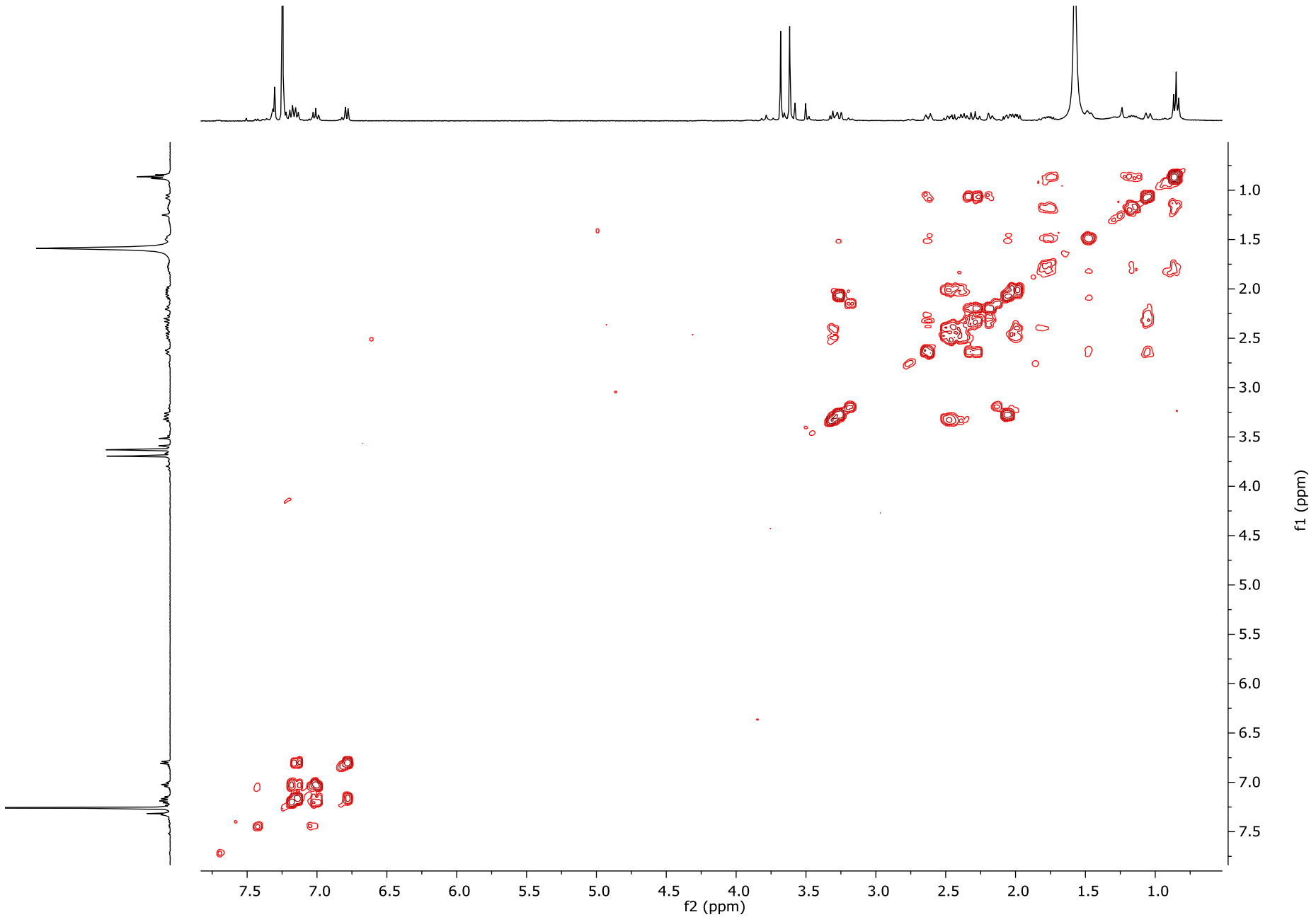

Figure S70. COSY spectrum for 3-epicorynoxine B (**18**) ($CDCl_3$, 500 MHz).

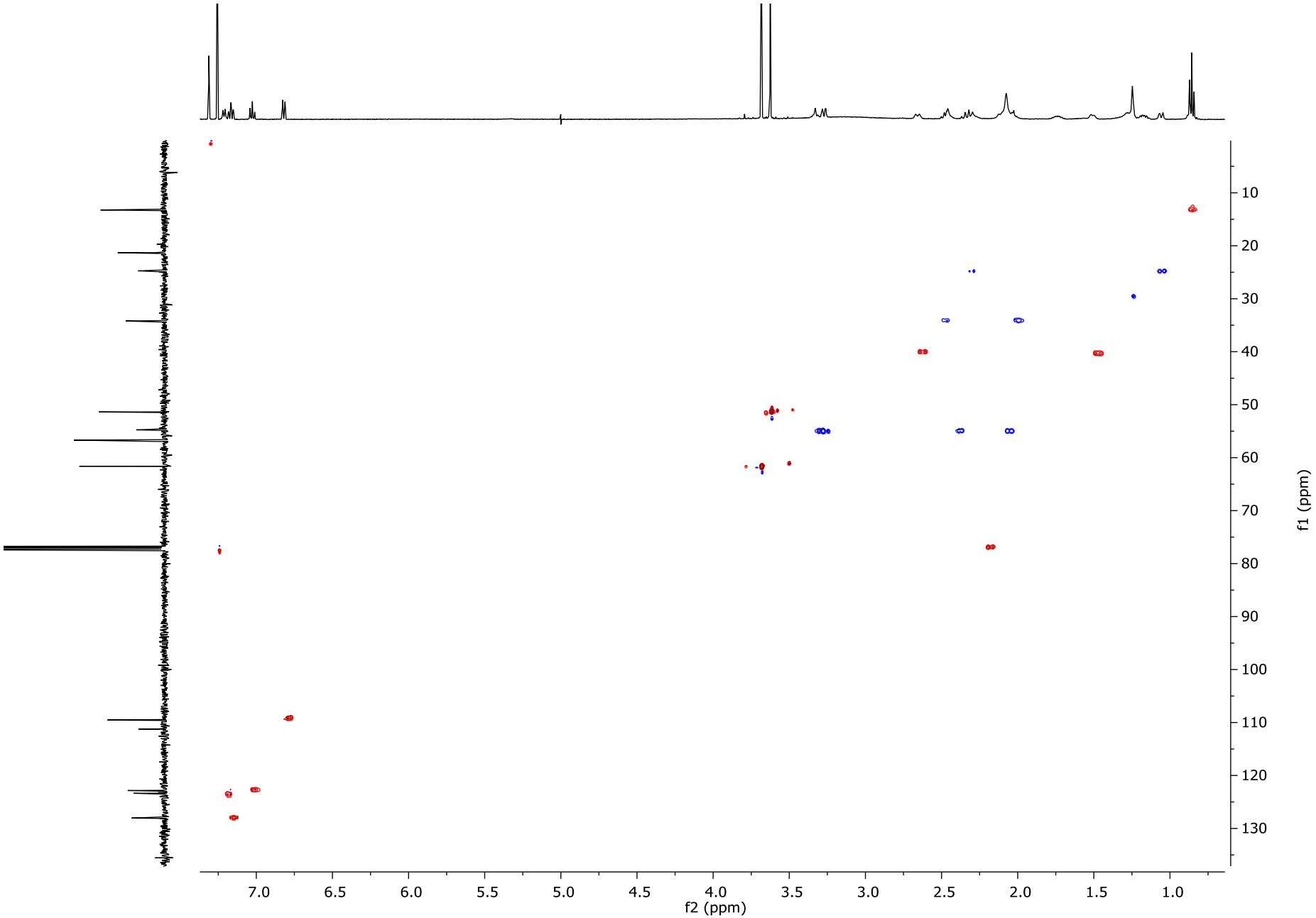

Figure S71. HSQC spectrum for 3-epicorynoxine B (**18**) ($CDCl_3$, 500 MHz).

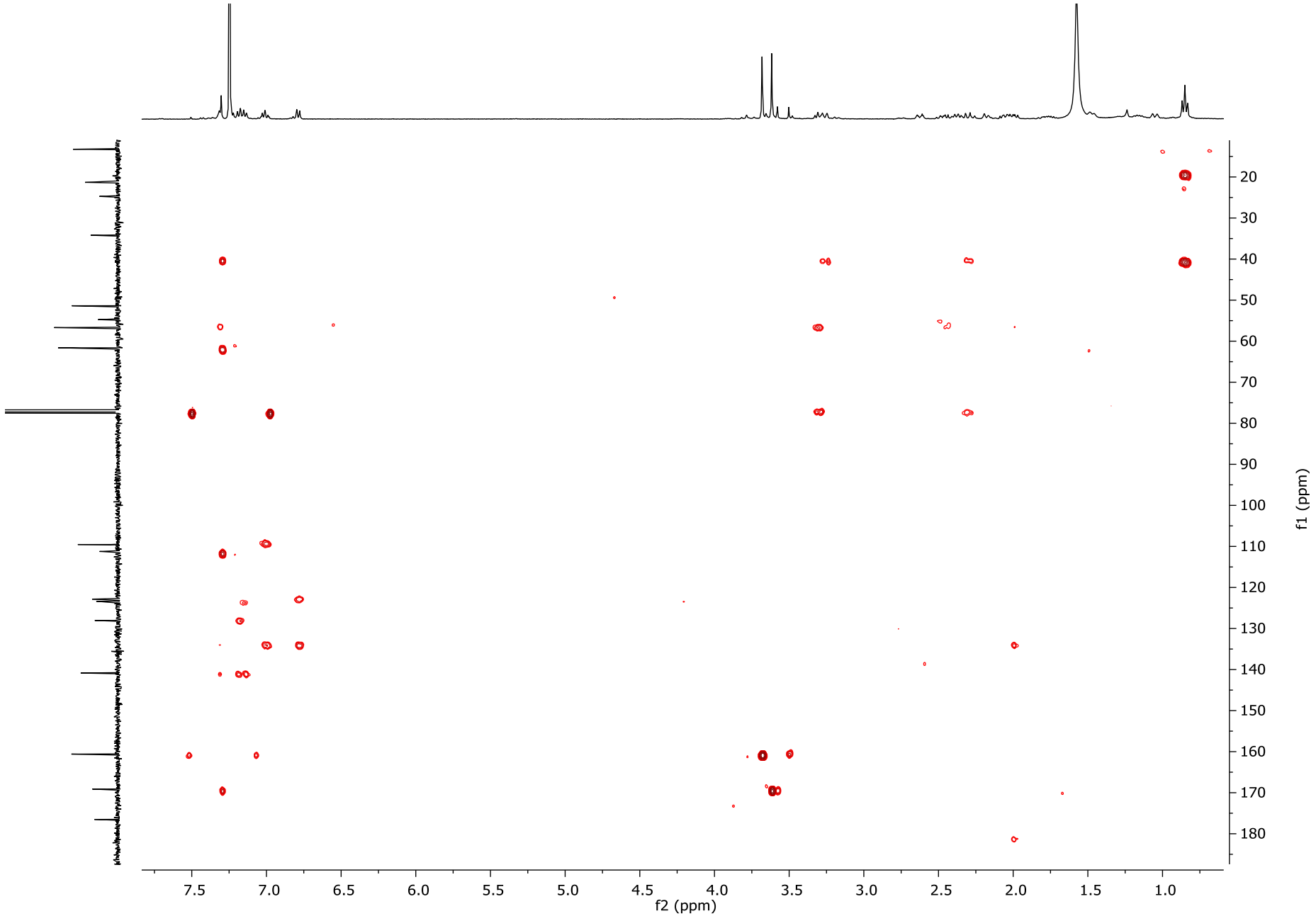

Figure S72. HMBC spectrum for 3-epicorynoxine B (**18**) ($CDCl_3$, 500 MHz).

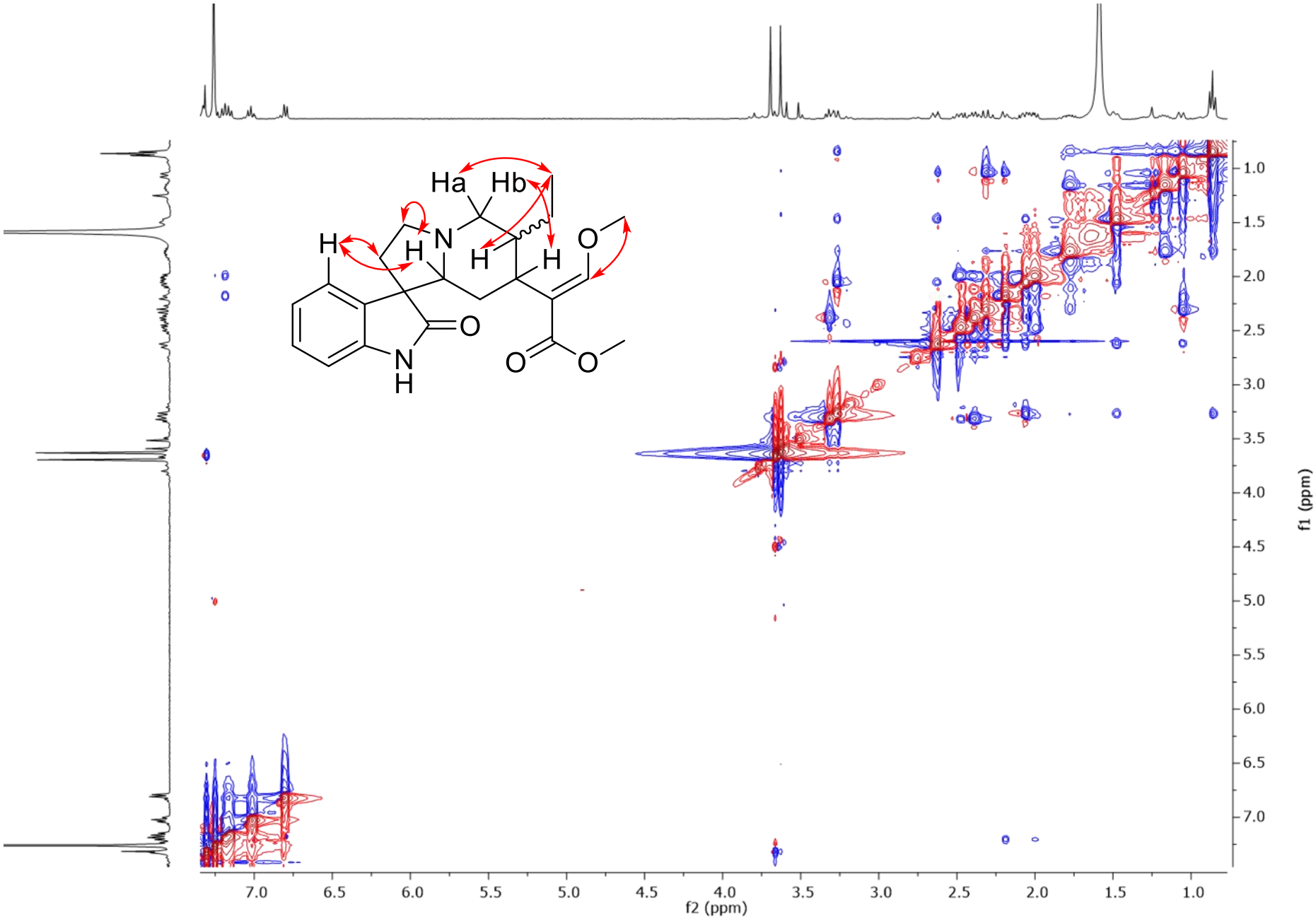

Figure S73. NOESY spectrum for 3-epicorynoxine B (**18**) ($CDCl_3$, 500 MHz).

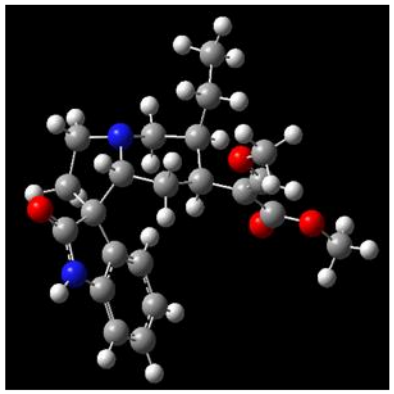

18a (ΔG 0.000 kcal/mol; P = 65.03%)

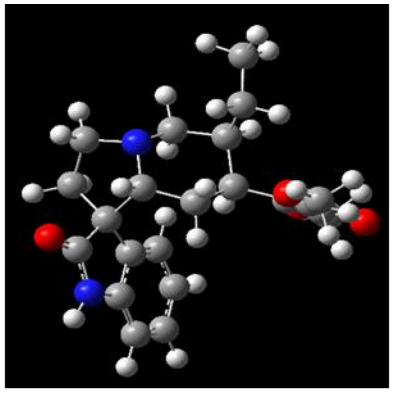

18b (ΔG 0.367 kcal/mol; P = 34.97%)

Figure S74. Two conformers used for the prediction of the ECD spectrum for **18**. The Boltzmann distributions are expressed as a percentage of population (P); the number of excited states considered for the calculation was n = 30.

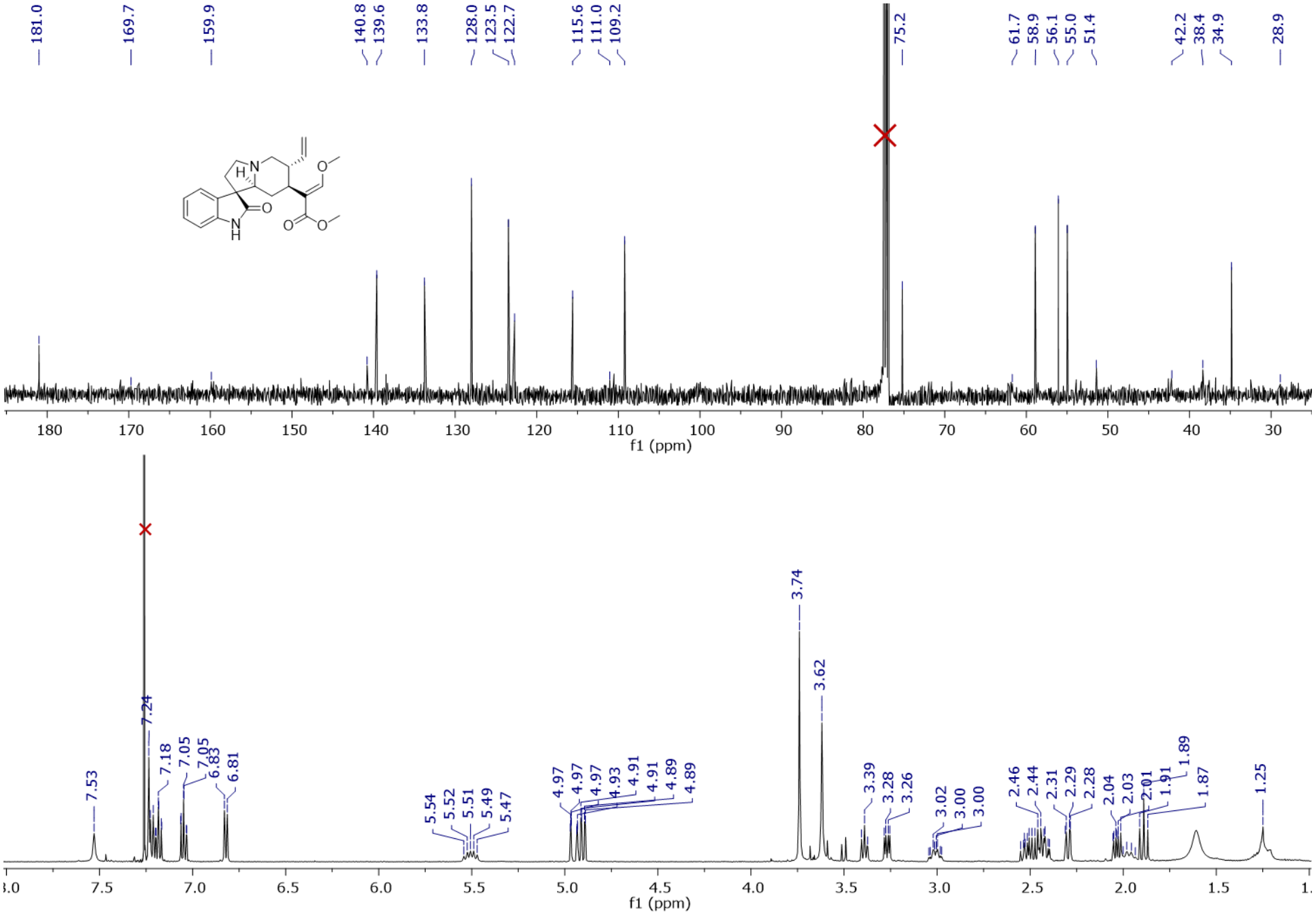

Figure S75. ^{1}H and ^{13}C NMR spectra for corynoxeine (**19**) ($CDCl_3$, 500 MHz and 125 MHz, respectively).

Table S8. Comparison of NMR Data for Compounds 15-19 ($CDCl_3$, 125 MHz and 500 MHz)

	corynoxine A (**15**)			corynoxine B (**16**)			3-epirhynchophylline (**17**)			3-epicorynoxine B (**18**)			corynoxeine (**19**)		
position	δ_C	type	δ_H (*J* in Hz)	δ_C	type	δ_H (*J* in Hz)	δ_C	type	δ_H (*J* in Hz)	δ_C	type	δ_H (*J* in Hz)	δ_C	type	δ_H (*J* in Hz)
2	182.4	C		182.3	C		181.2	C		182.2	C		181.0	C	
3	73.2	CH	2.41, dd (11.3, 2.7)	76.5	CH	2.24, bd (11.2)	77.4	CH	2.19, dd (11.4, 2.4)	77.0	CH	2.19, d (10.9)	75.2	CH	2.30, dd (11.3, 2.5)
5	54.0	CH_2	3.23, dd (8.7, 2.2) 3.20, dd (11.0, 2.16)	54.9	CH_2	3.33, m 2.50, m	55.1	CH_2	3.33, d (8.5) 2.40, m	54.8	CH_2	3.32, t (8.0) 2.39, m	55.0	CH_2	3.39, t (8.3) 2.47, m
6	34.9	CH_2	2.46, q (8.7) 2.03, dt (12.9, 8.5)	34.1	CH_2	2.46, m 2.03, m	34.2	CH_2	2.49, ddd (12.8, 10.0, 8.1) 2.01, ddd (12.9, 7.9, 1.3)	34.2	CH_2	2.49, m 2.01, dd (12.9, 8.3)	34.9	CH_2	2.52, m 2.04, ddd (13.6, 7.2, 1.8)
7	57.5	C		56.6	C		56.4	C		56.7	C		58.9	C	
8	134.7	C		133.7	C		133.8	C		135.6	C		133.8	C	
9	125.0	CH	7.45, d (7.4)	123.2	CH	7.19, d (7.4)	123.3	CH	7.20, d (7.5)	123.4	CH	7.20, d (7.8)	123.5	CH	7.22, d (7.8)
10	122.5	CH	7.05, td (7.6, 1.0)	122.5	CH	7.01, td (7.5, 1.0)	122.5	CH	7.02, td (7.6, 1.0)	122.9	CH	7.02, td (7.5)	122.7	CH	7.05, td (7.6, 1.0)
11	127.4	CH	7.17, td (7.7, 1.3)	127.9	CH	7.16, td (7.7, 1.0)	127.8	CH	7.16, td (7.7, 1.2)	128.1	CH	7.17, t (7.7)	128.0	CH	7.18, td (7.7, 1.2)
12	109.5	CH	6.86, d (7.7)	109.5	CH	6.87, d (7.7)	109.1	CH	6.81, d (7.7)	109.6	CH	6.80, d (7.7)	109.2	CH	6.82, d (7.7)
13	140.0	C		141.2	C		140.9	C		140.9	C		140.8	C	
14	25.4	CH_2	2.36, ddd (12.8, 9.4, 2.3) 0.92, dt (13.2, 3.0)	25.0	CH_2	2.37, td (12.5, 12.1) 1.04, dt (12.3, 2.8)	25.0	CH_2	2.31, m 1.06, dt (12.4, 2.6)	24.8	CH_2	2.30, m 1.06, d (12.0)	28.9	CH_2	2.47, m 1.89 t (10.9)
15	38.9	CH	2.76, dt (13.3, 3.6)	39.9	CH	2.64, dt (12.9, 3.4)	40.2	CH	2.64, dt (12.9, 3.4)	39.0	CH	2.64, qt (12.8, 2.9)	38.4	CH	3.01, qd (11.5, 3.8)
16	111.8	C	-	111.4	C	-	111.5	C	-	111.3	C	-	111.0	C	
17	160.3	CH	7.23, s	160.6	CH	7.29, s	160.6	CH	7.31, s	160.6	CH	7.32, s	159.9	CH	7.24, s
18	13.0	CH_3	0.87, t (7.4)	13.4	CH_3	0.86, t (7.4)	13.5	CH_3	0.86, t (7.4)	13.3	CH_3	0.86, t (7.3)	115.6	CH_2	4.95, ddd (17.2, 2.01, 0.8) 4.90, dd (10.2, 2.1)
19	19.4	CH_2	1.10, dqd (15.7, 7.8, 2.9) 1.65, dq (14.3, 7.2)	19.3	CH_2	1.77, ddq (14.2, 11.1, 7.1) 1.18, m	19.3	CH_2	1.78, ddq (13.6, 11.2, 7.2) 1.18, dq (14.7, 7.7)	19.8	CH_2	1.80, m 1.17, dq (14.5, 7.3)	139.6	CH_2	5.51, dt (18.0, 9.1)
20	40.3	CH	1.49, dt (11.4, 2.6)	40.3	CH	1.50, d (11.0)	40.5	CH	1.48, bd (11.1)	39.6	CH	1.48, d (10.6)	42.2	CH	1.97. dd (12.8, 10.3)
21	54.7	CH_2	2.15, dd (11.2, 2.7)	55.0	CH_2	3.28, dd (11.1, 2.1) 2.11, dd (9.8, 2.4	55.1	CH_2	3.28, dd (11.1, 2.1) 2.07, dd (11.2, 3.3)	54.5	CH_2	3.28, dd (11.6) 2.07, m	56.1	CH_2	3.27, dd (10.8, 4.1)
22	169.2	C	-	169.2	C	-	169.3	C		169.2	C		169.7	C	
17-OCH_3	61.2	CH_3	3.51, s	61.6	CH_3	3.57, s	61.7	CH_3	3.67, s	61.7	CH_3	3.69, s	61.7	CH_3	3.74, s
22-OCH_3	51.3	CH_3	3.59, s	51.4	CH_3	3.61, s	51.4	CH_3	3.63, s	51.4	CH_3	3.63, s	51.4	CH_3	3.62, s
NH			8.40, s			8.91, s			7.62, s			-			7.53, s

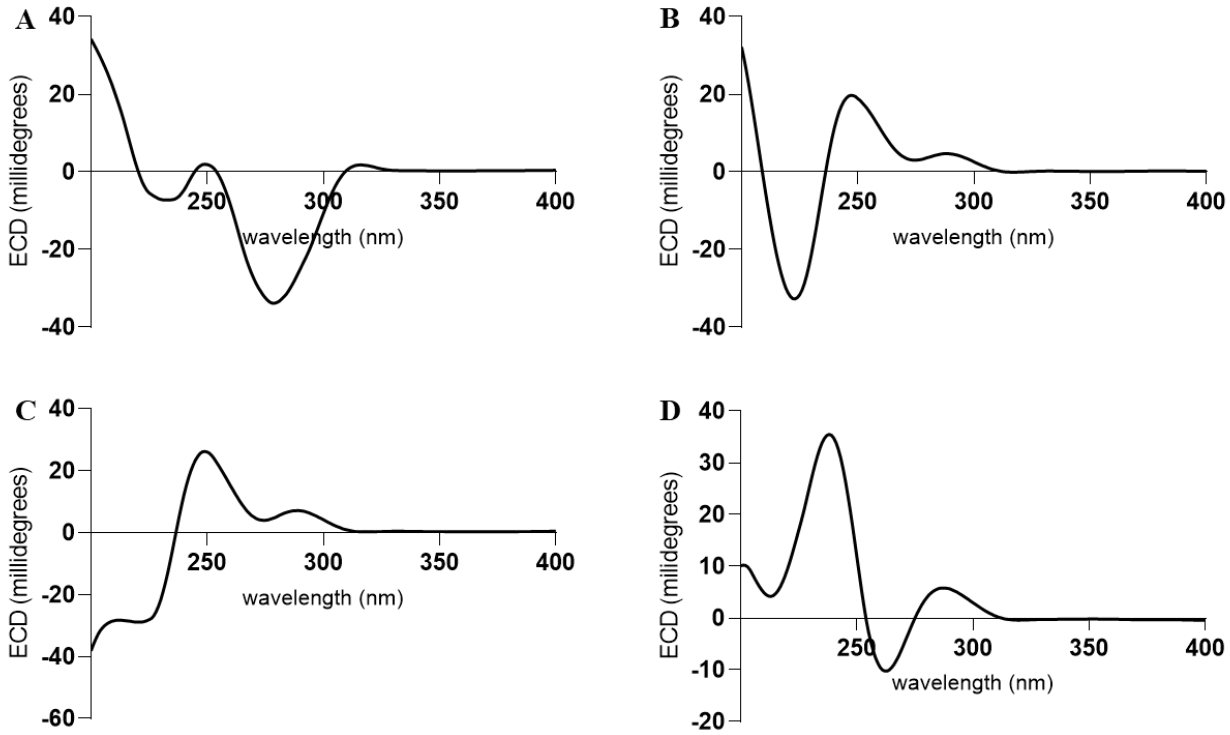

Figure S76. Comparison of the ECD spectra acquired in CH_3OH for A) corynoxine A (**15**), B) 3-epirhynchophylline (**17**), C) 3-epicorynoxine B (**18**), and D) corynoxeine (**19**).

Table S9. Confidence level data for the comparison of calculated and experimental VCD spectra.

Compound	S_E[a]	S_{-E}[b]	ESI[c]
Mitragynine (**1**)	70.0	4.6	65.4
Isopaynantheine (**6**)	59.9	8.6	51.2
Epiallo-isopaynantheine (**7**)	62.3	8.6	53.7
Corynoxine A (**15**)	67.2	7.3	59.9
3-epirhynchophylline (**17**)	57.7	8.7	48.9
3-epicorynoxine B (**18**)	58.2	8.9	49.3

[a]VCD spectral similarity for the proposed configuration. [b]VCD spectral similarity for the opposite proposed configuration. [c]Enantiomeric similarity index.

VCD Measurements. The samples were dissolved in $CHCl_3$ and placed in a BaF_2 cell with a path-length of 100 μm. In both cases, the baseline was generated by subtracting the spectrum of the solvent acquired under the same conditions.

Computational Methods. The minimum energy structures were built with Spartan'10 software. The conformational analysis was performed using the Monte Carlo search protocol under the MMFF94 molecular mechanics force field. The conformers were submitted to Gaussian'09 for calculation of their geometry optimization, performed using the B3LYP/cc-pVTZ level of theory. The optimized values were used to calculate vibrational frequencies, dipole transition moments, and rotational strengths. Individual VCD spectra were obtained as the sum of Lorentzian bands with a half-width of 9 cm^{-1} for each frequency value.

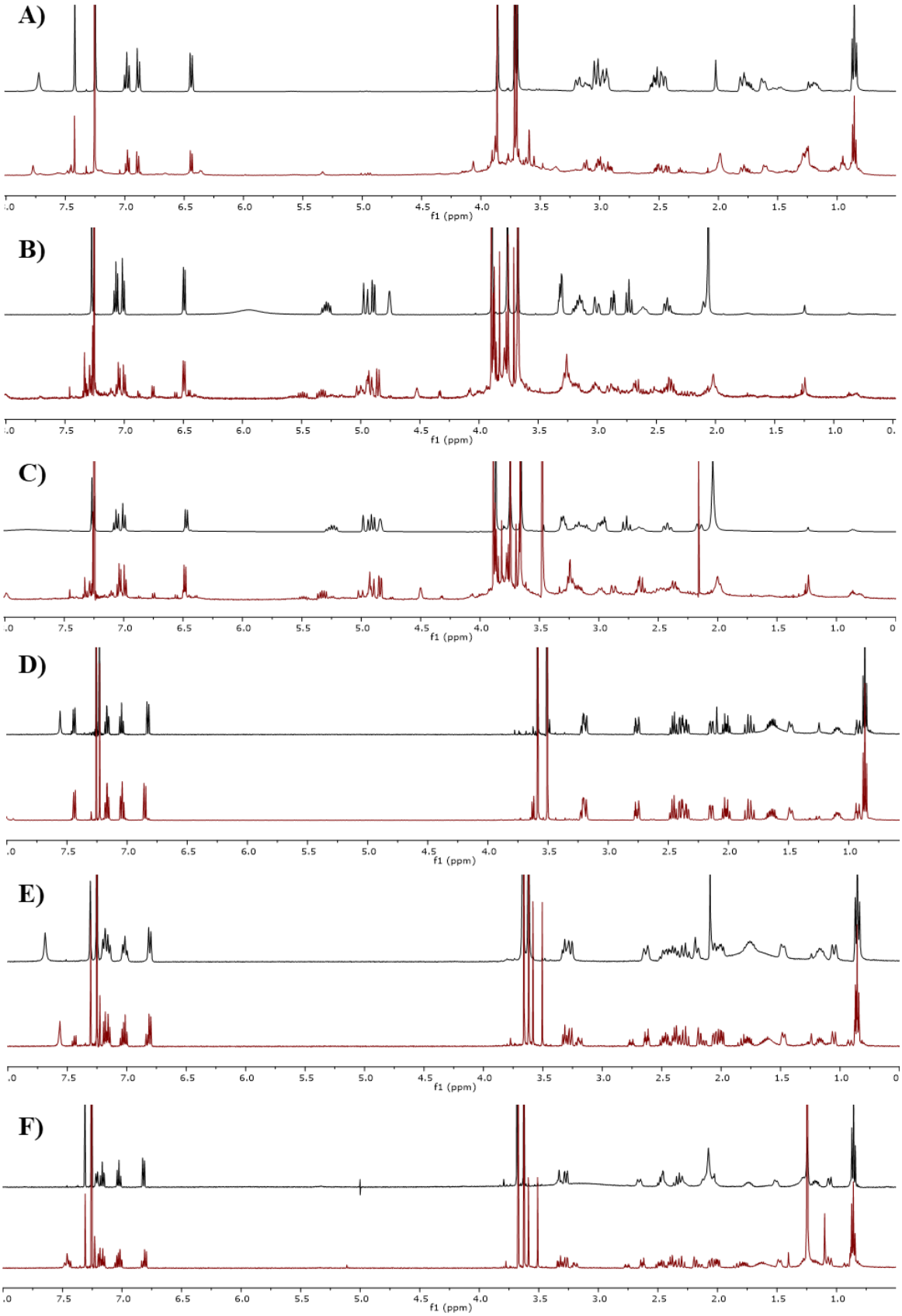

Figure S77. Comparison of the ^{1}H NMR before (black) and after (red) the acquisition of the VCD experiment. A) mitragynine (**1**), B) isopaynantheine (**6**), C) epiallo-isopaynantheine (**7**), D) corynoxine A (**15**), E) 3-epirhyncophylline (**17**), and F) 3-epicorynoxine B (**18**).